Aus dem Institut für Landschaftsökologie und Ressourcenmanagement
Professur für Landschaftsökologie und Landschaftsplanung
der Justus-Liebig-Universität Gießen

Application of remote sensing in ecosystem health assessment in times of global change

Inaugural-Dissertation
zur Erlangung des Doktorgrades der Naturwissenschaften
im Fachbereich Agrarwissenschaften, Ökotrophologie und
Umweltmanagement der Justus-Liebig-Universität Gießen

vorgelegt von

Mojdeh Safaei

Gießen, December 2024

Mit Genehmigung des Fachbereichs Agrarwissenschaften,

Ökotrophologie und Umweltmanagement

der Justus-Liebig-Universität Gießen

Prüfungskommission

1. Gutachter:	Prof. Dr. Till Kleinebecker
2. Gutachter:	Prof. Dr. Lutz Breuer
Prüfer:	Prof. Dr. Jan Siemens
Prüferin:	Prof. Dr. Suzanne Jacobs
Vorsitzende(r):	Prof. Dr. Joachim Aurbacher

Tag der Disputation: 09.12.2024

Erklärung gemäß der Promotionsordnung des Fachbereichs 09 vom 07. Juli 2004 § 17 (2)

„Ich erkläre: Ich habe die vorgelegte Dissertation selbständig und ohne unerlaubte fremde Hilfe und nur mit den Hilfen angefertigt, die ich in der Dissertation angegeben habe.

Alle Textstellen, die wörtlich oder sinngemäß aus veröffentlichten Schriften entnom-men sind, und alle Angaben, die auf mündlichen Auskünften beruhen, sind als solche kenntlich gemacht.

Bei den von mir durchgeführten und in der Dissertation erwähnten Untersuchungen habe ich die Grundsätze guter wissenschaftlicher Praxis, wie sie in der „Satzung der Justus-Liebig-Universität Gießen zur Sicherung guter wissenschaftlicher Praxis“ nie-dergelegt sind, eingehalten.“

Mojdeh Safaei

09.12.2024, Gießen

Contents

Chapter 1 - Synthesis

Application of remote sensing in dynamic ecosystem health assessment in times of global change

Introduction

State of research

Ecosystems provide a range of services that are of fundamental importance to human well-being, health, and livelihoods (IPBES, 2023; SDG, 2023), and those services can be directly linked with Sustainable Development Goals (SDG, 2019). In the next decades, climate change, Land Use/Land Cover Changes (LULCCs), and biological invasions are expected to drastically alter a multitude of ecosystem functions and services (IPBES, 2023; IPCC, 2023), and they will have a negative influence on biodiversity and ecosystem health at the global level. Among terrestrial ecosystems, forests and rangelands play a pivotal role in maintaining ecosystem health by safeguarding vital services to combat the negative impacts of global change. These ecosystems are also threatened by biological invasions as changes in canopy structure (e.g. crown thinning) and phenology may open a window of opportunity for invasive species (Große-Stoltenberg et al., 2023). Thus, assessing ecosystem health is crucial to our understanding of how ecosystems respond to environmental changes and therefore for achieving the SDGs.

Early research on ecosystem health identified and quantified factors that define the state of an ecosystem (Schaeffer et al., 1988). In 1994, the National Research Council (NRC) defined the term health in relation to rangelands and woodlands as **the degree to which the integrity of the soil, vegetation, water, and air, as well as the ecological processes, are balanced and sustained** (National Research Council, 1994). Later on, Costanza and Mageau (1999) defined a healthy ecosystem considered **one that is sustainable and has the ability to maintain its structure and function over time in the face of external stress**. Thus, a healthy ecosystem has the ability to remain stable (i.e. a high level of resistance or resilience) in the face of disturbances (Gunderson, 2000) and degradation occurs when energy flow, nutrient cycling, and hydrological regimes are negatively impacted. Therefore, assessment of ecosystem health can provide information related to ecosystem degradation and the identification of its causes (Li et al., 2014).

Traditionally assessment of ecosystem health was conducted based on field ecological data (Ludwig et al., 1996) considering socioeconomic consequences (Rapport et al., 1998) and extensively used in rangelands and forests (Jorgensen and Costanza, 2005; Tongway and Smith, 1989). For rangelands, there has been a quest for swift, qualitative, on-ground indicators to effectively monitor changes in ecosystem health , particularly regarding their capacity to preserve soil resources and sustain stability at assessment sites (Ludwig et al., 2023, 1996). Forest health assessment has also become an important aspect of terrestrial ecosystem management as well as in the study of consequences of ongoing climate change (Saha et al., 2021). Forest health was closely tied to the ecological concepts such as disturbance, vitality, resilience, decline, and mortality (Witzell et al., 2022). Traditional forest monitoring methods have not totally succeeded in delivering a comprehensive and comparable system for observing forest ecosystems, their health conditions, and changes across different spatial, temporal, and scaling levels (Lausch et al., 2017).

Methods such as Interpreting Indicators of Rangeland Health (IIRH) provide early warning tool of potential ecological problems and help to prioritize areas for monitoring, restoration, or management changes (Pellant et al., 2020). IIRH and other qualitative health assessment (Rapport et al., 1998) provided relatively quick assessments of the functionality status such as nutrient and hydrological status and soil stability (Heller et al., 2023; National Research Council, 1994). However, the assessment needs an experienced and well-trained multidisciplinary team to be reproducible (Lepak et al., 2022). Moreover, assessing ecosystem health using qualitative field data has distinct spatio-temporal limitations and IIRH are unsuitable for applications with large spatial extent (Pellant et al., 2020)

Advancements in remote sensing technology enabled the assessment and monitoring of ecosystem health more effectively than ever before (Bao et al., 2022; Lei et al., 2023; Li et al., 2014). The increasing availability of high-resolution satellite and digital spatial data such as soil parameters (Das and Panday, 2024) help monitor ecosystem health and hence support the achievement of SDGs by quantifying the level to which goals are reached. However, the question is how to develop metrics derived from remotely sensed data that are relevant for ecosystem status, and that account for the dynamic nature of ecosystem health. Remote sensing of vegetation indices enables the monitoring of ecosystem conditions at large spatial extents and could support monitoring and management efforts accounting for temporal variability (Ge et al., 2021; Li et al., 2022; Philipp et al., 2021). One of the most common approaches to describe ecosystems using remote sensing is

the creation of land-use/land cover (LULC) maps. Multiple concerns of these discrete, categorical representations exist including a lack of capacity to recognize ecosystem conditions in a dynamic manner. Thus, static outputs fail to represent the complexity of ecosystem conditions and its temporal variability (Coops and Wulder, 2019). Continuous space-borne data can monitor indicators of various processes (Lausch et al., 2017) and measure disturbances such as coniferous forest die-off (Larysch et al., 2022) in an extensive, continuous, and repetitive manner. Consequently, metrics calculated from remotely sensed time series data such as Dynamic Habitat Indices (DHIs), which rely on productivity properties based on Normalized differences Vegetation Index (NDVI) or Leaf Area Index (LAI) provide a baseline of the (natural) variability in ecosystem health, degradation and biodiversity (Coops et al., 2008; Razenkova et al., 2020).

In recent years, a growing concern with documenting and forecasting the impacts of rangeland/forest drought, climate warming, land-use change, and biological invasion has driven increased interest in the potential use of remote sensing in both static and dynamic manner in ecology. Phenological shifts have been among the most obvious and thoroughly documented biological responses to climate and land-use changes (Richardson et al., 2013; Song et al., 2021). For example, time series analyses reveal shifts in plant blooming and leaf-out in spring as global warming has accelerated since the 1980s (e.g. Vitasse et al., 2022) affecting ecosystem structures and functions (Zhou et al., 2023) and thus affect ecosystem health. Therefore, remote sensing metrics can help to refine the understanding of the existing relationship between vegetation and disturbances such as forest drought (Ivits et al., 2014) and plant invasions (Große-Stoltenberg et al., 2023). Hence, the central focus of my proposed dissertation project revolves around utilizing remotely sensed metrics and indices extracted from earth observation data to statically and dynamically explore the health of terrestrial ecosystems, considering the impacts of climate change.

Objectives

The main aim of this thesis was the assessment of terrestrial ecosystem health status with indicators derived from remote sensing data and to improve our understanding in times of climate change particularly using publicly available data. To this end, I present three studies dealing with a) a comparison of field-based data with remotely sensed data for mapping terrestrial ecosystem health in drylands considering scale issues, b) the use of Dynamic Habitat Indices (DHIs) to assess forest health in central European forests, and c) linking dynamic indicators to other environmental characteristics across different LULCs in a central European landscape. Below, I explain these

objectives:

Maintaining the structure and functionality of ecosystems is crucial for preserving soil integrity, nutrient cycling, and hydrological cycles (Ludwig et al., 2023). Various indicators for terrestrial ecosystem health have been developed, focusing on both qualitative and quantitative measures (O'Brien et al., 2016). Qualitative field data has limitations in assessing ecosystem functioning due to spatial and temporal constraints (Pellant et al., 2020). Integrating quantitative metrics from remote sensing data can address these limitations, although remote sensing also has accuracy constraints in assessing ecosystem health (Ludwig et al., 2007). Methodological approaches combining remote sensing with ground-based field data need further exploration to scale up assessments without losing crucial functional information (Frazier et al., 2023). The challenge lies in effectively scaling up from qualitative field-based measures to broader quantitative assessments using remote sensing data. Thus, the **first objective** addresses the challenge of aligning field-based observations to remote sensing data at various spatial scales to map terrestrial ecosystem health in drylands. Motivated by the need to monitor indicators of ecosystem health tied to United Nations SDGs, we propose a preliminary workflow. This approach scales and connects qualitative field assessments with landscape characteristics derived from remote sensing imagery, exemplified in central Iran. This method offers a foundation for further research to refine and expand upon and testing its applicability across different spatial and temporal scales, which is crucial for advancing landscape ecology.

Continuous measurements such as vegetation cover metrics offer more direct insights into ecosystem functioning compared to discrete classifications (Coops and Wulder, 2019). Metrics derived from remotely sensed time series data, like Dynamic Habitat Indices (DHIs), which capture vegetation productivity properties, provide a baseline for assessing natural variability in ecosystem health and degradation (Coops et al., 2008). Hence, the **second objective** of this thesis was to apply dynamic ecosystem health indicators using space-borne data and to detect the dynamic health status of coniferous forest before, during and after a severe drought event.

Combining DHIs with additional spatial information on ecosystem properties could contribute to a deeper understanding of ecosystem dynamics at the landscape level. Therefore, further exploration is needed to integrate DHIs with environmental factors influencing vegetation productivity. To our knowledge, a comprehensive assessment of how the DHI changes for different LULC types across different environmental conditions related to precipitation and soil

conditions has not yet been studied. Hence, the **third objective** was to investigate the potential of DHIs to capture variability in soil properties and drought conditions across LULC types in a Central European landscape.

Chapter outline

The dissertation comprises three manuscripts, all of which have already been published in international peer-reviewed scientific journals.

Chapter 2 (study 1 or objective 1): **Safaei M**, Bashari H, Kleinebecker T, Fakheran S, Jafari R, Große-Stoltenberg A (2023) Mapping terrestrial ecosystem health in drylands: Comparison of field-based information with remotely sensed data at watershed level. Landscape Ecology 38: 705-724 [doi: 10.1007/s10980-022-01454-4]

In the first study, a field survey was conducted to identify key indicators of health status using the IIRH assessment (Pellant et al., 2020). Two land use/land cover (LULC) maps were created based on 2016 Landsat OLI and 1987 Landsat TM imagery, using the supervised Maximum Likelihood Classification algorithm. The study aimed to determine if past terrestrial ecosystem health could be estimated by analyzing two-time steps. Different multivariate statistical methods such as cluster analyses and non-metric multi-dimensional scaling were employed to compare terrestrial ecosystem health patterns, addressing also the challenges of remote sensing data for monitoring landscapes. According to the results, soil surface loss, plant mortality, and invasive species were identified as important indicators of health and "healthy" sites had lower amounts of spectral heterogeneity. By linking field data with remote sensing indices, we improved the interpretation of ecological metrics and patterns. Through multivariate and cluster analyses, we assigned health status clusters to landscape indices, moving beyond traditional patch-based metrics. This approach demonstrates how landscape metrics can assess ecological processes at the watershed level, highlighting the potential for monitoring land degradation from space.

Chapter 3 (study 2 or objective 2): **Safaei M**, Kleinebecker T, Weis M, Große-Stoltenberg A (2024) Tracking effects of extreme drought on coniferous forests from space using Dynamic Habitat Indices. Heliyon [DOI:https://doi.org/10.1016/j.heliyon.2024.e27864]

Second study examines the impact of extreme droughts and heatwaves on the health of coniferous forests in Central Europe, focusing on the federal state of Hesse, Germany, using DHIs

of four consecutive years (2017-2020). Results show significant alterations in these indicators across both undamaged and damaged forest sites, indicating a shift in ecosystem functioning. The study underscores the potential of DHIs in capturing drought effects on Central European forests and suggests the applicability of this approach at larger scales and in diverse land cover types globally.

Chapter 4 (Study 3 or Objective 3): **Safaei M**, Kleinebecker T, Große-Stoltenberg A (2023) Potential of the satellite-based Dynamic Habitat Index (DHI) to capture changes in soil properties and drought conditions across Land Use/ Land Cover types. Geocarto International 38: 2292162 [doi.org/10.1080/10106049.2023.2292162]

Third study assesses the responsiveness of the DHI to changing environmental conditions across various LULC types. Results show distinct DHI patterns across different LULC types, with notable responses to the extreme drought in 2018. Integration of DHI with ancillary geodata improves traditional categorical LULC maps, offering applications in biodiversity and ecosystem research. These integrated products could aid decision-makers in formulating sustainable land management strategies and contribute to SDG indicators related to land degradation by identifying deviations from typical DHI profiles in response to disturbances and environmental stress.

Conclusions

Main Results

The studies of this dissertation project revealed that new practical approaches are required for the assessment of ecosystem health including spatially explicit identification, early warning signs, and thresholds of disturbances. It also revealed that remote sensing tools can be effectively applied to identify health status (Kooistra et al., 2023) from the sub catchment to regional scales within heterogeneous environments, and can be applied at even larger spatial scales. Freely available long-term optical remote sensing data offers a unique opportunity to investigate health status, especially when historical field records are not available. The first study (chapter 2) provided a workflow to derive a good estimation of changes in health status over time. However, validating remotely sensed information on terrestrial ecosystem health with expert field assessments is mandatory and enhances data-driven rangeland health evaluations (Herrick et al., 2019).

The second study (chapter 3) demonstrates that DHIs are an effective and straightforward tool for monitoring the health of coniferous forests at large spatial scales, providing valuable

spatio-temporal information (Lausch et al., 2017). Using multitemporal remote sensing data clearly mirrored the dynamics of vegetation greenness and successfully identified the impacts of disturbances, such as forest dieback in central European coniferous forests due to severe droughts (Schuldt et al., 2020a). By comparing the DHI component values between damaged and non-damaged sites, early warning indicators of ecosystem degradation and changes in ecosystem functioning could be derived.

Integrating DHIs with spatial environmental information additionally deepens our understanding of ecosystem dynamics at the landscape scale (Michaud et al., 2012) and is particularly valuable for ecological landscape assessments. Here (chapter 4), by integrating remote sensing with other geospatial data, we showed that composite vegetation indices and land surface phenological products from satellite time-series data can complement common LULC maps, allowing for a more detailed analysis of the links between LULC and ecosystem functioning (Coops and Wulder, 2019). This integration can aid decision-makers in developing sustainable land management strategies and supports SDG, such as SDG 15.3.1 related to land degradation, by identifying deviations in land use and land cover due to disturbance and/or environmental stress (Sims et al., 2021).

In summary, in this thesis I present a framework to assess terrestrial ecosystem health in two different landscape settings: an arid to semi- arid region in Iran and a temperate suboceanic European landscape in Germany. The proposed workflows can built the basis for a remote-sensing scheme to identify and map health status, and to define thresholds of ecosystem degradation for landscapes prone to disturbances (Li et al., 2014). Therefore, establishing a strong link between in situ and earth observations based on health concept are suggested to significantly increase the benefit of remote sensing for landscape ecology research (Wu and Hobbs, 2002). Our methodological approach utilized publicly available data and free, open-source software. This provides a foundation for further studies in climate change monitoring, landscape planning, and ecosystem management (Richardson et al., 2013).

A conceptual framework for ecosystem health assessment

The case studies presented in this thesis, spanning arid and semi-arid regions in central Iran and the temperate suboceanic climate of the Federal State Hesse located in central Germany, led to the development of a conceptual framework for the assessment of terrestrial ecosystem health that is potentially transferable to other environmental settings. This framework is based on

both field indicators and remote sensing metrics considering scaling issues (Figure 1-1). The concept of terrestrial ecosystem health is inherently intricate and multifaceted in ecosystem assessment (Herrick et al., 2019; Lei et al., 2023; Ludwig et al., 2023; O'Brien et al., 2016; Pellant et al., 2020; Rapport et al., 1998). Although measuring ecosystem health can be achieved by field work directly, these kinds of measurement are both time consuming and costly (Ludwig et al., 2007). Therefore, we applied simple filed measures (study 1) coupled them with remote sensing metrics that reliably indicate ecosystem health in terms of how well a landscape can conserve essential resources. However, due to the complexity within and among different ecosystem elements, coupled with their myriad interactions and reactions, the development of a health framework solely based on a limited set of indicators was challenging (Ludwig et al., 2023, 2007) (Figure 1-1). Thus, while identifying such indicators was no easy feat, crucial considerations for the selection of indicators are outlined below:

1. **Environmental context**: It is imperative to tailor index selection to suit specific environmental conditions and climates, as one method may not universally apply across different environmental contexts (Herrick et al., 2019). For example, indicators mentioned in the IIRH protocol and the way to collect data are specifically designed for arid and semi-arid landscapes and are not directly applicable to the central European landscape.

2. **Regional history**: Understanding the ecological history of a region is pivotal in indicator selection (Puig-Gironès and Real, 2022). For instance, semi-arid areas with a history of intense livestock grazing require different indicators compared to regions in Central Europe prone to droughts and pest infestations.

3. **Indicator diversity:** Qualitative and quantitative indicators, whether field-based or derived from remote sensing, offer a range of options (Lepak et al., 2022; Li et al., 2014). Selection of indicators should consider factors like budget, available expertise, and study area size.

4. **Monitoring feasibility**: The feasibility of ground indicator monitoring varies. This impacts the effectiveness of health monitoring efforts (Ludwig et al., 2007). The IIRH protocol is not suitable for yearly monitoring, but the DHI based on time series data provide an opportunity to thoroughly investigate the variation of productivity indices across years.

5. **Scale consideration**: When choosing indices applicable to both ground and remote sensing methods, careful attention to scale and scaling are crucial for accurate assessments (Frazier et al., 2023). In our case in semi-arid landscapes, we selected remote sensing metrics with the same ecological concept as field indicators.

6. **Temporal and spatial dynamics**: Satellite imagery's temporal and spatial resolution (Razenkova et al., 2020b) play a significant role in gauging ecosystem health over time and space.

7. **Time series analysis**: Time series data and dynamic modelling (Kooistra et al., 2023) provide valuable insights into health trends and changes over time.

8. **Integration with environmental variables**: Effective indices should integrate seamlessly with other environmental variables, enhancing their ability to capture changes accurately (Michaud et al., 2012). We show that composite remote sensing indices such as the DHI based on NDVI time series data are useful to characterize LULC types including their variation due to variable soil and changing drought conditions considering effects of severe drought years in Central European landscapes.

Considering the challenges discussed above and regardless of the specific type of terrestrial ecosystem (rangeland or forests in this thesis), ecosystem health can be understood as **the cohesive functioning of ecosystem components, with their structures performing optimally, even when the ecosystem is experiencing disturbances such as natural disasters, climate changes, or human activities** (Costanza and Mageau, 1999; Herrick et al., 2019; Lausch et al., 2017; Ludwig et al., 2023, 2007; National Research Council, 1994; O'Brien et al., 2016; Pellant et al., 2020; Rapport et al., 1998). For instance, in arid and semi-arid landscapes, soil protection and conservation were best achieved when vegetation cover and composition are at optimal levels, particularly in the face of heavy disturbance like strong grazing pressure (Ludwig et al., 2007). Or in the Central European landscape, variations in annual productivity were associated with soil characteristics, and drought had an impact on this productivity. The analysis indicated that as study sites transition from healthy to unhealthy, their structural and functional characteristics experience significant degradation. From the cases discussed, it is evident that maintaining healthy conditions and improving at-risk and unhealthy areas is crucial for rangeland and forest management. Thus, sustainable and multifaceted use of these lands should replace

excessive exploitation to prevent long-term damage and irreversible degradation (Hamdi et al., 2019; Heller et al., 2023; Schuldt et al., 2020).

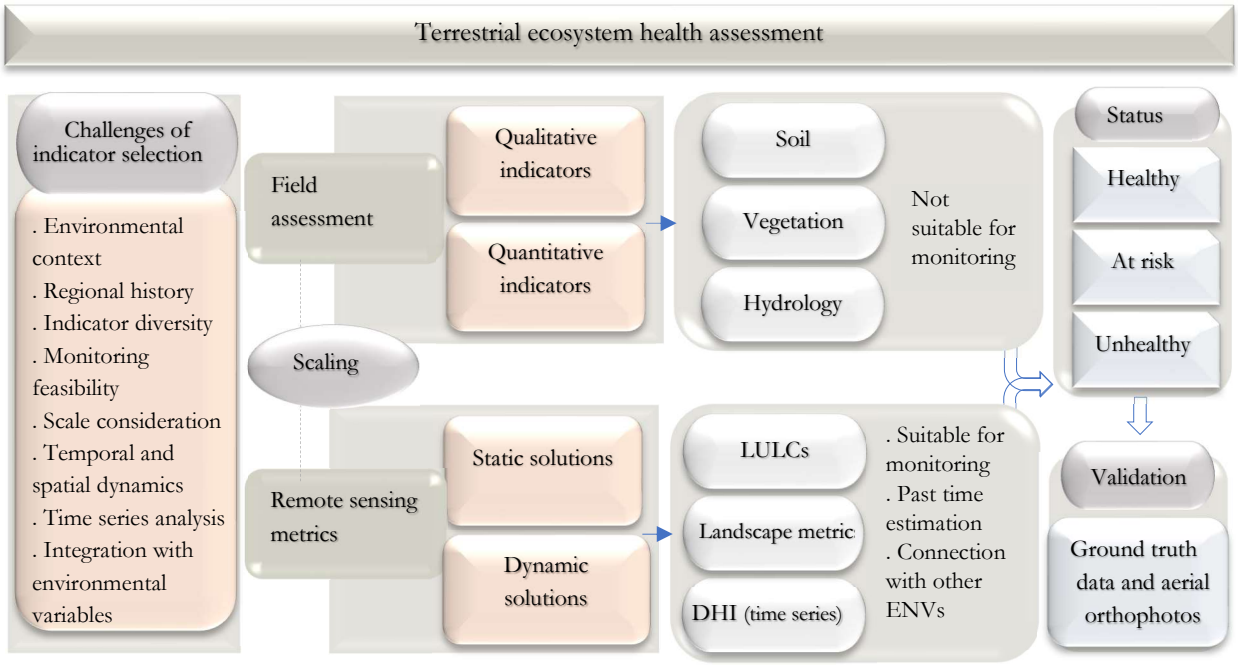

Figure 1-1 Conceptual framework of terrestrial ecosystem health assessment based on the three case studies presented in this thesis. We employed a set of qualitative and quantitative indicators, field and remote sensing metrics, single date and time-series data, different machine learning, multivariate and modelling methods under different climates to gain an understanding of terrestrial ecosystem health (here mainly forests and rangelands). The most important challenges we faced during our studies are presented in the figure as well. IIRH: Interpreting Indicators of Rangeland Health, ENVs: Environmental variables.

Future directions

Linking field and remotely sensed indices improved the interpretation of metrics and their corresponding ecological patterns and processes (Wu and Hobbs, 2002). By establishing this linkage, we highlighted the potential for space-based land degradation monitoring. Future research could focus on identifying ecological thresholds or tipping points (Andersen et al., 2009) and spatial early warning signals of ecosystem transitions to alternative stable states (Zou et al., 2024).

Using vegetation time series data like DHIs to capture the effects of droughts in forests can be an effective way to assess future tree mortality risks, especially with high-resolution optical data like PlanetScope or RapidEye images (Silveira et al., 2023). Combining these data with ecophysiological measurements (Schuldt et al., 2020a), sensory networks (Lausch et al., 2017), and

high-resolution bioclimatic data on terrestrial ecosystem drought could provide new insights into species die-off under extreme weather events. In regions where NDVI is less effective, such as semi-arid areas or tropical regions, alternative vegetation indices like the Enhanced Vegetation Index (EVI) or the Soil-Adjusted Vegetation Index (SAVI) could be tested (Chen et al., 2024). These integrated approaches can potentially identify damage before it becomes visibly apparent.

A significant limitation of vegetation indices from passive optical remote sensing is cloud cover, but recent advancements include the use of freely available synthetic aperture radar SAR (Zhang et al., 2019) data for forest drought monitoring, that can enhance DHI's capability to detect ecosystem changes. Incorporating structural data and canopy height information from LiDAR (Coops et al., 2018), supported by automated field measurements for calibration, is the next step to improve the identification of tipping points and regime shifts in terrestrial ecosystems health.

Management perspective

Based on the findings of this research, it seems necessary to implement a management plan at the national level and to allocate funds for the restoration of rangelands and forest. Therefore, the results of such research support land management planning and facilitate decision-making following the principles of sustainable development (SDG, 2023). Here, we underlined the importance of ecosystem structures and functions of rangelands and forests in different conditions, indicating that functional thresholds in unhealthy sites are extremely fragile (Ludwig et al., 2007). Identifying these thresholds is critical and managers must recognize that the conditions for plants and soil may undergo irreversible changes (Swift and Hannon, 2010). Informing managers about the value of the functions and services of natural ecosystems, in preventing the arbitrary conversion of forests and rangelands to other land uses plays an important role in land conservation (Scherzinger et al., 2024). The methodological approach developed in this thesis may help to implement more resilient landscape and sustainable land use, and remote sensing has shown great potential to get closer to the achievement of the SDGs.

References

Andersen, T., Carstensen, J., Hernández-García, E., Duarte, C.M., 2009. Ecological thresholds and regime shifts: approaches to identification. Trends in Ecology & Evolution 24, 49–57. https://doi.org/10.1016/j.tree.2008.07.014

Bao, Z., Shifaw, E., Deng, C., Sha, J., Li, X., Hanchiso, T., Yang, W., 2022. Remote sensing-based assessment of ecosystem health by optimizing vigor-organization-resilience model: A case study in Fuzhou City, China. Ecological Informatics 72, 101889. https://doi.org/10.1016/j.ecoinf.2022.101889

Chen, J., Yang, H., Jin, T., Wu, K., 2024. Assessment of terrestrial ecosystem sensitivity to climate change in arid, semi-arid, sub-humid, and humid regions using EVI, LAI, and SIF products. Ecological Indicators 158, 111511. https://doi.org/10.1016/j.ecolind.2023.111511

Coops, N.C., Kearney, S.P., Bolton, D.K., Radeloff, V.C., 2018. Remotely-sensed productivity clusters capture global biodiversity patterns. Scientific Reports 8, 16261. https://doi.org/10.1038/s41598-018-34162-8

Coops, N.C., Wulder, M.A., 2019. Breaking the Habit(at). Trends in Ecology & Evolution 34, 585–587. https://doi.org/10.1016/j.tree.2019.04.013

Coops, N.C., Wulder, M.A., Duro, D.C., Han, T., Berry, S., 2008. The development of a Canadian dynamic habitat index using multi-temporal satellite estimates of canopy light absorbance. Ecological Indicators 8, 754–766. https://doi.org/10.1016/j.ecolind.2008.01.007

Costanza, R., Mageau, M., 1999. What is a healthy ecosystem? Aquatic Ecology 33, 105–115. https://doi.org/10.1023/A:1009930313242

Das, S., Panday, D., 2024. Chapter 29 - Soil health assessment and spatial characterization using remote sensing, in: Dharumarajan, S., Kaliraj, S., Adhikari, K., Lalitha, M., Kumar, N. (Eds.), Remote Sensing of Soils. Elsevier, pp. 455–467. https://doi.org/10.1016/B978-0-443-18773-5.00034-X

Frazier, A.E., Kedron, P., Donovan, M.K., 2023. Advancing a science of scaling in landscape ecology. Landscape Ecology 38, 613–617. https://doi.org/10.1007/s10980-022-01591-w

Ge, W., Han, J., Zhang, D., Wang, F., 2021. Divergent impacts of droughts on vegetation phenology and productivity in the Yungui Plateau, southwest China. Ecological Indicators 127, 107743. https://doi.org/10.1016/j.ecolind.2021.107743

Große-Stoltenberg, A., Lizarazo, I., Brundu, G., Gonçalves, V., Osco, L., Masemola, C., Müllerová, J., Werner, C., Kotze, I., Oldeland, J., 2023. Remote Sensing of Invasive Australian Acacia Species: State of the Art and Future Perspectives. pp. 474–495. https://doi.org/10.1079/9781800622197.0029

Gunderson, L.H., 2000. Ecological resilience—in theory and application. Annual review of ecology and systematics, 31(1), 425-439.

Hamdi, Z.M., Brandmeier, M., Straub, C., 2019. Forest Damage Assessment Using Deep Learning on High Resolution Remote Sensing Data. Remote Sensing 11. https://doi.org/10.3390/rs11171976

Heller, N.E., McManus Chauvin, K., Skybrook, D., Barnosky, A.D., 2023. Including stewardship in ecosystem health assessment. Nature Sustainability 6, 731–741. https://doi.org/10.1038/s41893-023-01096-7

Herrick, J.E., Shaver, P., Pyke, D.A., Pellant, M., Toledo, D., Lepak, N., 2019. A strategy for defining the reference for land health and degradation assessments. Ecological Indicators 97, 225–230. https://doi.org/10.1016/j.ecolind.2018.06.065

IPBES, 2023. Thematic Assessment Report on Invasive Alien Species and their Control of the Intergovernmental Science-Policy Platform on Biodiversity and Ecosystem Services. IPBES Secretariat, Bonn, Germany. https://doi.org/10.5281/zenodo.7430682

IPCC, 2023. Climate Change 2023: Synthesis Report. Contribution of Working Groups I, II and III to the Sixth Assessment Report of the Intergovernmental Panel on Climate Change [Core Writing Team, H. Lee and J. Romero (eds.)]. IPCC, Geneva, Switzerland, pp. 35-115, doi: 10.59327/IPCC/AR6-9789291691647.

Ivits, E., Horion, S., Fensholt, R., Cherlet, M., 2014. Drought footprint on European ecosystems between 1999 and 2010 assessed by remotely sensed vegetation phenology and productivity. Global Change Biology 20, 581–593. https://doi.org/10.1111/gcb.12393

Jorgensen, S., Costanza, R., 2005. Fu-Liu Xu., 2005. Handbook of ecological indicators for assessment of ecosystem health.

Kooistra, L., Berger, K., Brede, B., Graf, L.V., Aasen, H., Roujean, J.-L., Machwitz, M., Schlerf, M., Atzberger, C., Prikaziuk, E., Ganeva, D., Tomelleri, E., Croft, H., Reyes Muñoz, P., Garcia Millan, V., Darvishzadeh, R., Koren, G., Herrmann, I., Rozenstein, O., Belda, S., Rautiainen, M., Rune Karlsen, S., Figueira Silva, C., Cerasoli, S., Pierre, J., Tanır Kayıkçı, E., Halabuk, A., Tunc Gormus, E., Fluit, F., Cai, Z., Kycko, M., Udelhoven, T., Verrelst, J., 2023. Reviews and syntheses: Remotely sensed optical time series for monitoring vegetation productivity. Biogeosciences Discussions 2023, 1–67. https://doi.org/10.5194/bg-2023-88

Larysch, E., Stangler, D.F., Puhlmann, H., Rathgeber, C.B.K., Seifert, T., Kahle, H.-P., 2022. The 2018 hot drought pushed conifer wood formation to the limit of its plasticity: Consequences for woody biomass production and tree ring structure. Plant Biology 24, 1171–1185. https://doi.org/10.1111/plb.13399

Lausch, A., Erasmi, S., King, D.J., Magdon, P., Heurich, M., 2017. Understanding Forest Health with Remote Sensing-Part II—A Review of Approaches and Data Models. Remote Sensing 9. https://doi.org/10.3390/rs9020129

Lei, J., Li, C., Yang, W., 2023. Ecosystem health assessment and approaches to improve Sichuan Province

based on an improved vigor organization resilience model. Ecological Indicators 155, 110925. https://doi.org/10.1016/j.ecolind.2023.110925

Lepak, N., Newingham, B.A., Kachergis, E., Toledo, David, Moffitt, J., 2022. Where do qualitative assessments fit in an era of increasingly quantitative monitoring? Perspectives from Interpreting Indicators of Rangeland Health. Rangelands 44, 39–49. https://doi.org/10.1016/j.rala.2021.07.008

Li, M., Ge, C., Zong, S., Wang, G., 2022. Drought Assessment on Vegetation in the Loess Plateau Using a Phenology-Based Vegetation Condition Index. Remote Sensing 14. https://doi.org/10.3390/rs14133043

Li, Z., Xu, D., Guo, X., 2014. Remote Sensing of Ecosystem Health: Opportunities, Challenges, and Future Perspectives. Sensors 14, 21117–21139. https://doi.org/10.3390/s141121117

Ludwig, J.A., Bastin, G.N., Chewings, V.H., Eager, R.W., Liedloff, A.C., 2007. Leakiness: A new index for monitoring the health of arid and semiarid landscapes using remotely sensed vegetation cover and elevation data. Ecological Indicators 7, 442–454. https://doi.org/10.1016/j.ecolind.2006.05.001

Ludwig, J.A., Tongway, D., Hodgkinson, K.C., Freudenberger, D., Noble, J., 1996. Landscape Ecology, Function and Management: Principles from Australia's Rangelands.

Ludwig, J.A., Tongway, D.J., Hindley, N., 2023. Can simple, on-ground vegetation and soil measures reliably indicate the health of rangelands? An application in Australia's semi-arid woodlands. Rangel. J. 45, 235–245.

Michaud, J.-S., Coops, N.C., Andrew, M.E., Wulder, M.A., 2012. Characterising spatiotemporal environmental and natural variation using a dynamic habitat index throughout the province of Ontario. Ecological Indicators 18, 303–311. https://doi.org/10.1016/j.ecolind.2011.11.027

National Research Council, 1994. Rangeland Health: New Methods to Classify, Inventory, and Monitor Rangelands. The National Academies Press, Washington, DC. https://doi.org/10.17226/2212

O'Brien, A., Townsend, K., Hale, R., Sharley, D., Pettigrove, V., 2016. How is ecosystem health defined and measured? A critical review of freshwater and estuarine studies. Ecological Indicators 69, 722–729. https://doi.org/10.1016/j.ecolind.2016.05.004

Pellant, M., Shaver, P.L., Pyke, D.A., Herrick, J.E., Lepak, N., Riegel, G., Kachergis, E.J., Newingham, B.A., Toledo, D.P., Busby, E.F., 2020. Interpreting Indicators of Rangeland Health, Version 5: Bureau of Land Management Technical Reference 1734-6, p. 187, https://pubs.er.usgs.gov/publication/70215720.

Philipp, M., Wegmann, M., Kübert-Flock, C., 2021. Quantifying the Response of German Forests to Drought Events via Satellite Imagery. Remote Sensing 13. https://doi.org/10.3390/rs13091845

Puig-Gironès, R., Real, J., 2022. A comprehensive but practical methodology for selecting biological

indicators for long-term monitoring. PLOS ONE 17, e0265246. https://doi.org/10.1371/journal.pone.0265246

Rapport, D.J., Costanza, R., McMichael, A.J., 1998. Assessing ecosystem health. Trends in Ecology & Evolution 13, 397–402. https://doi.org/10.1016/S0169-5347(98)01449-9

Razenkova, E., Radeloff, V.C., Dubinin, M., Bragina, E.V., Allen, A.M., Clayton, M.K., Pidgeon, A.M., Baskin, L.M., Coops, N.C., Hobi, M.L., 2020a. Vegetation productivity summarized by the Dynamic Habitat Indices explains broad-scale patterns of moose abundance across Russia. Scientific Reports 10, 836. https://doi.org/10.1038/s41598-019-57308-8

Richardson, A.D., Keenan, T.F., Migliavacca, M., Ryu, Y., Sonnentag, O., Toomey, M., 2013. Climate change, phenology, and phenological control of vegetation feedbacks to the climate system. Agricultural and Forest Meteorology 169, 156–173. https://doi.org/10.1016/j.agrformet.2012.09.012

Saha, A., Ghosh, M., Pal, S.C., 2021. Chapter 4 - Forest health assessment using advanced geospatial technology in Buxa reserve forest, sub-Himalayan West Bengal, India, in: Kumar Shit, P., Pourghasemi, H.R., Adhikary, P.P., Bhunia, G.S., Sati, V.P. (Eds.), Forest Resources Resilience and Conflicts. Elsevier, pp. 49–61. https://doi.org/10.1016/B978-0-12-822931-6.00004-6

Schaeffer, D.J., Herricks, E.E., Kerster, H.W., 1988. Ecosystem health: I. Measuring ecosystem health. Environmental Management 12, 445–455. https://doi.org/10.1007/BF01873258

Scherzinger, F., Schädler, M., Reitz, T., Yin, R., Auge, H., Merbach, I., Roscher, C., Harpole, W.S., Blagodatskaya, E., Siebert, J., Ciobanu, M., Marder, F., Eisenhauer, N., Quaas, M., 2024. Sustainable land management enhances ecological and economic multifunctionality under ambient and future climate. Nature Communications 15, 4930. https://doi.org/10.1038/s41467-024-48830-z

Schuldt, B., Buras, A., Arend, M., Vitasse, Y., Beierkuhnlein, C., Damm, A., Gharun, M., Grams, T.E.E., Hauck, M., Hajek, P., Hartmann, H., Hiltbrunner, E., Hoch, G., Holloway-Phillips, M., Körner, C., Larysch, E., Lübbe, T., Nelson, D.B., Rammig, A., Rigling, A., Rose, L., Ruehr, N.K., Schumann, K., Weiser, F., Werner, C., Wohlgemuth, T., Zang, C.S., Kahmen, A., 2020. A first assessment of the impact of the extreme 2018 summer drought on Central European forests. Basic and Applied Ecology 45, 86–103. https://doi.org/10.1016/j.baae.2020.04.003

SDG, 2023. The Sustainable Development Goals Report 2023: Special Edition - July 2023. New York, USA: UN DESA. © UN DESA. https://unstats.un.org/sdgs/report/2023/.

SDG, 2019. The Sustainable Development Goals Report 2019, 2019th ed. United Nations.

Silveira, E.M.O., Pidgeon, A.M., Farwell, L.S., Hobi, M.L., Razenkova, E., Zuckerberg, B., Coops, N.C., Radeloff, V.C., 2023. Multi-grain habitat models that combine satellite sensors with different resolutions explain bird species richness patterns best. Remote Sensing of Environment 295,

113661. https://doi.org/10.1016/j.rse.2023.113661

Sims, N.C., Newnham, G.J., England, J.R., Guerschman, J., Cox, S.J.D., Roxburgh, S.H., Viscarra Rossel, R.A., Fritz, S., Wheeler, I., 2021. Good Practice Guidance. SDG Indicator 15.3.1, Proportion of Land That Is Degraded Over Total Land Area. Version 2.0. United Nations Convention to Combat Desertification, Bonn, Germany.

Song, Y., Zajic, C.J., Hwang, T., Hakkenberg, C.R., Zhu, K., 2021. Widespread Mismatch Between Phenology and Climate in Human-Dominated Landscapes. AGU Advances 2, e2021AV000431. https://doi.org/10.1029/2021AV000431

Swift, T.L., Hannon, S.J., 2010. Critical thresholds associated with habitat loss: a review of the concepts, evidence, and applications. Biological Reviews 85, 35–53. https://doi.org/10.1111/j.1469-185X.2009.00093.x

Tongway, D., Smith, E.M., 1989. Soil surface features as indicators of rangeland site productivity. Rangeland Journal 11, 15–20.

Vitasse, Y., Baumgarten, F., Zohner, C.M., Rutishauser, T., Pietragalla, B., Gehrig, R., Dai, J., Wang, H., Aono, Y., Sparks, T.H., 2022. The great acceleration of plant phenological shifts. Nature Climate Change 12, 300–302. https://doi.org/10.1038/s41558-022-01283-y

Witzell, J., Tapia, C.R., Aldea, J., Löf, M., 2022. Chapter 3 - Forest diversity and productivity: Implications for forest health in future climates, in: Asiegbu, F.O., Kovalchuk, A. (Eds.), Forest Microbiology. Academic Press, pp. 49–59. https://doi.org/10.1016/B978-0-323-85042-1.00009-4

Wu, J., Hobbs, R., 2002. Key issues and research priorities in landscape ecology: An idiosyncratic synthesis. Landscape Ecology 17, 355–365. https://doi.org/10.1023/A:1020561630963

Zhang, K., Ali, A., Antonarakis, A., Moghaddam, M., Saatchi, S., Tabatabaeenejad, A., Chen, R., Jaruwatanadilok, S., Cuenca, R., Crow, W.T., Moorcroft, P., 2019. The Sensitivity of North American Terrestrial Carbon Fluxes to Spatial and Temporal Variation in Soil Moisture: An Analysis Using Radar-Derived Estimates of Root-Zone Soil Moisture. Journal of Geophysical Research: Biogeosciences 124, 3208–3231. https://doi.org/10.1029/2018JG004589

Zhou, H., Min, X., Chen, J., Lu, C., Huang, Y., Zhang, Z., Liu, H., 2023. Climate warming interacts with other global change drivers to influence plant phenology: A meta-analysis of experimental studies. Ecology Letters 26, 1370–1381. https://doi.org/10.1111/ele.14259

Zou, Y., Zohner, C.M., Averill, C., Ma, H., Merder, J.,…., GFBI consortium, 2024. Positive feedbacks and alternative stable states in forest leaf types. Nature Communications 15, 4658. https://doi.org/10.1038/s41467-024-48676-5

Chapter 2

Mapping terrestrial ecosystem health in drylands: Comparison of field-based information with remotely sensed data at watershed level

Mojdeh Safaei[1]*, Hossein Bashari[2], Till Kleinebecker[1,3], Sima Fakheran[2], Reza Jafari[2], André Große-Stoltenberg[1,3]

1 Division of Landscape Ecology and Landscape Planning, Institute of Landscape Ecology and Resource Management, IFZ Research Centre for Biosystems, Land Use and Nutrition, Justus Liebig University Giessen, Heinrich-Buff Ring 26-32, 35392 Giessen, Germany

2 Department of Natural Resources, Isfahan University of Technology, Isfahan 84156-83111, Iran

3 Center for International Development and Environmental Research (ZEU), Senckenbergstraße 3, 35390 Giessen, Germany

Landscape Ecology 38, 705–724 (2023). https://doi.org/10.1007/s10980-022-01454-4

Abstracts

Context: Combining field-based assessments with remote-sensing proxies of landscape patterns provide the opportunity to monitor terrestrial ecosystem health status in support of Sustainable Development Goals (SDG).

Objectives: Linking qualitative field data with quantitative remote-sensing imagery to map terrestrial ecosystem health (SDG15.3.1"land degradation neutrality").

Methods: A field-based approach using the Interpreting Indicators of Rangeland-Health (IIRH) protocol was applied to classify terrestrial ecosystem health status as healthy, at-risk, and unhealthy at the watershed level. Quantitative complex landscape metrics derived from Landsat spaceborne data were used to explore whether similar health statuses can be retrieved on a broader scale. The assignment of terrestrial ecosystem health classes based on field and the remotely sensed metrics were tested using multivariate and cluster analysis methods.

Results: According to the IIRH assessments, soil surface loss, plant mortality, and invasive species were identified as important indicators of health. According to the quantitative landscape metrics, healthy sites had lower amounts of spectral heterogeneity, edge density, and resource leakage. We found a high agreement between health clusters based on field and remote-sensing data (NMI= 0.91) when using a combined approach of Density-Based Spatial-Clustering of Applications with Noise (DBSCAN) and k-means clustering together with non-metric multi-dimensional scaling (NMDS).

Conclusions: We provide an exemplary workflow on how to combine qualitative field data and quantitative remote-sensing data to assess SDGs indicators related to terrestrial ecosystem health. As we used a standardized method for field assessments together with publicly available satellite data, there is potential to test the generalizability and context-dependency in other arid and semi-arid rangelands.

Keywords Sustainable Development Goals (SDGs); Land Degradation Neutrality (LDN); semi-arid ecosystems; Central Zagros Mountains Iran; Self-Organizing Map (SOM); Density-Based Spatial Clustering of Applications with Noise (DBSCAN); Procrustes Analysis (PA); Moving Standard Deviation Index (MSDI); landscape ecology and planning, Normalized mutual information (NMI)

Introduction

Arid and semi-arid ecosystems cover ~45% of the globe and provide important ecosystem services related to water supply, preserving biodiversity, flood protection, food security, and the storage and capture of carbon (UN 2019; Berdugo et al. 2020). However, the ecological functioning of these drylands is currently threatened by ecosystem degradation, unsustainable land management practices, accelerated urbanization rates, and changing demographics (IPBES 2018; IPBES 2019; Berdugo et al. 2020). These factors are recognized as the most critical drivers for the depletion of natural resources (van der Zanden et al. 2016) and terrestrial ecosystem health (Lausch et al. 2016). The ecosystem degradation in drylands is negatively affecting ecosystem functions and services and indirectly threatening the well-being of at least 3.2 billion people worldwide with costs of more than 10% of the global gross product per year (IPBES 2018; UN 2019). Thus, understanding how arid and semi-arid ecosystems respond to ongoing environmental change is crucial in achieving sustainable development goals (SDGs) (https://sdgs.un.org/goals). Each SDG is assigned certain indicators that are ideally sensitive, unambiguous, quick and easy to sample, temporally consistent, and applicable to a wide range of ecosystems (Prince 2019). More specifically, fulfilling SDGs should be measurable by employing both qualitative and quantitative indicators (Hák et al. 2016). For example, SDG15 "Life on Land" addresses the urgency of stopping the degradation of natural habitats along with the integration of biodiversity and ecosystem values into development processes and local planning (UN 2019). SDG 15.3.1, in particular, addresses the need to accomplish land degradation neutrality (LDN) (Sims et al. 2021). The degree of land degradation can be quantifying sub-indicators such as i) land cover and land cover change, ii) land productivity, and iii) carbon stocks above and below ground (UN 2019; Prince 2019). Therefore, spatial indicators of terrestrial ecosystem health as monitoring and decision-making tools are important for land managers to combat land degradation. However, scaling issues can apply when translating terrestrial ecosystem information from the field level to broader levels in space and time (Wu and Hoobs 2002). Linking ecological information between finer and larger scales constitutes a fundamental challenge in landscape ecological research as well as a practical land management challenge because some ecological processes might only be noticeable at a certain level, and interactions might occur between levels. Additionally, to assess the effects of land management, it is important to select appropriate spatial units for the studied ecological processes considering the fact that there is a spatial hierarchy of ecosystems and that there are linkages between systems, for example via sediment transport, groundwater movement,

runoff, and microclimate (Bailey 1985). In a broader sense, spatially-explicit knowledge of scaling is an essential requirement to understand patterns and processes of ecosystem health status.

Terrestrial ecosystem health can be understood as the degree to which vegetation, climate, and soil integrity are capable of sustaining self-organized structures and processes (NRSC 1994). Thus, a healthy ecosystem can be regarded as resilient against disturbance (Gunderson 2000). In contrast, degradation occurs when different ecosystem states related to energy flow, nutrient cycling, and hydrological regimes are negatively affected. Particularly for semi-arid lands, protecting the structure and functionality of the ecosystems and actively restoring degraded drylands are essential to ensure soil integrity, nutrient cycling, and water retention (Pyke et al. 2002; Briske et al. 2005). As a result, a wide range of terrestrial ecosystem health indicators has been developed (van der Zanden et al. 2016; Estevez et al. 2017) with the emphasis on utilizing both qualitative and quantitative indicators (Duniwayet al. 2010). The Interpreting Indicators of Rangeland Health (IIRH) protocol (see Pyke et al. 2002) is regarded as an international standard to assess land health and degradation in drylands (Duniway et al. 2010, Herrick et al. 2019). IIRH is a qualitative assessment of ecological processes using 17 observable indicators and it is designed for assessing ecosystem health and functions in rangelands. However, assessing ecosystem functioning based on qualitative field data has distinct spatio-temporal limitations. These drawbacks can be investigated by properly integrating quantitative metrics from remotely sensed data (Toevs et al. 2011). A variety of remote sensing data has been used to assess and monitor ecosystem health across a range of scales (Li et al. 2014). However, remote sensing data has certain limitations in accurately assessing the state of ecosystem health (Li et al. 2014). Thus, methodological approaches combining and verifying remote sensing data with ground-based field sampling information on ecosystem health require further investigation.

The question is, however, how to scale up from the qualitative field-based measures to a broader scale using quantitative remote sensing data without losing crucial functional information. An integrated approach that combines field data, experimental manipulations, GIS, remote sensing, and modelling is essential for advancing a science of scale (Wu and Hobbs 2002). Integrating remote sensing with in situ data is challenging, but it has a large potential to deepen our understanding of sustainable use of ecosystems and ecosystem resilience (Cavender-Bares et al. 2022). Common remote sensing products are land-use land cover (LULC) maps. LULC change analysis allows for mapping changes of landscape structural and functional characteristics

(Matsushita et al. 2006) and supports monitoring SDG 15.3.1 (Prince 2019). LULC changes are among the main anthropogenic factors needed for health assessment in semi-arid land ecosystems (Soffianian and Madanian 2015; Baranian et al. 2017; Molaeinasab et al. 2018; Safaei et al. 2021). Beyond the commonly used Normalised Difference Vegetation Index (NDVI) (Tucker 1979), complex remote sensing-based indices that are linked to landscape functionality and degradation (Tanser and Palmer 1999; Bastin et al. 2002) as well as landscape metrics (Frank et al. 2012, Inkoom et al. 2018) have been applied to map ecosystem functioning. An example of a complex remote-sensing index is the Moving Standard Deviation Index (MSDI). It can capture the spectral diversity across images and has been applied in rangelands to map ecosystem degradation caused by overgrazing and improper management (Tanser and Palmer 1999; Jafari et al. 2008). Another example is the Leakiness Index (LI) (Bastin et al. 2002; Ludwig et al. 2007). The LI can be applied to assess sub-catchment-level resource leakage based on the hydrological regime, digital elevation models (DEM), and vegetation cover. As a result, the LI has emerged as a promising ecological index with a high potential to monitor terrestrial ecosystem health status across arid and semi-arid landscapes (Ludwig et al. 2007).

To our knowledge, the LI has been underutilized in terrestrial ecosystem health assessments. Because all remote sensing approaches present scaling issues at least to some extent (Torgerson 1958), and as data availability, transferability, and uncertainty in estimating valid health indicators remains challenging (Li et al. 2014), more research is required on using landscape metrics or complex indices for valid upscaling of field assessments based on remote sensing data to aid mapping terrestrial ecosystem health. In this study, we used multivariate methods to compare field-based, terrestrial ecosystem health indicators from the watershed scale with the landscape level by means of remote sensing. Based on a case study for central Iran, the main aim of our study is to link qualitative field data with quantitative remote sensing data to identify SDG indicators related to terrestrial ecosystem health that can be monitored from space. By quantifing LULC changes over 28 years using remote sensing metrics and assigning health classes in each sub-catchment, the proportion of land degradation related to SDG15.3.1 was estimated. We use a standardized field protocol, publicly available satellite data and mainly free and open-source software so the methodology described here can be tested and applied in other arid and semi-arid rangelands as a decision support tool to conduct land degradation zoning and to prioritize regions for restoration efforts.

Material and methods

Study area

This study was carried out in central Iran across an area of 2238 square km located between 33°04'18" and 32°36'23" E and 49°38'40" and 50°19'25" N (Figure 2-1). The region has a mean annual precipitation and temperature of 538 mm and 10.1 °C, respectively, and the climate is considered to be Mediterranean type (DeMartonne 1962). The natural landscape of this region, which is part of the vast central Zagros Mountains, traditionally provides forage for livestock, water, and other ecosystem services to the local people. Overgrazing and droughts with varying severities and magnitudes along with the dieback of oak tree forests (*Quercus persica* Jaub. & Spach), and other valuable rangeland species such as *Astragalus verus* (Olivier) and *Astragalus adscendens* (Boiss. & Hausskn. ex Boiss) have resulted in substantial changes in LULC (Safaei et al. 2021). Although many oak forests in Iran suffer from oak charcoal rot, which is caused by two opportunistic fungi, *Biscogniauxia mediterranea* and *Obolarina persica*, the incidence of this disease has not been reported in the study area so far (Ahmadi et al. 2020).

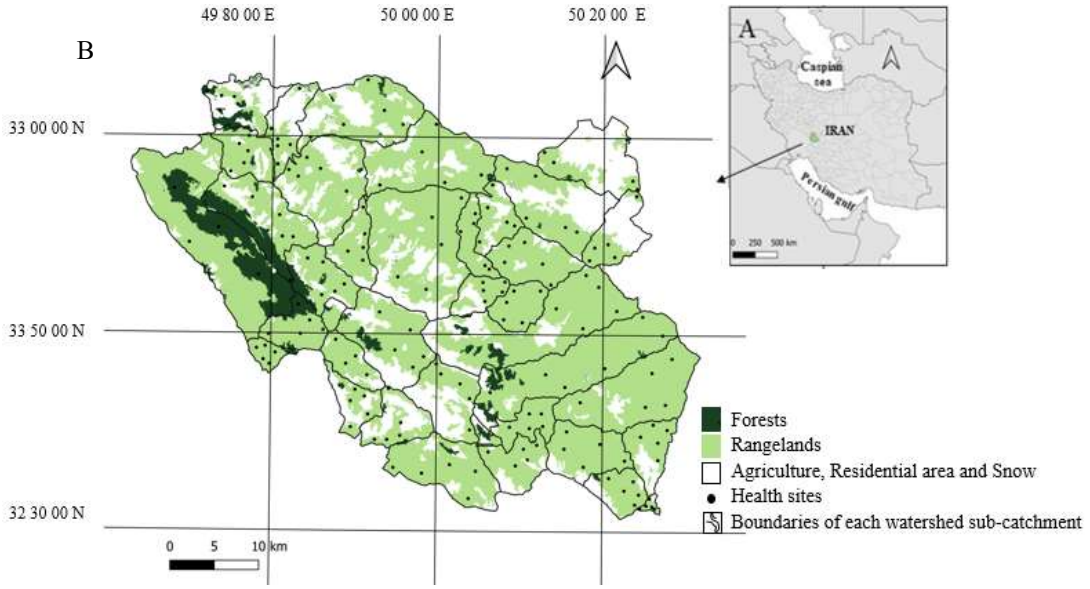

Figure 2-1 (A) Study region in western Isfahan Province, Iran. The region was divided into 40 sub-catchments. Each sub-catchment has been assigned a health class that is derived from five replications of IIRH (Interpreting Indicators of Rangeland Health) protocol assessments. (B) Sites of health assessment in the forest and rangelands were distributed using stratified random sampling. Photos show examples of landscape views with the recording of a few health indicators at some evaluation sites. (C) Rangeland in near reference state condition dominated by tall grass with shrubs, subdominant annual grasses, and rarely connected patches of bare ground. (D) Shrub community (Astragalus versus) with dead and dying branches and leaves (shown in red circles). (E) Native shrub with good vigor and reproductive capability (red circle). (F) Rills in a steep slope are the result of geologically sensitive formation. (G) Degraded rangeland site with large patches of bare ground. (H) Open forest dominated by oak trees.

We developed an exemplary workflow that links qualitative field data (Fig. 2-2, Step 1) with quantitative remote sensing data (Fig. 2-2, Step 2) for identifying and assessing SDG indicators related to terrestrial ecosystem health in semi-arid lands using different multivariate analyses (Fig. 2-2, Step 3). Finally, we tested whether this combination of analyses can be used to assess the state of terrestrial ecosystem health in the past (Fig. 2-2, Step 4). All steps of our workflow are illustrated in Figure 2-2.

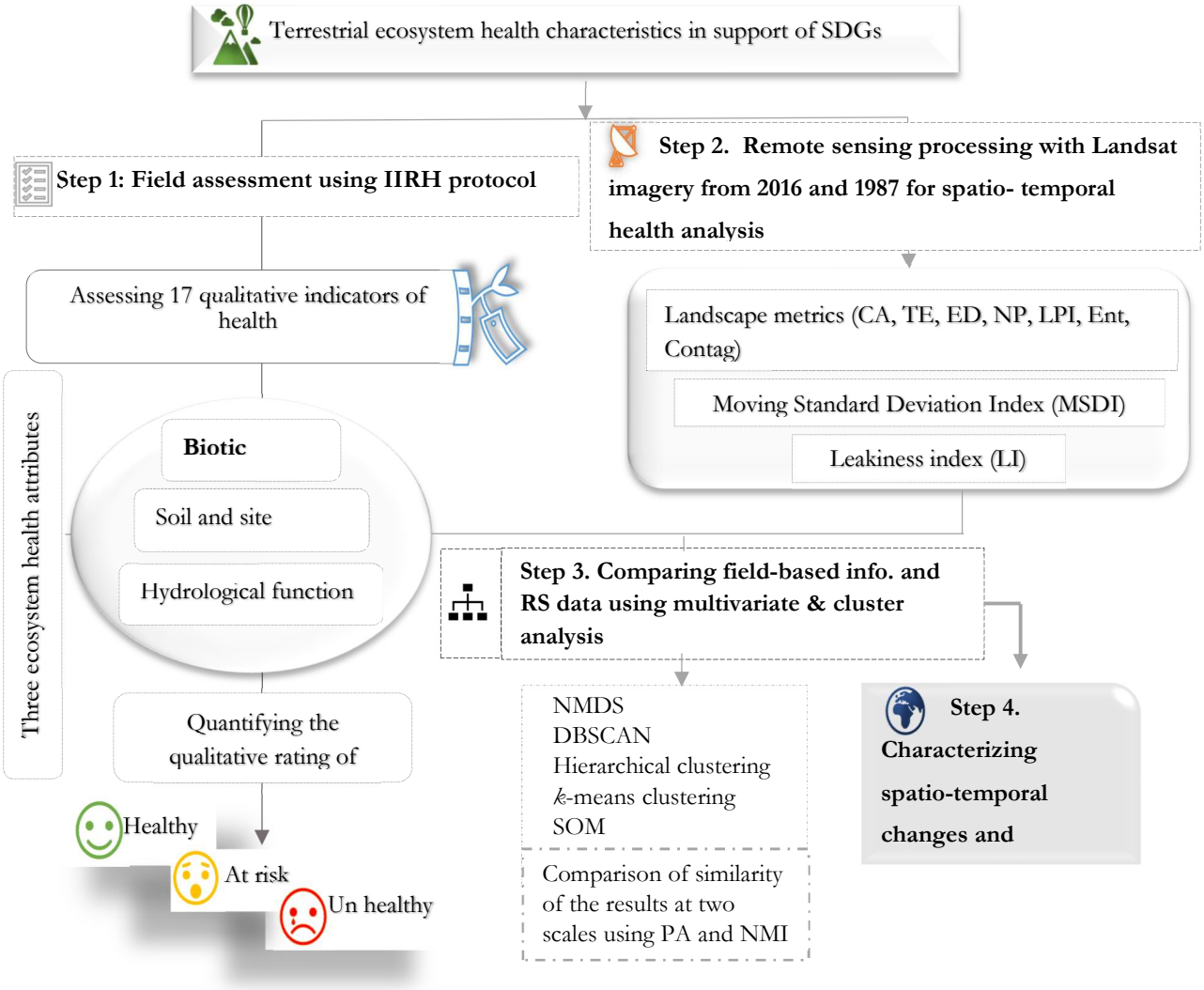

Figure 2-2 Graphical illustration of the workflow linking field and remote sensing data to aid our understanding of the health status of arid and semi-arid ecosystems. CA: Total (Class) Area, TE: Total Edge, ED: Edge Density, NP: Number of Patches, LPI: Largest Patch Index, Ent: Entropy, Cont: Contagion, LI: Leakiness index, MSDI: moving standard deviation index, NMDS: Non-Metric Multi-Dimensional Scaling, DBSCAN: , SOM: Self Organizing Map, PA: Procrustes analysis, NMI: Normalized Mutual Information.

Field data collection through IIRH protocol and analysis of terrestrial ecosystem health

A field survey was conducted at the sub-catchment scale to determine the most important indicators of health status according to the IIRH assessment given by Pyke et al. (2002). We considered sub-catchments as our sampling unit because their hydraulic gradient is crucial for the calculation of functionality (Ludwig et al. 2007). Of the 40 sub-catchments, rangelands were dominating in 35, and forests were dominating in 5 sub-catchments. Since the study area was large

(2238 km^2), careful selection of health sites at the sub-catchment scale that reflected the overall condition of each sub-catchment was important. To avoid misevaluations, the scaling of health data from sampling point to sub-catchment was done using stratified random strategy to cover the representative site conditions in each sub-catchment and the 17 Interpreting Indicators of Rangeland Health (IIRH) were assessed (Table 2-1). Based on the IIRH protocol (Pyke et al. 2002; Pellant et al. 2020), two sites, one rangeland, and one forest, were selected as ecological reference sites. An ecological reference site is a well-managed landscape unit in which ecological processes (i.e., energy flow, nutrient cycling, and hydrological condition) are working within the natural range of variability, and the vegetation has adequate resilience and/or resistance to typical disturbances (Pyke et al. 2002). The 17 ecological indicators were utilized to identify three ecosystem attributes that reflect ecosystem functionality including (i) soil and site stability, (ii) hydrological function, and (iii) biotic integrity (Table 2-1) (Pyke et al. 2002; Pellant et al. 2020). They were manually recorded on evaluation sheets in five replicates at different locations in each sub-catchment. The five replicates were representative for the degree of health in each sub-catchment. The deviation of the 17 measured indicators in each sub-catchment from the reference area conditions was rated in five quality categories (extreme to total, moderate to extreme, moderate, slight to moderate, and none to slight) (see Pellant et al. (2020) for a detailed IIRH description). As it is shown in Table 2-1, the deviation of nine indicators were used to rate soil and site stability, 10 indicators to rate hydrological function, and nine indicators to rate biotic integrity based on a preponderance of evidence approach using a two way table in the R package "base" (R Core Team 2021). Finally, a health class including healthy, at risk and unhealthy status was assigned to sub-catchment using the preponderance of evidence of three health attributes ((i) soil and site stability, (ii) hydrological function, and (iii) biotic integrity). To prevent or reduce observer bias, fieldwork was performed by two fixed observers who worked together on the same site with a sound ecological knowledge of the study area in two months during June and July 2015. Information related to the 40 sub-catchments, as well as the assigned health status for the three ecosystem attributes, are given in the Supplementary file 1 (Table S.1).

Table 2-1 A brief description of the 17 Interpreting Indicators of Rangeland Health (IIRH) indicators and their relation to the three attributes of terrestrial ecosystem health. The indicators are sorted under the attributes to which they relate. Boxes that traverse multiple attributes contain indicators that relate to more than one attribute (descriptions and structure of the table were adopted from Pyke et al. 2002 and Pellant et al. 2020)

<table>
<tr><th>Soil and site stability</th><th>Hydrological function</th><th>Biotic integrity</th></tr>
<tr><td colspan="2">1. Rills: small erosional rivulets that are generally linear</td><td>12. Functional/structural groups: a suite of species that are grouped together because of similar morphology, photosynthesis pathways, nitrogen-fixing ability, life cycle, etc.</td></tr>
<tr><td colspan="2">2. Water flow patterns: path that water takes as it moves across the soil surface</td><td>13. Plant mortality/decadence: the proportion of dead/decadent plants</td></tr>
<tr><td colspan="2">3. Pedestals/Terrecettes: the movement of soil by wind/water</td><td rowspan="2">15. Annual production: total above-ground biomass as a measure of the vegetation available to harvest the sun's energy</td></tr>
<tr><td colspan="2">4. Bare ground: exposed mineral or organic soil not covered by vegetation, gravel /rock, litter or biological crust</td></tr>
<tr><td colspan="2">5. Gullies: channel that has been cut into the soil by moving water</td><td>16. Invasive plants: invasive exoticand noxious weed</td></tr>
<tr><td>6. Wind-scoured, blowout, and/or depositional areas: finer soil particles have been redistributed from depositional areas interspaces and deposited near an obstruction</td><td colspan="2">14. Litter amount: dead organic material in contact with the soil surfacethat influences several ecological processes</td></tr>
<tr><td>7. Litter movement: redistribution of litter by water or wind</td><td>10. Plant community composition & distribution relative to infiltration reflects the contributions of functional/structural groups and their associated species in modifying infiltration.</td><td>17.The reproductive capability of perennial plants: measure of potential for seed or tiller production, not presence of seedlings/new clonal plants</td></tr>
<tr><td colspan="3">8. Soil surface resistance to erosion: reduced soil surface stability usually reflects lower soil biotic integrity because of organic matter and biological decomposition processes</td></tr>
<tr><td colspan="3">9. Soil surface loss or degradation: loss or degradation of soil surface (organic matter) affects site potential</td></tr>
<tr><td colspan="3">11. Compaction layer: near-surface layer of dense soil caused by repeated impact or disturbance of the soil surface</td></tr>
</table>

Remotely sensed landscape metrics across terrestrial ecosystem health classes

Two LULC maps with a pixel size of 30 m including forest, rangelands in good, moderate and poor conditions, agriculture, residential area, snow and ice classes were produced based on 2016 Landsat OLI imagery with 6 bands (bands 2 to 7) with an overall accuracy of 94% (see Safaei et al. 2021) and 1987 Landsat TM imagery with 4 bands (bands 1 to 4) (Soffianian and Madanian 2015) with an overall accuracy of 84%, respectively applying the supervised Maximum Likelihood Classification (MLC). Both images were downloaded from the United States Geological Society (USGS) Earth Resources Observation and Science (EROS) Center (https://earthexplorer.usgs.gov/). We consider two-time steps to see whether the estimation of terrestrial ecosystem health in the past is possible. The validity of the 2016 LULC map was assessed using 401 field points assessed in 2016 (Safaei et al. 2021). The validity of the 1987 LULC map was tested using 86 reference points from aerial photographs of 1985 (National Cartographic Center; ncc.gov.ir).

Five landscape metrics including the (i) number of patches, (ii) total edge, (iii) edge density, (iv) largest patch area, and (v) total class area (see Table 2-2) were quantified at landscape level in each sub-catchment using Fragstats 4.2 (McGarigal et al. 2012). (vi) Entropy and (vii) contagion metrics, two indicators of fragmentation, were measured using the Guidos Toolbox 3 (Vogt and Riitters 2017). The (viii) MSDI, a proxy for landscape degradation patterns (Tanser and Palmer 1999), was computed using a 3×3 window filter moving across the Landsat OLI 2016 red band. The (ix) LI, a functionality indicator, was calculated based on a DEM with a spatial resolution of 30m using 1:25000 topographic maps (National Cartographic Center; ncc.gov.ir) (Safaei et al. 2021) (Table 2-2), and the NDVI (Tucker 1979) from Landsat OLI imagery for 2016. See Ludwig et al. (2007) for details about the LI. The ecological concept of the selected metrics is more similar to the assessed terrestrial indicators. All metrics were calculated at landscape level in each sub-catchment.

Table 2-2 Landscape metrics and indices used in this research (descriptions for landscape metrics adopted from McGarigal et al. 2012)

Metrics	Equation	Description	Reason and relevance
(ED) Edge Density (Meters per Hectare)	$ED = \frac{\sum_{k=1}^{m} e_{ik}}{A} \times 10000$	eik = total length (m) of an edge in landscape involving patch type (class) i; includes landscape boundary and background segments involving patch type i. A = total landscape area (m^2).	all edges in the landscape in relation to the landscape area.

Metrics	Equation	Description	Reason and relevance
(LPI) Largest Patch Index (Percent)	$LPI = \frac{max(a_{ij}) \times 100}{A}$	aij = area (m2) of patch ij A = total landscape area (m^2)	the percentage of the landscape covered by the largest patch in the landscape
(TE) Total Edge (Meters)	$TE = \sum_{k=1}^{m} e_{ik}$	Total length (m) of an edge in landscape	it measures the configuration of the landscape because a highly fragmented landscape will have many edges.
(CA) Total (Class) Area (Hectares)	$CA = \sum_{j=1}^{n} a_{ij} \left(\frac{1}{10000}\right)$	aij = Area (m^2) of patch ij.	the core area is the area unaffected by the edges of the patch
(NP)Number of Patches	$NP = n_i$	ni = Number of patches in the landscape of patch type (class) i.	get the number of patches of the corresponding patch type
Contagion (Percent)	$\left[1 + \frac{\sum_{i=1}^{m}\sum_{k=1}^{m}\left[(P_i)\left(\frac{g_{ik}}{\sum_{k=1}^{m} g_{ik}}\right) \times \left[\ln(\right.\right.\right.}{2\ln(m)}$	Pi =Proportion of the landscape by patch type (class) i. gik =Number of ies (joins) between pixels of patch types i and k based on the double-count method. nber of patch types (classes) present in the e, including the landscape border if present.	contagion refers to the tendency of patch types to be spatially aggregated; that is, to occur in large, aggregated or "contagious" distributions.
Entropy (Percent)	$S=\sum_i P_i log P_i$	Pi = Disorder of pixels in a raster map	based on the Shannon's theory (Shannon 1948) and considers disorder of pixels in a raster map.
(LI) Leakiness index (Ludwig et al., 2007)	$LI = 1 - \left[\frac{L_{max} - L_{calc}}{L_{max} - L_{min}}\right]^k$ $Lmax = \frac{L_{calc}}{\left[1 - \sqrt[3]{1 - LI}\right]}$	Lmax = maximum leakiness, Lmin = minimum leakiness, Lcalc =progressively accumulates resources from pixel to pixel	can assess resource leakage based on the hydrologic regime, Digital Elevation Model (DEM), and vegetation cover
(MSDI)The moving standard deviation index (Tanser and Palmer 1999)	$\text{MSDI} = \sqrt{\sum_{1}^{N}(\frac{DN_i - \text{DN}'}{N})^2}$	N= the pixel number of the filter (N= 9), DN_i = the digital number of pixel (i) in pixels, DN' = the average digital number value of pixels	capture the spectral diversity across images and has been applied in rangelands to map ecosystem degradation caused by overgrazing and improper management

Analysis of variance (ANOVA) followed by a post hoc Tukey test for unequal sample sizes (α=0.05) was performed to assess whether landscape metrics showed significant differences among health classes. Only the landscape metric ED met the assumptions for ANOVA. For all other

remotely sensed indices, a Kruskal-Wallis test followed by a Dunn's test with a bh p-value adjustment (α=0.05) for the multiple comparisons was applied. Autocorrelations among the remotely sensed data were checked using the R packages "tseries" (R Core Team 2021; Trapletti and Hornik 2020).

Linking field-based indicators with remote sensing metrics

To test if the sites can be grouped into the three health classes "healthy", "at risk" and "unhealthy" based on the NMDS, an unsupervised cluster analysis was conducted on the remotely sensed data and a supervised cluster analysis was conducted on the field data. (Tables 1 and 2). Non-Metric Multi-Dimensional Scaling (NMDS) (Kruskal 1964) with different distance measures including Euclidean, Manhattan, Mahalanobis, and Bray-Curtis were employed. The returning stress values for the different dissimilarity indices were used to identify the best dimensional ordination fit of field and remotely sensed data. Minimum stress solution was sought with Procrustean rotation (Gower 1971). The two-dimensional NMDS with 20 runs was performed in the "vegan" R package (Dixon 2003; R Core Team 2021). Terrestrial ecosystem health field indicators and remotely sensed metrics that were significantly correlated with the ordination axes were plotted in the two-dimensional ordination space.

Since it is challenging to identify the best algorithm a priori (e.g. Kozakura et al. 2017), different clustering algorithms were employed. Common types of clustering methods were tested including DBSCAN (Hahsler et al. 2019), *k*-means clustering (Johnson 1967), hierarchical clustering (Johnson 1967), and Self-Organizing Map (SOM) (Vialaneix et al. 2020). The clustering algorithm DBSCAN can identify clusters of any shape containing outliers and noise in the dataset. The goal of DBSCAN is to measure the number of objects close to a given point and then to identify dense regions (Ester et al. 1996). *k*-means clustering aims to partition "n" observations into "k" clusters based on the nearest mean (Kriegel et al. 2016), whereas hierarchical clustering is one of the most popular clustering techniques in machine learning. It places similar observations close to each other with no need to pre-specify the number of clusters as in *k*-means clustering (Johnson 1967). Finally, the Self Organizing Map (SOM) algorithm which is part of Artificial Neural Networks (ANNs) techniques, includes dimensionality reduction and data clustering. The SOM can be used for providing the geographic topology of the input data (Kohonen 2001; van der Zanden et al. 2016). We conducted the DBSCAN, the combination of DBSCAN+*k*-means clustering, hierarchical clustering, and SOM clustering analysis for both field qualitative indicators

and remotely sensed quantitative metrics using the R packages "dbscan"(R Core Team 2021; Hahsler et al. 2019), "factoextra" (R Core Team 2021; Kassambara and Mundt 2020), "SOMbrero", and "kohonen" (Kohonen 2001; R Core Team 2021; Vialaneix et al. 2020).

We compared the patterns of terrestrial ecosystem health using different multivariate and cluster analyses considering the challenges of monitoring landscapes using remote sensing data to quantify and identify the spatio-temporal characteristics at watershed scale (Wu and Qi 2000). The combination of DBSCAN+*k*-means clustering was applied to check if the performance of clustering can be increased when combining methods.

Comparison of qualitative field indicators and quantitative remote sensing indices

The degree to which ecological processes and spatial patterns of both field and remote sensing level are related can be identified by testing if the assignment of terrestrial ecosystem health classes based on field indicators matched the characterization based on remotely sensed indicators. The multivariate spaces of both levels were compared using Procrustes analysis (PA) (Gower 1971). In PA, the ordination solutions are rotated to minimize the sum of squared residuals and maximize similarity (Gower 1971). Procrustes analysis has been successfully applied to test the relation between multivariate data sets in ecology including both field and remote sensing data (Feilhauer et al. 2010; Magiera et al. 2013; Große-Stoltenberg et al. 2018). The clustering was compared using the Normalized Mutual Information measure (NMI) (Chiquet et al. 2020). The Normalized Mutual Information measure shows the consistency between two clustering results (Formula. 1).

$$I(U,V) = \sum_{p=1}^{P}\sum_{q=1}^{Q} \frac{|U_p \cap V_p|}{N} log \frac{N|U_p \cap V_p|}{|U_p| \times |V_p|}$$

Where $|U_p| and |V_p|$ represent the cardinality of the p-th and q-th clusters in U and V clusters on a set of data, respectively (Kozakura et al. 2017). A zero NMI value corresponds to no mutual information (e.g. no correlation between the clustering results of the field and remote sensing based NMDS ordinations), while a value of one indicates a perfect correlation.

Thus, both NMI and PA help to evaluate the similarity of datasets generated by multivariate analysis and cluster analysis, respectively (Kozakura et al. 2017). The PA was performed using the

function "protest" in the R package "vegan" (R Core Team 2021; Dixon 2003) and NMI was calculated in "NMI" and "aricode" packages of R (R Core Team 2021; Chiquetet al. 2020).

Transferability of quantitative remote sensing indices to the past time

In addition, we tested whether this combination of indicators and clustering methods can be used to assess the state of terrestrial ecosystem health in the past. Therefore, after validating the remotely sensed indicators and clustering methods against field data for 2016 (see previous paragraph), metrics and clusters were computed for satellite imagery in 1987 to investigate health status in the past. The reason for choosing 1987 was because shortly thereafter extensive LULC conversions (e.g. converting rangelands to dry farmlands) caused a sharp decline in the size of rangelands and heavy grazing occurred that considerably affected the rangeland health (Baranian et al. 2017; Safaei et al. 2021), so distinct changes could be expected. While satellite data were available for 1987, there was no IIRH assessment available. Thus, after testing the validity of our approach for 2016, the RS indicators were applied to the 1987 data to derive a health status map. The plausibility of the 1987 map and the change of ecosystem health from 1987 to 2016 was assessed using published literature. Based on the available ecological report and a publication from that time (Bassiri et al. 1989; Bassiri and Iravani 2009) ecological information about the health status of the sub-catchments was obtained. The visual interpretation of the LULC map obtained from Landsat 7 in 1987 (see Supplementary file 3; Fig S.1) and 86 points drived from the aerial photographs in 1981 (National Cartographic Center; ncc.gov.ir) helped to compare good, moderate and poor rangelands as well as dense, semi-sparse and sparse forest (see Safaei et al. 2021) to health classes derived from NMDS. Expert assessments from the combination of these three data sets have been used to validate health classes in the past. Finally, to determine the efficacy of integrating field and remotely sensed data for estimating SDGs 15.3.1, we quantified site-based data to assess the three health classes including healthy, at risk and unhealthy derived from geospatial information. The measurement unit for indicator 15.3.1 is the spatial extent (km^2) calculated as the proportion of land that is degraded relative to the total land area (percentage) (Table 2-3) (Prince 2019; UN 2019; Sims et al. 2021).

Table 2-3. Calculating the SDG15.3.1 by comparing the status of the three helth classes "healthy", "at risk", and "unhealthy" in 1987 and 2016.

SDG15.3.1 Equation	**Explanation (Sims et al. 2021)**
A (Degraded)= A (Stable) + A (Negative) - A (Positive)	A (Stable or unchanging): Areas of land that have persisted state since the baseline period A (Negative or declining): Areas that have degraded since the baseline period A (Positive or improving): Areas that have improved from a degraded state to a non-degraded state wince the baseline period.
$P = \frac{\text{A (Degraded)}}{\text{A (Total)}}$	the proportion of land that is degraded (%)

Results

Qualitative field assessment following the IIRH protocol: indicators and health class assignment

According to the IIRH protocol, nine, 11, and 20 sites were classified as healthy, at-risk, and unhealthy at the watershed level, respectively (Figure 2-3). Among the 17 indicators, the presence of structural and functional groups, vegetation composition, productivity, and litter volume was capable of discriminating healthy sites from unhealthy ones. The most important indicators in unhealthy sites were compaction layer, plant mortality, rills and water flow pattern, invasive species, and surface soil condition. The region has no gully formation, making this factor ineffective in site discrimination and health evaluation.

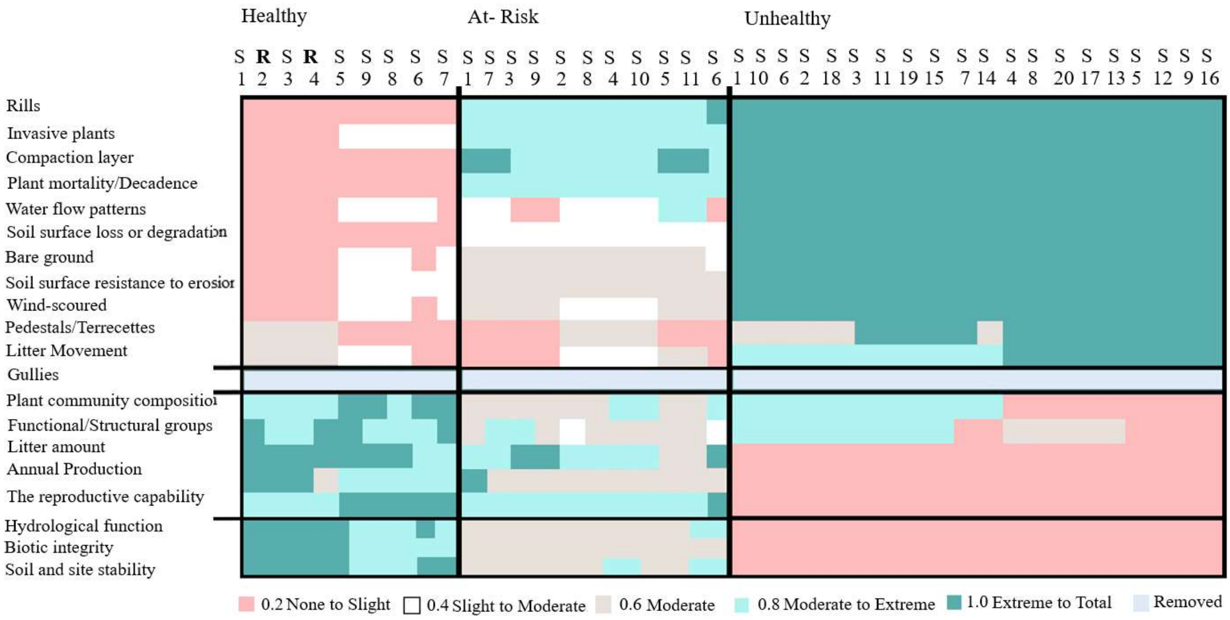

Figure 2-3 The two-way table provides an overlay of 17 health indicators (rows) in sites with different health status (columns) of evaluation sites (S) and reference sites (R). The color gradient from pink (0) to green (1) indicates the increasing importance of the index in each site. The horizontal black lines differentiate the three functional attributes from the 17 indicators Due to the lack of gullies in the study area, no scores were included (grey colored line in the middle of the figure). The vertical black lines seperate the three health classes.

Remotely sensed landscape metrics across terrestrial ecosystem health classes

Healthy sites had the largest patch sizes (LPI) (Fig. 2-4A) as well as the lowest edge length (Fig. 2-4C, and 2-4G) and lowest number of patches (NP) (Fig.2-4B) compared to at-risk and unhealthy sites ($p < 0.05$), while the total class area (CA), (Fig. 2-4D) was similar across health classes. The entropy metric showed that the degree of disorder in each site was low in healthy and high in at risk and unhealthy sites (Fig. 2-4E), indicating that these were more fragmented than healthy ones. Accordingly, contagion showed an opposite trend relative to entropy, highlighting that regions with a low spatial contagion, i.e. unhealthy sites, were severely fragmented (Fig. 2-4F).

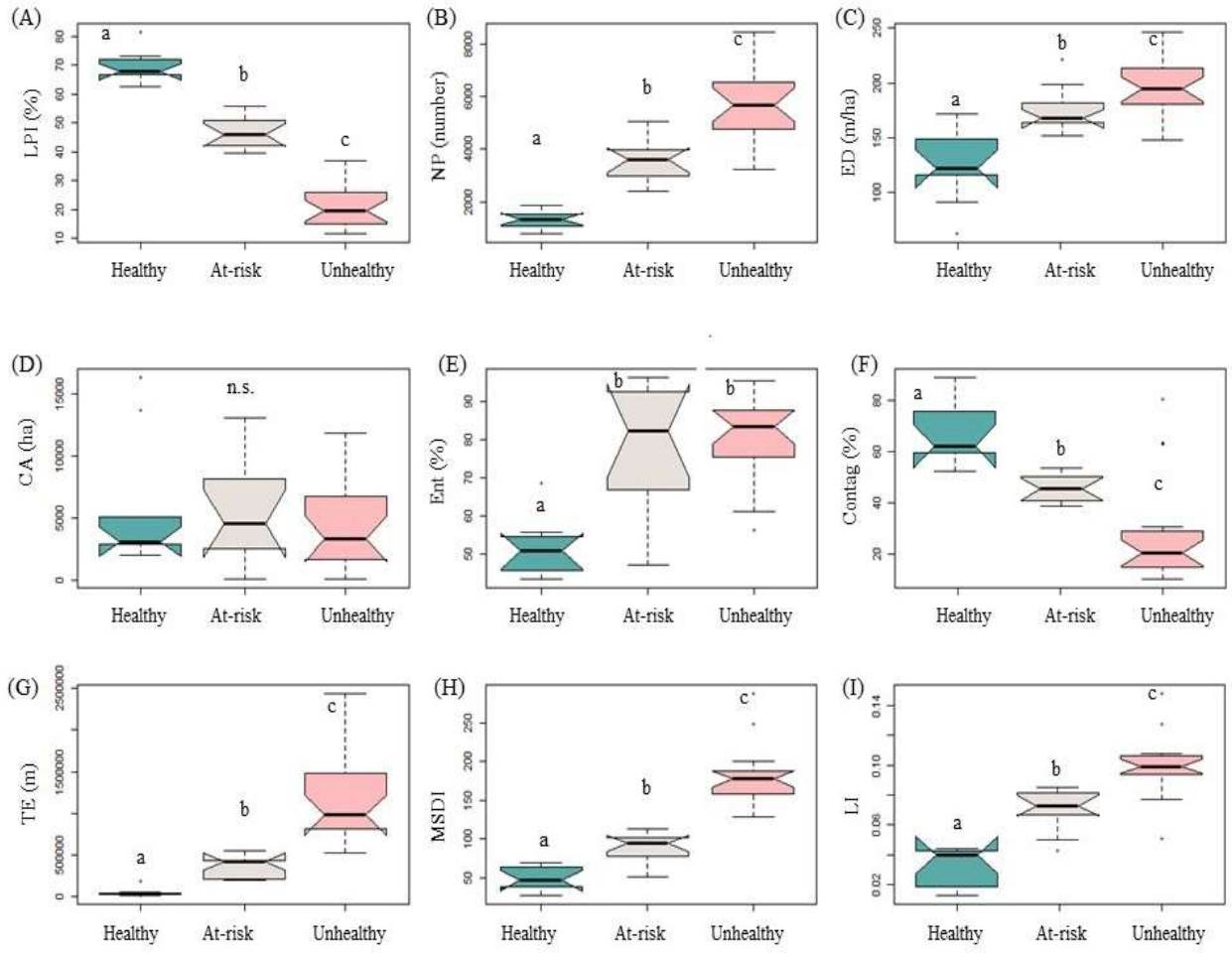

Figure 2-4. Boxplots of landscape metrics across different health classes. A: LPI (largest patch index); B: NP (number of patches); C: ED (edge density); D: CA (total class area); E: Ent (Entropy); F: Contag (Contagion); G: TE (Total edge); H: MSDI (moving standard deviation index); I: LI (leakiness index). Lowercase letters indicate significant differences across health classes after Tukey test (P< 0.05). n.s. in Fig. 2-4D indicates no significant differences across classes. Both the MSDI index and the LI were significantly lower for healthy sites than for unhealthy ones (Fig. 2-4H, I) indicating lower degradation with lower water and soil resource loss at healthy sites.

Comparison of qualitative field indicators and quantitative remote sensing indices

The multivariate analysis (NMDS) coupled with clustering (DBSCAN, *k*-means clustering, hierarchical clustering, and SOM) performed well (Table 2-4) to categorize both field qualitative and remotely sensed quantitative data (Fig. 2-5). Among the different distance measures (Euclidean, Manhattan, Mahalanobis, and Bray-Curtis), Manhattan performed best with the lowest stress value (0.022) for the qualitative field data, while Euclidean performed best with the lowest stress value (0.067) for remotely sensed data (Supplementary file 5; Fig S.3 and S.4).

Based on the NMDS for field health indicators (Fig. 2-5A), higher values for soil surface loss and degradation, plant mortality and decadence, compaction layer, soil surface resistance to erosion, rills, and water flow patterns were related to unhealthy sites. In contrast, higher values for structural and functional groups, annual production, the reproductive capability of perennial plants, and plant community composition were related with healthy sites. The NMDS revealed that larger patch values were associated with healthy sites (Fig. 2-5B). High edge density, number of patches, entropy, MSDI, and leakiness values were related to unhealthy sites. These data confirmed the results obtained from the univariate analyses of single measures (Fig. 2-4).

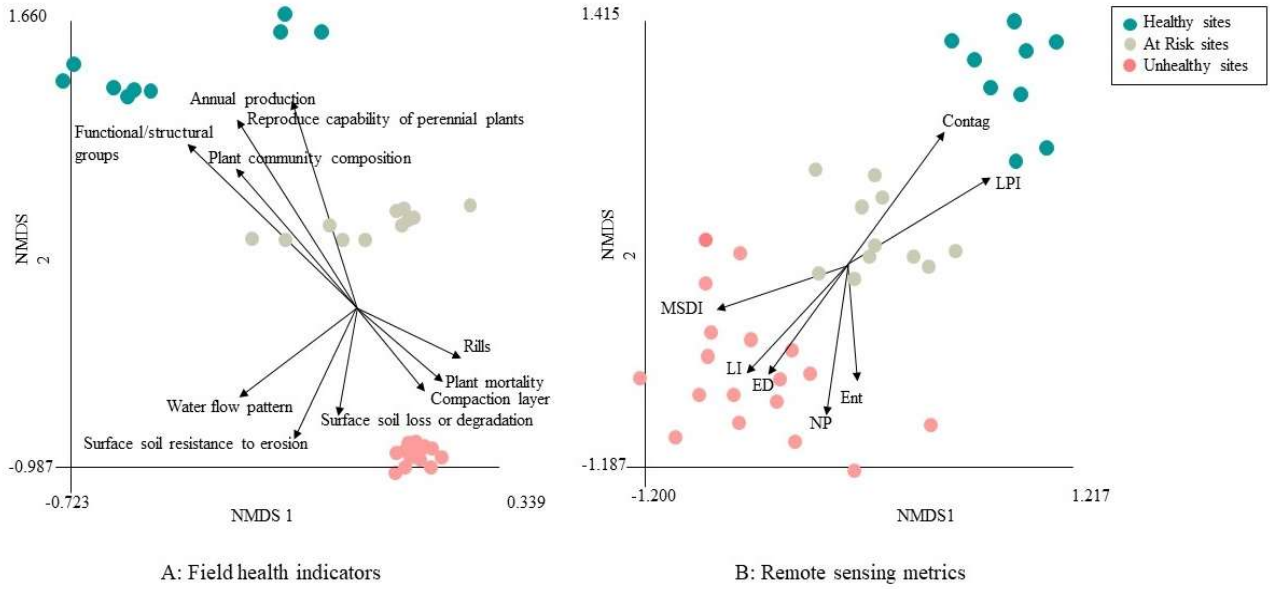

Figure 2-5 Two-dimensional ordination NMDS of 40 sample sites. (A) 10 vectors of health indicators significantly correlated (p= 0.001, α= 0.05) with the 2-D ordination axes (stress 0.14 Manhattan Metric); (B) Seven vectors of remotely sensed metrics significantly correlated (p= 0.001, α= 0.05) with the 2-D ordination axes, (stress: 0.07 Bray-Curtis Metric). Each color includes groups of sites assigned to the three health classes. MSDI: moving standard deviation index, LI: leakiness index, Ent: entropy, Contag: contagion, LPI: largest patch index, NP: number of patches, ED: edge density.

We used PA to determine if similar NMDS relationships of health indicator data and sites can be retrieved from both field-based indicators and remotely sensed metrics to validate the metrics derived from remote sensing analyses. There was a high Procrustes correlation derived from the symmetric Procrustes residual (0.88) between terrestrial ecosystem health groups based on field indicators (Fig. 2-5A) and derived from remotely sensed metrics (Fig. 2-5B) (Supplementary file 4; Figure S.2).

The NMI differed between clustering approaches. The minimum was 0.54 (DBSCAN and k-means clustering, raw data) while the combination of DBSCAN and k-means clustering on two-dimensional NMDS data performed best (NMI = 0.91). The NMI value for the SOM on NMDS data showed the second-best performance (NMI= 0.84) (see Table 2-4, Supplementary file 5 and 6; Fig. S. 3, and S. 4). Collectively, NMI differed between methods and data types, although using a combination of clustering methods based on ordinated data performed best.

Table 2-4 Normalized mutual information value for each clustering method. A zero NMI value corresponds to no mutual information, whereas one indicates a perfect correlation. Each NMI value is calculated based

on the correlation of clusters between remotely sensed quantitative data and field qualitative assessment data.

Method*	Types of data	NMI
DBSCAN	Raw data	0.57
	Ordination score	0.57
DBSCAN+ *k*-means clustering	Raw data	0.54
	Ordination score	0.91
SOMbrero	Raw data	0.75
	Ordination score	0.84
Hierarchal clustering*	Raw data	0.67
	Ordination score	0.64

*Graphical results of different methods are shown in Supplementary file 5; Fig. S3. Hierarchical clustering is presented by heatmaps based on ward linkage and Manhattan distance. Since DBSCAN+ *k*-means clustering and SOM performed best, they were used to produce health status maps for 2016 (Fig. 2-6A, B, C, Table 2-3).

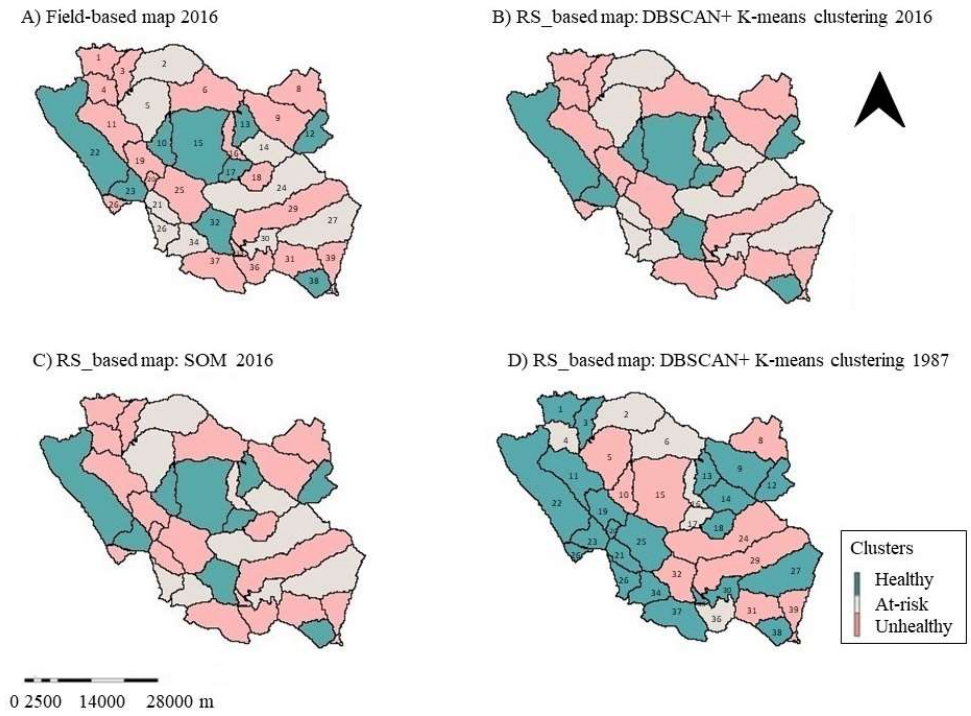

Figure 2-6 Terrestrial ecosystem health status maps across space and time and comparing methods. (A) Field assessment in 2016, (B) DBSCAN+ k-means clustering on NMDS scores of remote sensing (RS) data in 2016, (C) Self-organizing map on NMDS scores of RS data in 2016, and (D) DBSCAN+ k-means clustering on NMDS scores of RS data in 1987.

Compared to the field-based map, both DBSCAN + *k*-means clustering and SOM overestimated the health status for one site ("At-risk" instead of "Unhealthy", site 16), SOM additionally underestimated the status for a further site ("Unhealthy" instead of "At-risk", site 21). Generally, both field and remote-based maps of terrestrial ecosystem health were consistent (Fig. 2-6A, B, C; Table 2-3), and inconsistencies of the RS-based maps accounted for 2.5% (DBScan and *k*-means clustering) and 5% (SOM), respectively. Finally, a LULC map with an overall accuracy of 84% (See Supplementary file 3; Fig. S1) was created for 1987, and a terrestrial ecosystem health status map for 1987 was produced following the classification approach for 2016 (Fig. 2-6D and see Supplementary file 5 and 6; Fig. S3, 4). Compared to 2016, there were 23 healthy sites, 11 unhealthy sites, and six at risk. There was a clear degradation of ecosystem health status in the Western part of the study area (Fig. 2-6D). The interpretation of the aerial images and the LLC maps (Supplementary file 3; Fig. S1), indicated that degradation occurred due to the conversion of forest in 1987 to poor and moderate rangelands in 2016 (Supplementary file 3; Fig. S1A, C, D). The increasing number of patches and total edge, as well as the decreasing largest patch index, has resulted in a higher level of fragmentation.

Discussion

The overall results of this study illustrate that standardized field assessments of terrestrial ecosystem health in drylands following the established IIRH protocol can be accurately reproduced with satellite data by combining multivariate methods together with unsupervised cluster analysis in this region. So we present an exemplary workflow on how to integrate a standardized in situ data set with publicly available satellite imagery to monitor land degradation (SDG indicator 15.3.1) . The best approach, DBSCAN+ *k*-means clustering, reached a very high correlation (PA=0.88 and NMI=0.91) between field and spaceborne data. Only the status of one out of 40 sites, which accounted for 0.93% of the total area, was misclassified by one health class ("at-risk" instead of "unhealthy). Therefore, if field indicators of ecosystem health are linked with the appropriate RS metrics, there is potential for combining the data at different scales and extents, which could be tested in further studies in other rangelands to explore the transferability of our approach. Indeed, integrating in situ ecological data with remote sensing is both promising and challenging (Cavender-Bares et al. 2022). there is an urgent need for identifying indicators that anticipate change in terrestrial ecosystem health caused by human impacts to allow for timely management at the landscape scale (Briske et al. 2005; Estevez et al. 2017), because human, social and economic

development relies on the health of natural habitats (UN 2019). Due to the complexity and the variety of available indicators, assessing terrestrial ecosystem health status across field and RS scale is a challenging task, but integrating expert knowledge and ecological data with remote sensing data has a large potential (Herrick et al. 2019), and in this study we present an exemplary methodological approach on how to deal with this challenge. In the following discussion, we describe the efficacy of combining field-based and remote sensing methods in determining health indices regarding structural and functional changes across health status.

Field assessment and IIRH protocol: health classes and indicators influencing terrestrial ecosystem health

Even though the IIRH protocol is a well-established method, adequate information of the studied ecological units is essential to interpret its indicators (Pyke et al. 2002). The classification of our study sites into three groups (healthy, at-risk, and unhealthy) based on the indicators defined in the IIRH protocol directly provide useful information for land managers and decision-makers. Here, both the unhealthy and the at-risk sites were characterized by a clear deviation of indicators from the optimal state for all three attributes (soil and site stability, hydrological function, and biotic integrity). On the other hand, the healthy sites were characterized by good status of indicators related mainly to biotic integrity. The differences in the ratings of IIRH attributes were likely due to a combination of disturbances associated with the proximity to nomadic and rural areas, land-use/cover conversion to abandoned rainfed lands, and decreasing coverage of under-canopy perennial plants (Duniway et al. 2010; Molaeinasab et al. 2018). Such disturbances lead to soil degradation and erosion, decreasing the frequency of productive, perennial, and palatable grass species like *Bromus tomentellus* and *Agropyron tricophorum*, and increasing the frequency of annual, toxic, and invasive plants in the study area (Safaei et al. 2021). This combination of disturbances affects various ecosystem functions and explains the combination of indicators in all three attributes, which are relevant for the unhealthy ecosystem status. Thus, integrating "moment-in-time assessments" such as the IIRH (Pyke et al. 2002) with scientific knowledge of ecosystem processes of a region can help to stimulate the understanding of terrestrial ecosystem health status. Since healthy ecosystems significantly reduce the destructive impact of human and natural disasters in arid and semi-arid ecosystems (Li et al. 2014; Lausch et al. 2016; Estevez et al. 2017; Molaeinasb et al. 2018), this understanding could help to develop expert knowledge-based benchmarks (Herrick et al. 2019) to support UN sustainable development indicators (Hák et al. 2016) in terms of land degradation neutrality (LDN, SDG.15.3.1).

Assessment of terrestrial ecosystem health using remotely sensed metrics

In the studied area, remote sensing methods have been successfully applied to assess terrestrial ecosystem health status and to investigate impacts on ecosystem functioning and services. There has been a lot of discussion about how to relate landscape metrics to ecological processes (Wu and Hobbs 2002; Bastin et al. 2002; Lausch et al. 2016; Robinson and Weckworth 2016). However, scale issues and data availability as well as uncertainty in estimating health indicators from remote sensing can limit the applicability and accuracy (Li et al. 2014). For example, the diagnostic value of vegetation indices such as the NDVI to assess ecosystem degradation can be increased when changes in the spectral reflectance are linked to the underlying ecosystem processes using scientific knowledge (Herrick et al. 2019). In semi-arid lands, there are various methods to determine terrestrial ecosystem health using structural and functional indicators (Estevez et al. 2017; Berdugo et al. 2020). Here, we examined changes in landscape metrics related to landscape function (LI) and landscape degradation (MSDI) in rangeland and forest ecosystems. The LI can be used to assess and monitor changes in leakiness status of various landscapes and at different scales. Combining coarse or fine scale satellite imagery with low- or high-resolution DEM allows for LI to be derived at different spatial scales (Ludwig et al. 2007). Most landscape indices such as the LI and MSDI differed significantly between health classes and showed the same trend as, for example, the number of patches and the largest patch area. Indeed, decreasing terrestrial ecosystem health in this region can lead to an increasing the number of fragmented patches and leakage of resources, showing less integrated ecosystems with a higher degree of fragmentation (Safaei et al. 2021). The spectral heterogeneity was relatively high in degraded and unhealthy sites. Results from this and other studies all found that the MSDI serves as an appropriate complementary or alternative method to expensive field investigation for measuring landscape status and land degradation in arid and semi-arid regions (Tanser and Palmer 1999; Jafari et al. 2008). On the basis of these findings, the current structural condition of these ecosystems, which stems from past changes and conversions, is an indication of increasing land degradation. Given that one significant consequence of landscape degradation and conversion is health reduction, numerous ecological consequences are expected to rise (Tanser and Palmer 1999). Due to the importance of landscape structure and functionality for land management, it would be beneficial to consider RS based landscape metrics such as LI and MSDI in future research to outline management practices and to identify appropriate management strategies.

Integration of field-based indicators with remote sensing metrics to map and assess terrestrial ecosystem health status across spatio-temporal scales

The validation of remotely sensed information on terrestrial ecosystem health with expert field assessments can contribute to a science-based and data-driven assessment of rangeland health (Herrick et al. 2006; Herrick et al. 2019). In this study, comparing field data with remote sensing metrics using multivariate statistical methods turned out to be a promising approach for clustering terrestrial ecosystem health classes at the landscape scale in the studied area. We compared eight clustering methods to identify the appropriate clustering approaches on both field-based and remote sensing metrics, as the performance of different classification algorithms might vary clearly for a chosen dataset (Abbas 2008; Wiwie et al. 2015). The accuracy between maps using field and remote sensing data differed between best-performing clustering methods and pre-processing procedures. Here, DBSCAN combined with *k*-means clustering using NMDS ordination data showed the best performance in terms of concordance between field and remote sensing assessments of terrestrial ecosystem health gradients. Our results outline the potential of NMDS to deal with mixed data types (McCune and Grace 2002), the utility of Procrustes rotation of ordination data coupled with cluster analysis to assess survey data at larger spatial scales (Gonzalez-Mejia et al. 2018), and of combining distance and density-based clustering algorithms (Dash et al. 2001). Our results particularly highlight the recent popularity of DBSCAN (Ester 1996; Saha 2021). It has the typical characteristic to group data points with many nearby neighbors and to accurately identify clusters containing outliers and noise in the dataset (Ester et al. 1996). The results of this and other studies (Kozakura et al. 2017) demonstrated that combining clustering algorithms is a promising avenue to approximate clusters and to find the optimal clustering method suited to different types of ecological data. This approach enabled us to identify appropriate RS indicators of land degradation such as complex vegetation indices that cannot be calculated from field data alone (Toevs et al. 2011). The linkage between field and remotely sensed indices helped to better interpret the numerical appearance of metrics and the respective ecological patterns and processes. With the assignment of health status clusters to the landscape indices using a combination of multivariate analysis and cluster analysis, we go beyond the patch-based metrics (Wu and Hobbs 2002) and illustrate how landscape metrics can be applied to assess ecological processes at the watershed level, which highlights the potential to monitor land degradation from space. Further studies to test the transferability of our approach to other rangelands or across spatial scales are possible as we used a standardized field protocol, mainly free and open source software as well as

publicly available satellite data. Future directions could include identifying ecological thresholds (Andersen et. al 2009) or spatial early warning signals of ecosystem transitions to alternative stable states (Kéfi et al. 2014) based on complex remote-sensing indices and the IIRH protocol to test the integrity of land degradation monitoring in rangelands in the field, from space and based on ecological conceptual frameworks and theory.

The primary challenge in defining the benchmark of land degradation is the lack of historical data (Herrick et al. 2019). However, from a remote sensing perspective, the use of archive data from long-lasting satellite programs such as Landsat (Wulder et al. 2016) can partly fill such data gaps. Here, the remote sensing-based model for the assessment of terrestrial ecosystem health in 2016 was validated by field surveys and projected to Landsat data from 1987 (Fig. 2-6). From 1987 to 2016, decreasing areas of forest and dense rangeland together with increasing fragmentation exert negative trends on the ecosystem health status (Supplementary file 3; Fig. S1). Briefly, terrestrial ecosystem health maps derived from field information and remotely sensed indicators were consistent. This allowed for a transfer of the methods to historical satellite data, which produced plausible results. Providing an overview of the current and past state of ecosystem conditions is important because it affects the delivery of services and, therefore, human well-being (Rendon et al. 2019). Decreasing soil quality (Molaeinasab et al. 2018), increasing soil erosion, dust problems, and tree mortality in unhealthy sites have been attributed to the long history of over-grazing with domestic livestock like sheep and goats, and the conversion of forests and rangelands to arable lands (Baranian et al. 2017). When transferring our remote sensing approach to assess terrestrial ecosystem health from 2016 to satellite data from 1987, we found 32% of degradation related to the SDG 15.3.1 and its main aim to achieve land degradation neutrality (Prince 2019; UN 2019). In fact, it has been estimated that the actual number of livestock in some parts of the western rangelands of Iran including the study area exceeds considerably the grazing capacity (Farahpour 2002). It is partly because herders rely more on other feed sources for their livestock such as hay from farming lands (Abolhassani 2011). It is worth mentioning that rangeland management of the study area changed considerably following the Nationalization of Rangelands and Forests Act (Ghorbani et al. 2013). Before the land reform, rangelands were managed by nomads in common, public rangelands, while private rangelands were controlled by landlords. As a result, the rangelands were in better condition due to appropriate management, specifically due to the lower number of livestock and herders compared to the present time. Based on the land reform law, all rangelands were allocated to the government, resulting in "tragedy of the

commons" dilemma (Baland and Platteau 1994). Another cause of rangeland health decline is extensive land conversion to farms by local farmers and villagers whose primary intention is to claim ownership of land rather than agricultural goods. These farmers are well aware that rainfed agriculture in degraded rangeland is not profitable but would help them acquire more land by taking advantage of an inefficient long-lasting land management system in the region (Baranian et al. 2017). The current approach holds bright prospects for outlining policies that contribute to the range and forestry development efforts, integrated management of resource exploitation, and reducing resource degradation (Matsushita et al., 2006; Miller 2008).

In summary, the presented workflow on how to combine ecological information from the field and from satellite to map ecosystem health in space and time is in line with Wu and Hobbs (2002), who introduced an integrated approach that combines field data, experimental manipulations, GIS, remote sensing, and modeling for developing a science of scale. Using a combination of multivariate and cluster analysis to compare field and remotely sensed data turned out to be suitable to map ecosystem degradation. As the quality and availability of data over large areas and extended time periods are critical for modeling (Wu and Hobbs 2002), and continuously gathering field data over large areas has limitations, complex remotely sensed indices that are verified against field data provide one of the best opportunities to overcome these challenges. Future research could investigate the combined use of different sensors and platforms including the analysis of time-series data, and the transfer to different sites and ecosystems.

Conclusion

In this paper, we showed that assessing rangeland health based on satellite data can coincide accurately with assessment based on common field approaches (IIRH protocol). Thus, there is potential for integration of standardized in situ data with remote sensing imagery to enable a continuous monitoring of land degradation (SDG 15.3.1). We presented a methodological approach on how this information on ecosystem health can be linked using multivariate statistics, cluster analysis, and complex remote sensing metrics based on publicly available satellite data. As spatial data-driven monitoring approaches are essential to achieve SDGs, this approach could contribute to the development of benchmarks for land health and monitoring of indicators for land degradation neutrality based on remote sensing. Identification of spatial indicators of degradation could also help to establish links to conceptual frameworks such as ecological regime shifts with the objective to determine spatial early warning signals of regime shifts to alternative stable states. In the next step,

our approach could be tested at the national or even continental scale in arid and semi-arid regions or could be transferred to other study areas and ecosystems to support monitoring land degradation neutrality from space.

Acknowledgment

We thank the anonymous reviewer whose comments and friendly suggestions helped improve and clarify this manuscript.

Funding

This research did not receive any specific grant from funding agencies in the public, commercial, or not-for-profit sectors.

Conflicts of interest

The authors declare that they have no known competing financial interests or personal relationships that could have appeared to influence the work reported in this paper.

Data availability

The datasets generated during the current study are available from the corresponding author on reasonable request.

Authorship

All authors contributed to the study conception and design. Material preparation and data collection were performed by MS, with significant guidance from AGS and HB. Analyses were performed by MS. The first draft of the manuscript was written by MS and commented by HB, AGS, TK, and SF to prepare the final manuscript. All authors approved the final manuscript.

References

Abbas, OA., 2008. Comparisons between data clustering algorithms. Int. Arab J. Inf. Technol. 5, 320-325.

Abolhassani, L., 2011 Rangeland management in Iran: A socio-economic analysis and case study of Semnan rangelands. Dissertation, Freiburg University.

Ahmadi, S., Ghaderi, F., Safaee, D., 2020. Oak charcoal rot disease in Iran. Plant Pathology 9: 118-128. In FarsiBailey RG 1985 The factor of scale in ecosystem mapping. Environ Manage 9: 271–275. https://doi.org/10.1007/BF01867299

Andersen, T., Carstensen, J., Hernandez-Garcia, E., Duarte, CM., 2009. Ecological thresholds and regime shifts: approaches to identification. Trends Ecol. Evol 24: 49-57. https://doi.org/10.1016/j.tree.2008.07.014

Baland, JM., Platteau, JP., 1994. Should Common Property Resources be Privatized? A re-examination of the tragedy of the commons. In: Terhal P, De Vries G ed, Development, transformation and state policy. Manohar Pub. Delhi

Baranian, E., Bashari, H., Mosaddeghi, MR., Bassiri, M., 2017. Soil aggregate stability and organic matter as affected by land use change in central Iran. Arch Agron Soil Sci 63: 1823-1837. https://doi.org/10.1080/03650340.2017.1308492

Bassiri, M., Iravani, M., 2009. Vegetation changes after 19 years of grazing exclosure in the central Zagros region. Rangeland 3: 155-170 In Farsi https://www.sid.ir/en/journal/ViewPaper.aspx?ID=170566

Bassiri, M., Jalalian, A., Vahabi, MR., 1989. Studies on habitate condition and seed production of native range plants in Fereydan region. Project report, college of Agriculture, Isfahan University of Technology. In Farsi

Bastin, GN., Ludwig, JA., Eager, RW., Chewings, VH., Liedloff, AC., 2002. Indicators of landscape function: comparing patchiness metrics using remotely-sensed data from rangelands. Ecol Indic 1, 247-260. https://doi.org/10.1016/S1470-160X0200009-2

Berdugo, M., Delgado-Baquerizo, M., Soliveres, S., Hernández-Clemente, R., Zhao, Y., Gaitán, JJ., Gross, N., Saiz, H., Maire, V., Lehmann, A., Rillig, MC., Solé, RV., Maestre, FT., 2020. Global ecosystem thresholds driven byaridity. Science 367: 787-790. 10.1126/science.aay5958

Briske, DD., Fuhlendorf, SD., Smeins, FE., 2005. State-and-transition models, thresholds, and rangeland health: A synthesis of ecological concepts and perspectives. Rangland Ecol Manag 58: 1-10. https://doi.org/10.2111/1551-5028200558<1:SMTARH>2.0.CO;2

Cavender-Bares, J., Schneider, F.D., Santos, M.J. et al. 2022. Integrating remote sensing with ecology and evolution to advance biodiversity conservation. Nat Ecol Evol. https://doi.org/10.1038/s41559-022-01702-5

Chiquet, J., Rigaill, G., Sundqvist, M., 2020. Aricode: efficient computations of sandard. clustering comparison measures. R package version 1.0.0. https://CRAN.R-project.org/package=aricode

DeMartonne, E., 1962 Une nouvelle fonctionclimatologique. L indiced' aridie. La Meterologie 2, 449-458

Dixon, P., 2003 VEGAN, a package of R functions for community ecology. J. Veg. Sci. 14: 927-930. https://doi.org/10.1111/j.1654-1103.2003.tb02228.x

Duniway, MC., Herrick, JE., Pyke, DA., David, TP., 2010. Assessing transportation infrastructure impacts on rangelands: test of a standard rangeland assessment protocol. Rangland Ecol Manag. 63, 524-536.10.2111/REM-D-09-00176.1

Ester, M., Kriegel, HP., Sander, J., Xu, X., 1996. A density-based algorithm for discovering clusters in large spatial databases with noise, In: Second International Conference on Knowledge Discovery and Data Mining. AAAI Press, United States, pp 226–231

Estevez, E., Rodríguez-Castillo, T., Álvarez-Cabria, M., González-Ferreras, A., Lezcano, M., Barquín, P., Peñas, F., 2017. Analysis of structural and functional indicators for assessing the health state of mountain streams. Ecol Indic. 72. 553-564. https://doi.org/10.1016/j.ecolind.2016.08.052

Farahpour, M., 2002. A planning support system for rangeland allocation in Iran: case of Chadegan sub-region. Dessertation, Wageningen Agricultural University

Feilhauer, H., Oerke, EC., Schmidtlein, S., 2010. Quantifying empirical relations between planted species mixtures and canopy reflectance with PROTEST. Remote Sens Environ 114, 1513-1521. https://doi.org/10.1016/j.rse.2010.02.006

Frank, S., Fürst, C., Koschke, L., Makeschin, F., 2012. A contribution towards a transfer of the ecosystem service concept to landscape planning using landscape metrics. Ecol Indic 21, 30-38. https://doi.org/10.1016/j.ecolind.2011.04.027

Ghorbani, M., Azarnivand, H., Mehrabi, A., Jafari, M., Nayebi, H., Seeland, K., 2013 The role of indigenous ecological knowledge in managing rangelands sustainably in northern Iran. Ecol Soc 18:15. http://dx.doi.org/10.5751/ES-05414-180215

Gonzalez-Mejia, A., Styles, D., Wilson, P., Gibbons, J., 2018. Metrics and methods for characterizing dairy farm intensification using farm survey data. PloS ONE, 13, e0195286. https://doi.org/10.1371/journal.pone.0195286

Gower, JC., 1971. Statistical methods of comparing different multivariate analyses of the same data. In: Hodson FR, Kendall DG, Tautu P ed, Mathematics in the archaeological and historical sciences. Edinburgh University Press, Edinburgh, pp 138– 149.

Große-Stoltenberg, A., Hellmann, C., Thiele, J., Oldeland, J., Werner, C., 2018. Invasive acacias differ from native dune species in the hyperspectral/biochemical trait space. J VegSci 29: 325– 335. https://doi.org/10.1111/jvs.12608

Gunderson, LH., 2000. Ecological Resilience-In Theory and Application. Annu Rev Ecol Syst 31. 425-439. https://doi.org/10.1146/annurev.ecolsys.31.1.425

Hahsler, M., Piekenbrock, M., Doran, D., 2019. dbscan: Fast Density-Based Clustering with R J Stat Softw 91: 1–30. 10.18637/jss.v091.i01

Hák, T., Janoušková, S., Moldan, B., 2016. Sustainable Development Goals: A need for relevant indicators. Ecol Indic 60: 565-573. https://doi.org/10.1016/j.ecolind.2015.08.003

Herrick, JE., Schuman, GE., Rango, A., 2006. Monitoring ecological processes for restoration projects. J Nat Conserv 143-4, 161-171. https://doi.org/10.1016/j.jnc.2006.05.001

Herrick, JE., Shaver, P., Pyke, DA., Pellant, M., Toledo, D., Lepak, N., 2019. A strategy for defining the reference for land health and degradation assessments. Ecol Indic 97: 225-230. https://doi.org/10.1016/j.ecolind.2018.06.065 Accessed 05 July 2018

IPBES, 2018. Summary for policymakers of the assessment report on land degradation and restoration of the Intergovernmental Science- Policy Platform on Biodiversity and Ecosystem Services. Scholes RJ, Montanarella L, Brainich E et al ed. IPBES secretariat, Bonn, https://www.ipbes.net/system/tdf/spm_3bi_ldr_digital.pdf?file=1&type=node&id=28335

IPBES, 2019. Global assessment report on biodiversity and ecosystem services of the Intergovernmental Science-Policy Platform on Biodiversity and Ecosystem Services. Brondizio ES, Settele J, Díaz S, Ngo HT ed. IPBES secretariat, Bonn, https://doi.org/10.5281/zenodo.3831673 Accessed 04 May 2019

Inkoom, JN., Frank, S., Greve, K., Walz, U., Fürst, C., 2018. Suitability of different landscape metrics for the assessments of patchy landscapes in West Africa. Ecol Indic 85, 117-127. https://doi.org/10.1016/j.ecolind.2017.10.031

Jafari, R., Lewis, MM., Ostendorf, B., 2008. An image-based diversity index for assessing land degradation in an arid environment in South Australia. J Arid Environ 72: 1282-1293. https://doi.org/10.1016/j.jaridenv.2008.02.011

Johnson, SC., 1967. Hierarchical clustering schemes. Psychometrika 32, 241–254. https://doi.org/10.1007/BF02289588

Kassambara, A., Mundt, F., 2020. factoextra: Extract and Visualize the Results of Multivariate Data Analyses. R package version 1.0.7. https://CRAN.R-project.org/package=factoextra

Kéfi, S., Guttal, V., Brock, WA., Carpenter, SR., Ellison, AM., Livina, VN., 2014. Early Warning Signals of Ecological Transitions: Methods for Spatial Patterns. PLoS ONE 93: e92097. https://doi.org/10.1371/journal.pone.0092097

Kohonen, T., 2001. Self-organizing maps. Springer, New York, Berlin, Heidelberg. https://doi.org/10.1007/978-3-642-56927-2

Kozakura, Y., Mori, T., Fujibuchi, W., 2017. Comparison of clustering methods for single-cell transcriptome analysis. IPSJ SIG Technical report 51: 9-26.

Kriegel. HP., Schubert, E., Zimek, A., 2016. The black art of runtime evaluation: Are we comparing algorithms or implementations? KAIS 52: 341–378 https://doi.org/10.1007/s10115-016-1004-2

Kruskal, JB., 1964. Non-metric multidimensional scaling: a numerical method. Psychometrica 29: 115–129. https://doi.org/10.1007/BF02289694

Lausch, A., Erasmi, S., King, JD., Magdon, P., Heurich, M., 2016. Understanding forest health with remote sensing -Part I-A review of spectral traits, processes and remote-sensing characteristics. Remote Sens 8:1029. https://doi.org/10.3390/rs8121029

Li, Z., Xu, D., Guo, X., 2014. Remote sensing of ecosystem health: opportunities, challenges, and future perspectives. Sensors. 14: 21117-21139. https://doi.org/10.3390/s141121117

Ludwig, JA., Bastin, GN., Chewings, VH., Eager, RW., Liedloff, AC., 2007. Leakiness: A new index for monitoring the health of arid and semi-arid landscapes using remotely sensed vegetation cover and elevation data. Ecol Indic. 7: 442-454. http://dx.doi.org/10.1016/j.ecolind.2006.05.001

Magiera, A., Feilhauer, H., Otte, A., Waldhardt, R., Simmering, D., 2013. Relating canopy reflectance to the vegetation composition of mountainous grasslands in the Greater Caucasus. Agric Ecosyst Environ, 177, 101-112. https://doi.org/10.1016/j.agee.2013.05.017

Matsushita, B., Xu, M., Fukushima, T., 2006. Characterizing the changes in landscape structure in the Lake Kasumigaura Basin, Japan using a high-quality GIS dataset. Landsc. Urban Plan 78: 241-250. https://doi.org/10.1016/j.landurbplan.2005.08.003

McCune, BP., Grace, J., 2002. Analysis of ecological communities. J Exp Mar Biol Ecol 289:303-305. https://doi.org/10.1016/S0022-09810300091-1

McGarigal, K., Cushman, S., Neel, M., Ene, E., 2012. FRAGSTATS v4: Spatial pattern analysis program for categorical maps. Computer software program. University of Massachusetts, Amherst. http://www.umass.edu/landeco/research/fragstats/fragstats.html

Miller, ME., 2008. Broad-scale assessment of rangeland health, Grand Staircase-Escalante National Monument, USA. Rangland Ecol Manag 61: 249-262. https://doi.org/10.2111/07-107.1

Molaeinasab, A,. Bashari, H., TarkeshEsfahani, M., Mosaddeghi, MR., 2018. Soil surface quality assessment in rangeland ecosystems with different protection levels, central Iran. CATENA. 171: 72-82. https://doi.org/10.1016/j.catena.2018.07.004

National Research Council NRSC, 1994. Rangeland health: new methods to classify, inventory, and monitor rangelands. Committee on rangeland classification. The National Academies Press, Washington. https://aim.landscapetoolbox.org/wp-content/uploads/2015/09/NRC_Rangeland_Health_1994.pdf Accessed 1994

Pellant, M., Shaver, PL., Pyke, DA., Herrick, JE., Lepak, N., Riegel, G., Kachergis, E., Newingham, BA., Toledo, D., Busby, FE., 2020. Interpreting indicators of rangeland health. National Operations Center, Denver. https://www.blm.gov/sites/blm.gov/files/docs/2020-12/IB2021-007_att1.pdf

Prince, SD., 2019. Challenges for remote sensing of the sustainable development goal SDG 15.3.1 productivity indicator, Remote Sens Environ, 234. https://doi.org/10.1016/j.rse.2019.111428

Pyke, D., Herrick, J., Shaver, P., Pellant, M., 2002. Rangeland health attributes and indicators for qualitative assessment. J Range Manage 55: 584–597. https://doi.org/10.1016/j.ecolind.2014.02.009

R Core Team, 2021. R: A language and environment for statistical computing. R Foundation for Statistical Computing, Vienna, Austria. https://www.r-project.org/

Robinson, HS., Weckworth, B., 2016. Landscape ecology: linking landscape metrics to ecological processes. McCarthy T, Mallon D, Snow Leopards, Academic Press, New York. pp 395-405. https://doi.org/10.1016/B978-0-12-802213-9.00029-8

Safaei, M., Jafari, R., Datta, P., Bashari, H., Pothier, D., Koch, B., 2021. Spatial scale effect of Sentinel-2, Landsat OLI, and MODIS imagery in the assessment of landscape condition of Zagros Mountains. Geocarto Int. https://doi.org/10.1080/10106049.2021.1914745

Saha, PK., Logofatu, D., 2021. Efficient Approaches for Density-Based Spatial Clustering of Applications with Noise. In: Maglogiannis I, Macintyre J, Iliadis L ed Artificial Intelligence Applications and Innovations. AIAI 2021. IFIP Advances in Information and Communication Technology, Springer, Cham. https://doi.org/10.1007/978-3-030-79150-6_15

Sims, NC., Newnham, GJ., England, JR., Guerschman, J., Cox, SJD., Roxburgh, SH., Viscarra Rossel, RA., Fritz, S., Wheeler, I., 2021. Good Practice Guidance. SDG Indicator 15.3.1, Proportion of Land That Is Degraded Over Total Land Area. Version 2.0. United Nations Convention to Combat Desertification, Bonn, Germany. https://www.unccd.int/publications/good-practice-guidance-sdg-indicator-1531-proportion-land-degraded-over-total-land

Soffianian, A., Madanian, M., 2015. Monitoring land cover changes in Isfahan Province, Iran using Landsat satellite data. Environ Monit Assess 187: 543. https://doi.org/10.1007/s10661-015-4442-5

United Nations UN, 2019. High-level political forum on sustainable development, convened under the auspices of the Economic and Social Council Special edition: progress towards the Sustainable Development Goals. https://undocs.org/E/2019/68. Accessed 8 May 2019

Tanser, FC., Palmer, AR., 1999. The application of a remotely-sensed diversity index to monitor degradation patterns in a semi-arid, heterogeneous, South African landscape. J Arid Environ 43: 477-484. https://doi.org/10.1006/jare.1999.0568

Toevs, GR., Karl, JW., Taylor, JJ., Spurrier, CS., Bobo, MR., Herrick, JE., 2011. Consistent indicators and methods and a scalable sample design to meet assessment, inventory, and monitoring information needs across scales. Rangelands 33: 14-20. https://doi.org/10.2111/1551-501X-33.4.14

Torgerson, WS., 1958. Theory and methods of scaling. John Wiley and Sons, New York, pp 245-247 https://doi.org/10.1002/bs.3830040308

Trapletti, A., Hornik, K., 2020. tseries: Time series analysis and computational finance. R package version 0.10-48. https://CRAN.R-project.org/package=tseries

Tucker, CJ., 1979. Red and photographic infrared linear combinations for monitoring vegetation. Remote Sens Environ 8: 127-150. https://doi.org/10.1016/0034-42577990013-0

van der Zanden, EH., Levers, Ch., Verburg, PH., Kuemmerle, T., 2016. Representing composition, spatial structure and management intensity of European agricultural landscapes: A new typology. Landsc Urban Plan 150:36-49. https://doi.org/10.1016/j.landurbplan.2016.02.005

Vialaneix, N., Maigne, E., Mariette, J., Olteanu, M., Rossi, F., Bendhaiba, L., Bolaert, J., 2020. SOMbrero: SOM bound to realize euclidean and relational outputs. R package version 1.3-1. https://cran.r-project.org/web/packages/SOMbrero/index.html

Vogt, P., Riitters, K., 2017. Guidos Toolbox: universal digital image object analysis. Eur J Remote Sens 50: 352-361. https://doi.org/10.1080/22797254.2017.1330650

Wiwie, C., Baumbach, J., Röttger, R., 2015. Comparing the performance of biomedical clustering methods. Nat Methods 12, 1033-1038. https://doi.org/10.1038/nmeth.3583

Wu, J., Qi, Y., 2000. Dealing with Scale in Landscape Analysis: An Overview, Geogr inf sci 6:1, 1-5. https://doi.org/10.1080/10824000009480528

Wu, J., Hobbs, R., 2002. Key issues and research priorities in landscape ecology: An idiosyncratic synthesis. Landsc Ecol 17:355–365. https://doi.org/10.1023/A:1020561630963

Wulder, MA., White, JC., Loveland, TR., Woodcock, CE., Belward, AS., Cohen, WB., Roy, DP., 2016. The global Landsat archive: status, consolidation, and direction. Remote Sens Environ 185: 271-283. https://doi.org/10.1016/j.rse.2015.11.032

Appendix

Supplementary file1: Table

In the IIRH assessment, 17 ecological indicators were utilized to identify three ecosystem attributes that reflect ecosystem functionality including (i) soil and site stability, (ii) hydrological function, and (iii) biotic integrity. Each of the 17 indicators has an ecological relationship with three functional attributes. For example, as shown in Table 1, the soil and site stability was assessed using the scores of indicators 1-9 and 11. Finally, in each sub-catchment, the preponderance of evidence approach related to the three functional attributes led us to assign healthy, at-risk, and unhealthy classes.

Table. Information related to the 40 sub-catchments. We used the preponderance of evidence approach to finding the appropriate category for each functional attribute. 1-17 shows the number of indicators from Table 1. SSS: soil and site stability, HF: Hydrological function, and BI: Biotic integrity.

Sites	X	Y	1	2	3	4	5	6	7	8	9	10	11	12	13	14	1	16	17	SSS	HF	BI	Health
1	385647.2	3654238.1	E_T	E_T	M	E_T	N_S	E_T	M_E	E_T	E_T	M_E	N_S	M_E	E_T	E_T	E_T	E_T	E_T	E_T	E_T	E_T	Unhealthy
2	392333.0	3654651.0	M_E	M_E	S_M	M	N_S	M	M	M	S_M	M	N_S	M	M_E	M	M	M_E	M	M	M	M	At Risk
3	388806.7	3653919.5	E_T	E_T	M	E_T	N_S	E_T	M_E	E_T	E_T	M_E	N_S	M_E	E_T	E_T	E_T	E_T	E_T	E_T	E_T	E_T	Unhealthy
4	385869.1	3649893.7	E_T	E_T	M_E	E_T	N_S	E_T	M_E	E_T	E_T	M_E	N_S	M_E	E_T	E_T	E_T	E_T	E_T	E_T	E_T	E_T	Unhealthy
5	393702.9	3645976.8	M_E	S_M	S_M	M	N_S	M	N_S	M	S_M	M	N_S	M	M_E	S_M	N_S	M_E	M	S_M	S_M	M	At Risk
6	406286.0	3648993.0	E_T	E_T	M	E_T	N_S	E_T	M_E	E_T	E_T	M_E	N_S	M_E	E_T	E_T	E_T	E_T	E_T	E_T	E_T	E_T	Unhealthy
7	398383.2	3644907.1	N_S	N_S	M	N_S	N_S	N_S	M	N_S	N_S	S_M	M_E	N_S	S_M	N_S	N_S	N_S	M	N_S	N_S	N_S	Healthy
8	424341.0	3648340.0	E_T	E_T	M_E	E_T	N_S	E_T	M_E	E_T	E_T	M_E	N_S	E_T	E_T	E_T	E_T	E_T	E_T	E_T	E_T	E_T	Unhealthy
9	421671.0	3641898.0	E_T	E_T	M_E	E_T	N_S	E_T	E_T	E_T	E_T	E_T	N_S	M_E	E_T	E_T	E_T	E_T	E_T	E_T	E_T	E_T	Unhealthy
10	397511.1	3640319.0	E_T	N_S	S_M	M	N_S	M	N_S	M	S_M	S_M	S_M	M_E	M_E	N_S	M	M_E	S_M	N_S	N_S	S_M	Healthy
11	385692.0	3642777.0	E_T	E_T	M	E_T	N_S	E_T	M_E	E_T	E_T	M_E	N_S	E_T	E_T	E_T	E_T	E_T	E_T	E_T	E_T	E_T	Unhealthy
12	426996.9	3640863.0	N_S	S_M	S_M	S_M	N_S	S_M	S_M	S_M	N_S	N_S	M_E	S_M	S_M	N_S	S_M	S_M	S_M	S_M	N_S	S_M	At Risk
13	412904.0	3640269.0	N_S	N_S	M	N_S	N_S	N_S	M	N_S	N_S	S_M	M_E	S_M	S_M	N_S	N_S	N_S	M	N_S	N_S	N_S	Healthy
14	414980.0	3638196.0	M_E	N_S	S_M	M	N_S	M	N_S	M	S_M	M	S_M	M	M_E	N_S	M	M_E	M	N_S	N_S	M	Healthy
15	401972.1	3640319.0	N_S	S_M	S_M	S_M	N_S	S_M	S_M	S_M	N_S	S_M	M_E	S_M	S_M	N_S	S_M	S_M	S_M	S_M	N_S	S_M	At Risk
16	409783.1	3639757.2	E_T	E_T	M	E_T	N_S	E_T	M_E	E_T	E_T	M_E	N_S	M_E	E_T	E_T	E_T	E_T	E_T	E_T	E_T	E_T	Unhealthy
17	410349.9	3634117.2	N_S	S_M	S_M	S_M	N_S	S_M	S_M	S_M	N_S	N_S	M_E	N_S	S_M	N_S	S_M	S_M	S_M	S_M	N_S	S_M	At Risk
18	412936.0	3632058.0	E_T	E_T	M_E	E_T	N_S	E_T	E_T	E_T	E_T	E_T	N_S	E_T	E_T	E_T	E_T	E_T	E_T	E_T	E_T	E_T	Unhealthy
19	390352.0	3637519.0	E_T	E_T	M_E	E_T	N_S	E_T	E_T	E_T	E_T	E_T	N_S	M_E	E_T	E_T	E_T	E_T	E_T	E_T	E_T	E_T	Unhealthy
20	394406.0	3631918.0	E_T	E_T	M_E	E_T	N_S	E_T	E_T	E_T	E_T	E_T	N_S	M_E	E_T	E_T	E_T	E_T	E_T	E_T	E_T	E_T	Unhealthy
21	395117.4	3627262.6	M_E	S_M	S_M	M	N_S	M	N_S	M	S_M	M	N_S	S_M	M_E	S_M	M	M_E	M	S_M	S_M	M	At Risk

22	377817.6	3641733.4	N_S	N_S	M	N_S	N_S	N_S	M	N_S	N_S	S_M	M_E	S_M	S_M	N_S	N_S	N_S	M	N_S	N_S	N_S	Healthy
23	391854.3	3630417.8	N_S	N_S	M	N_S	N_S	N_S	M	N_S	N_S	S_M	M_E	N_S	S_M	N_S	M	N_S	M	N_S	N_S	N_S	Healthy
24	424059.2	3633573.1	M_E	S_M	M	M	N_S	S_M	S_M	M	S_M	M	S_M	M	M_E	S_M	M	M_E	M	S_M	S_M	M	At Risk
25	399908.0	3629006.0	E_T	E_T	M_E	E_T	N_S	E_T	E_T	E_T	E_T	E_T	N_S	E_T	E_T	E_T	E_T	E_T	E_T	E_T	E_T	E_T	Unhealthy
26	387257.2	3627528.9	E_T	E_T	M	E_T	N_S	E_T	M_E	E_T	E_T	M_E	N_S	M_E	E_T	E_T	E_T	E_T	E_T	E_T	E_T	E_T	Unhealthy
27	431784.3	3623998.4	M_E	S_M	M	M	N_S	S_M	S_M	M	S_M	S_M	S_M	M	M_E	S_M	M	M_E	M	S_M	S_M	M	At Risk
28	397728.7	3622366.3	M_E	S_M	M	M	N_S	S_M	S_M	M	S_M	M	S_M	M_E	M_E	S_M	M	M_E	M	S_M	S_M	M	At Risk
29	421668.0	3624684.0	E_T	E_T	M_E	E_T	N_S	E_T	E_T	E_T	E_T	E_T	N_S	E_T	E_T	E_T	E_T	E_T	E_T	E_T	E_T	E_T	Unhealthy
30	416566.0	3619130.0	M_E	N_S	S_M	M	N_S	M	N_S	M	S_M	M	S_M	S_M	M_E	N_S	M	M_E	M	N_S	N_S	M	Healthy
31	422440.5	3615086.1	E_T	E_T	M_E	E_T	N_S	E_T	M_E	E_T	E_T	M_E	N_S	M_E	E_T	E_T	E_T	E_T	E_T	E_T	E_T	E_T	Unhealthy
32	406264.0	3623830.0	N_S	S_M	S_M	N_S	N_S	N_S	N_S	S_M	N_S	N_S	M_E	S_M	S_M	S_M	S_M	S_M	S_M	N_S	N_S	S_M	Healthy
33	411655.6	3618123.0	E_T	E_T	M_E	E_T	N_S	E_T	E_T	E_T	E_T	E_T	N_S	M_E	E_T	E_T	E_T	E_T	E_T	E_T	E_T	E_T	Unhealthy
34	402298.4	3622039.9	M_E	S_M	M	M	N_S	S_M	S_M	M	S_M	S_M	S_M	M	M_E	S_M	M	M_E	M	S_M	S_M	M	At Risk
35	411776.7	3617062.5	E_T	E_T	M_E	E_T	N_S	E_T	M_E	E_T	E_T	M_E	N_S	M_E	E_T	E_T	E_T	E_T	E_T	E_T	E_T	E_T	Unhealthy
36	417095.8	3614858.9	E_T	E_T	M_E	E_T	N_S	E_T	E_T	E_T	E_T	E_T	N_S	E_T	E_T	E_T	E_T	E_T	E_T	E_T	E_T	E_T	Unhealthy
37	405562.5	3615402.9	M_E	M_E	S_M	M	N_S	M	M	M	S_M	M	N_S	M	M_E	M	M	M_E	M	M	M	M	At Risk
38	426561.7	3640319.0	N_S	N_S	S_M	S_M	N_S	S_M	N_S	S_M	N_S	N_S	M_E	N_S	S_M	S_M	S_M	S_M	S_M	N_S	N_S	S_M	Healthy
39	431131.5	3617361.4	E_T	E_T	M_E	E_T	N_S	E_T	M_E	E_T	E_T	M_E	N_S	M_E	E_T	E_T	E_T	E_T	E_T	E_T	E_T	E_T	Unhealthy
40	430378.1	3610366.3	E_T	E_T	M_E	E_T	N_S	E_T	E_T	E_T	E_T	E_T	N_S	M_E	E_T	E_T	E_T	E_T	E_T	E_T	E_T	E_T	Unhealthy

T_T: Extreme to Total, M_E: Moderate to Extreme, M: Moderate, S-M: Slight to Moderate, and N_S: None to Slight

Supplementary file 2: Leakiness index

The leakiness index is a relatively new effective metric for monitoring landscape health (Ludwig et al., 2007). This index looks into major structural and structural aspects of a landscape, especially it's potential to lose or leak resources. This is a quantitative index built based on integrating vegetation data derived from satellite remote sensing imagery and DEM. This index considers vegetation configuration and soil loss impacts to explain landscape functionality. NDVI index (Tucker 1979) was derived from Landsat 8 imagery (Safaei et al. 2021). 1:25000 topographic maps (National Cartographic Center; ncc.gov.ir) (Table 2) were also used to produce DEM with a spatial resolution of 30 m. The importance of DEM and sub-catchment layers is that LI measures resource leakage based on hydrological conditions. Vegetation cover index, DEM, and sub-catchment boundary layers served as the input of Liv4 software to produce LI (Ludwig et al., 2007). The value of the LI varies between zero indicating higher function and one indicating lower function

$$LI = 1 - \left[\frac{L_{max} - L_{calc}}{L_{max} - L_{min}}\right]^{k}$$

$$Lmax = \frac{L_{calc}}{\left[1 - \sqrt[3]{1 - LI}\right]}$$

Lmax = maximum leakiness. In theory, if all pixels in a map have no vegetation cover to trap surface flows and soil sediments flowing, then the landscape have maximum potential leakiness (Ludwig et al., 2007).

Lmin = minimum leakiness. If all pixels in a landscape have 100% cover, and if we assume that this cover effectively traps any soil sediments flowing then the landscape have minimum potential leakiness (Ludwig et al., 2007).

Lcalc = progressively accumulates resources from pixel to pixel

Supplementary file 3: Figure

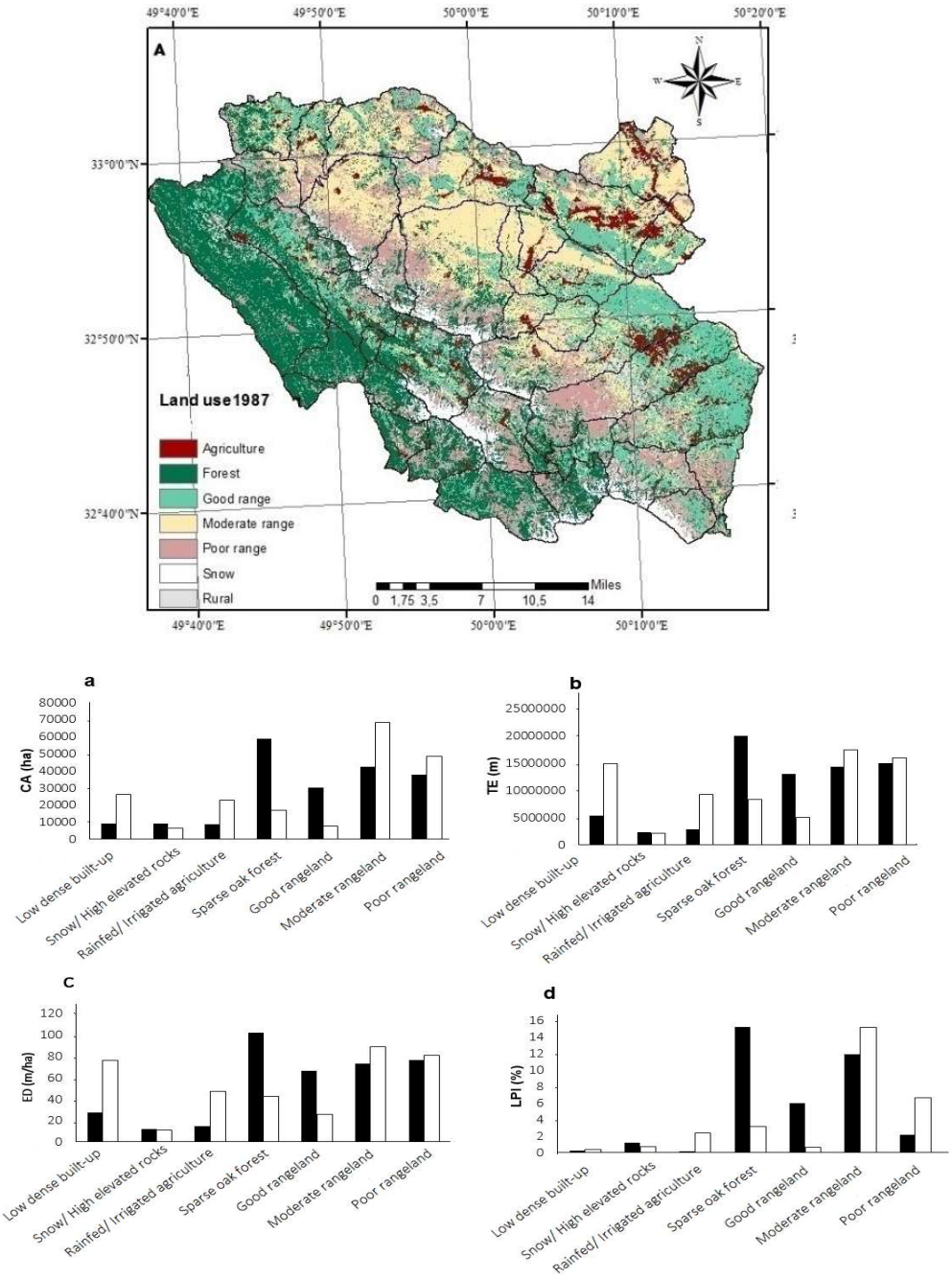

Fig. S1 Land-use/cover maps of the study area are derived from (A) Landsat TM 1987 and (B) Landsat OLI 2016 (Safaei et al. 2021). Graphs show landscape metrics change over a 30-year time period during 1987and 2016.

Results of the total class area (Figure S.1a) showed that the area occupied by forest in 1987 (58829 ha) was larger than that in 2016 (16955 ha). Good rangeland decreased from 30110 ha in 2016 to

7621 in 1987. Forest and good rangeland had negative growth rates of -21.5% and -11.5%, respectively, whereas moderate rangeland, built-up land, agriculture, and poor rangeland experienced positive rates, equivalent to 13%, 8.5%, 7.1%, and 5.5%, respectively. The values of total edge (Figure S.1b) and edge density (Figure S.1c) were consistent with the total class area. The largest patch index (Figure S.1d) presented similar changing trends. Based on the results, good rangeland and dense canopy cover forest decreased while poor rangeland increased during the period 1987-2016.

Supplementary file 4: Figure

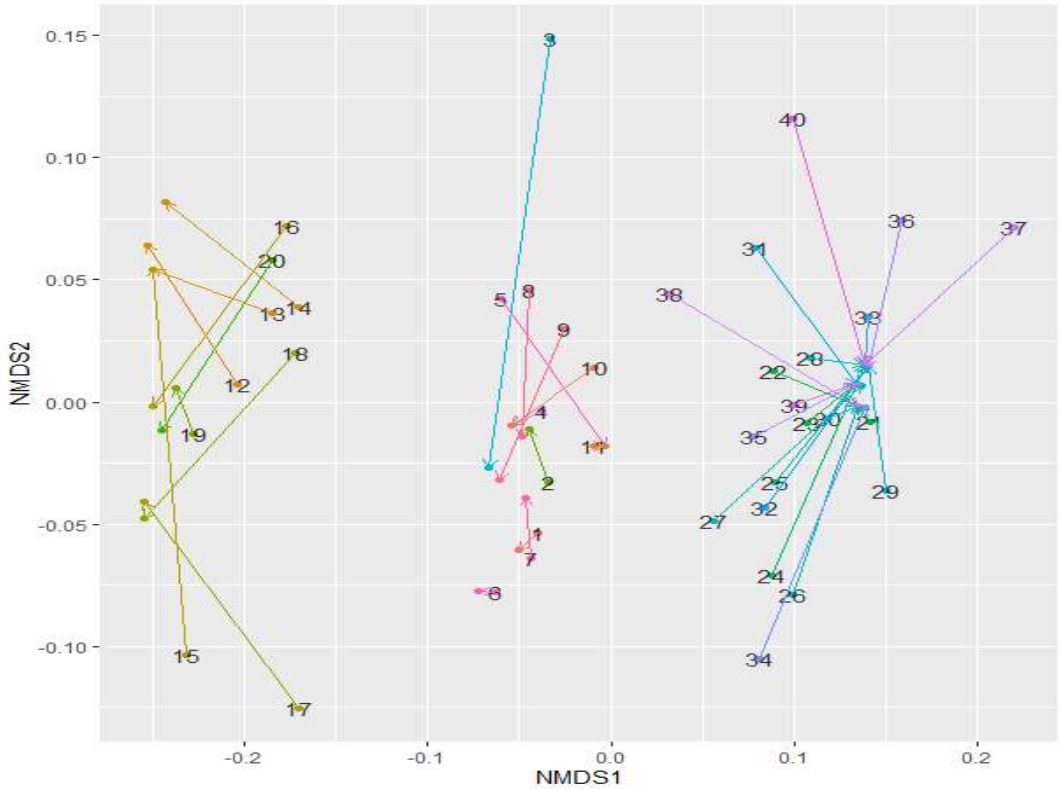

Fig. S2 Results of Procrustes rotations comparing the first two components of the original NMDS based on 17 heath indicators of field assessment (See table1) with NMDS on the remotely sensed metrics. Boxes mean sites numbers of the NMDS (field data) and blue lines connect target and rotated configurations of the second NMDS ordination. The permutation tests with 999 permutations confirmed the non-randomness of the patterns (p value= 0.001).

Supplementary file 5: Figure

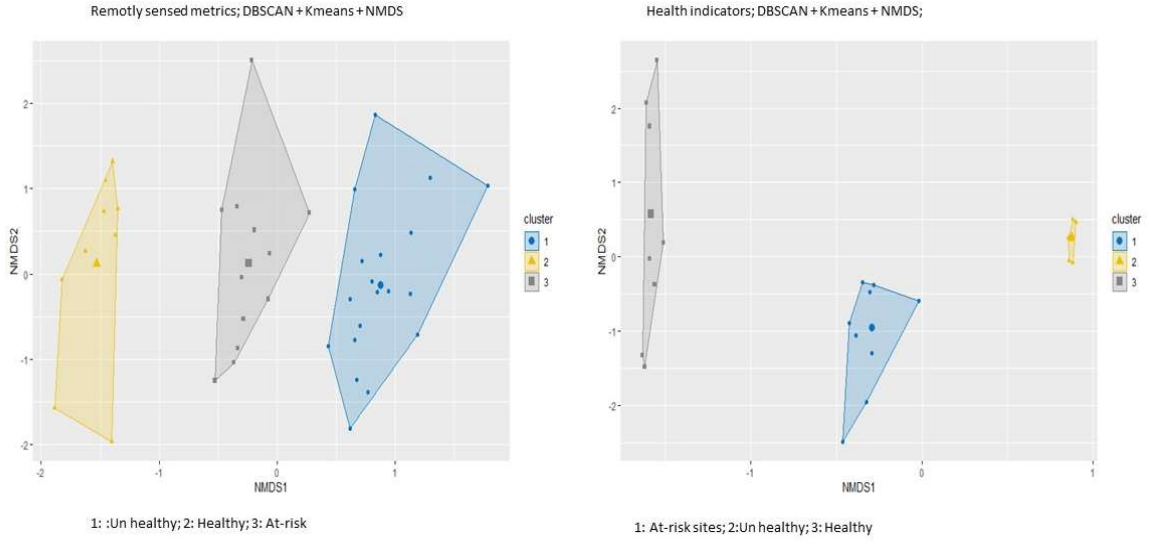

Fig. S3A: Visualization by dimensionality reduction DBSCAN+ K-means clustering on NMDS data a: remotely sensed metrics clustering and b: health indicators clustering (NMI=0.91)

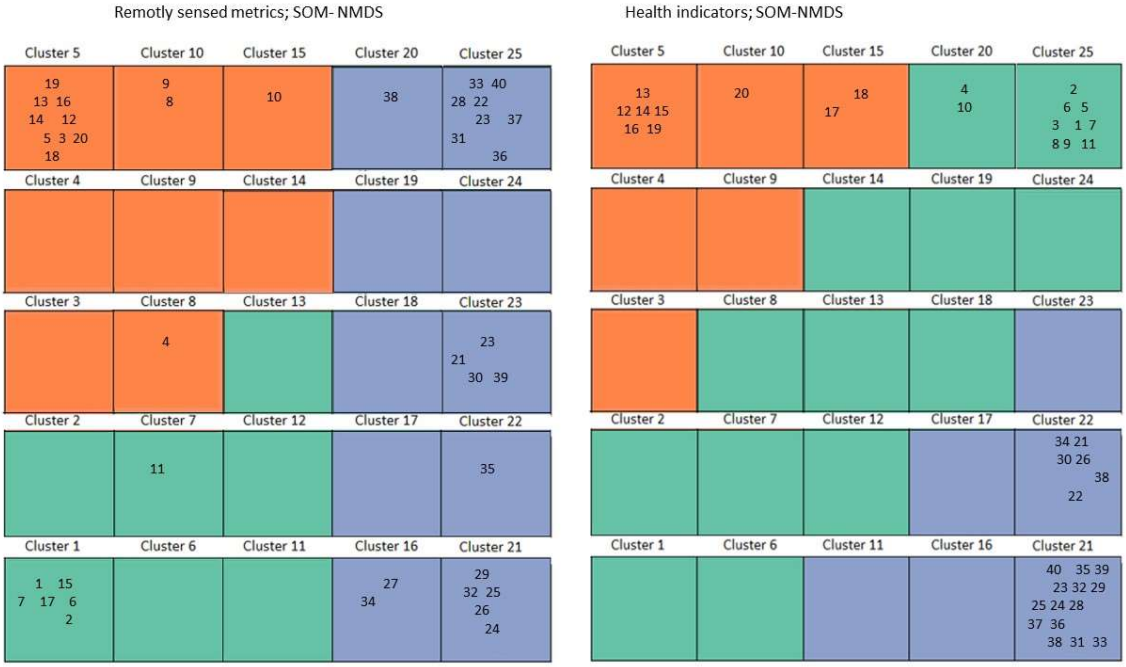

Fig. S3B Maps of 5 × 5 SOM grids with their cluster number and the distributions of variables and sites among the clusters. The super clusters indicate three general groups of health. Healthy clusters defined by field based and remotely sensed metrics and 40 studied sites (NMI=0.84). The dendrogram shows 25 nodes in super clusters. And girds show distance depends on the overall distance to their nearest neighbors. The same color means neighbors are closer distances, distance is less, whereas different colors indicate they have bigger distance.

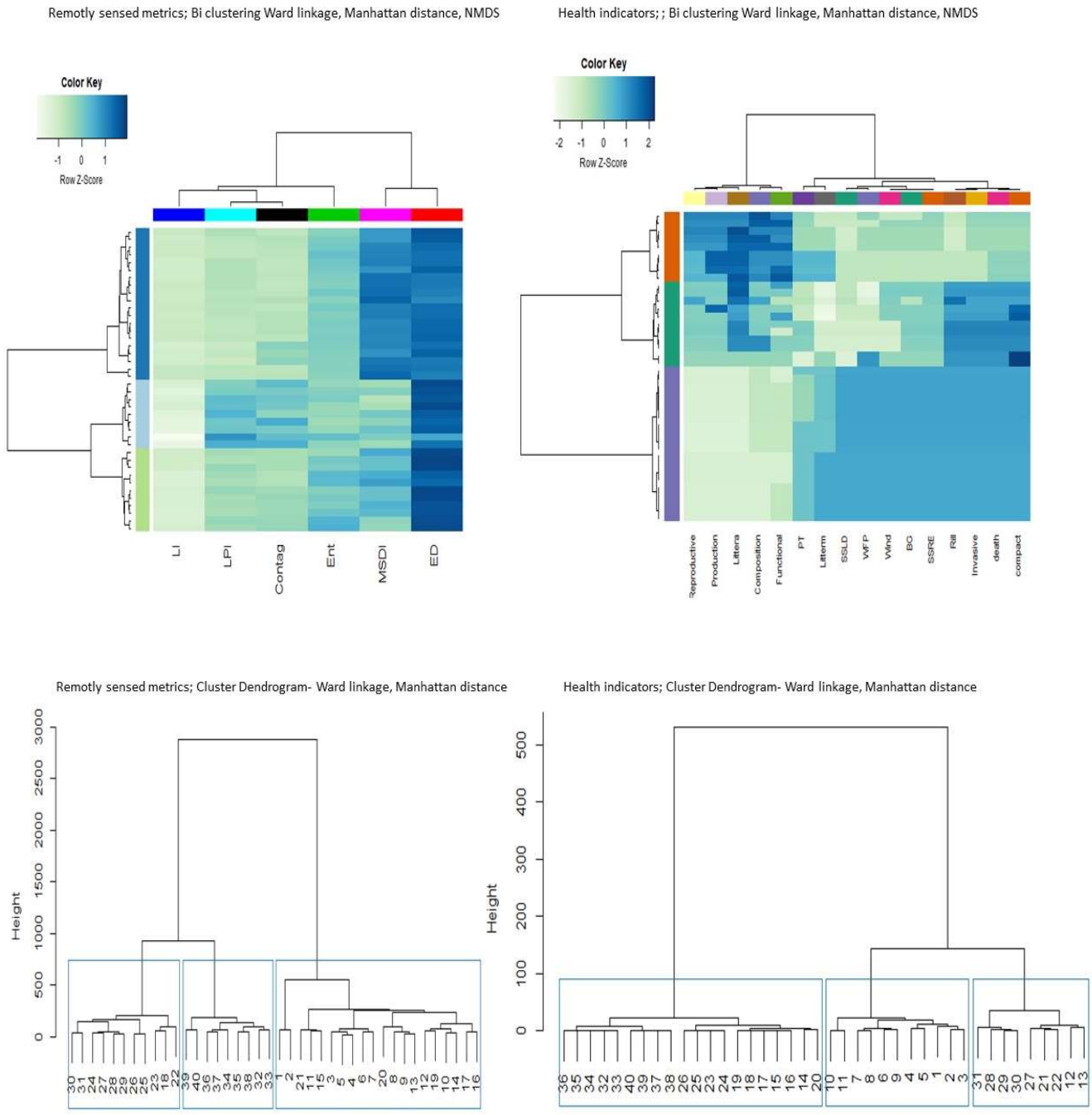

Fig. S3C Heatmaps with clustering results of Bi-clustering of sites and indicators. Each heatmap is separated by two dendrograms based on ward linkage and Manhattan distance. The upper dendrograms are the expression of indicators and metrics, and the lower dendrograms are the expression of sites (NMI= 0.67).

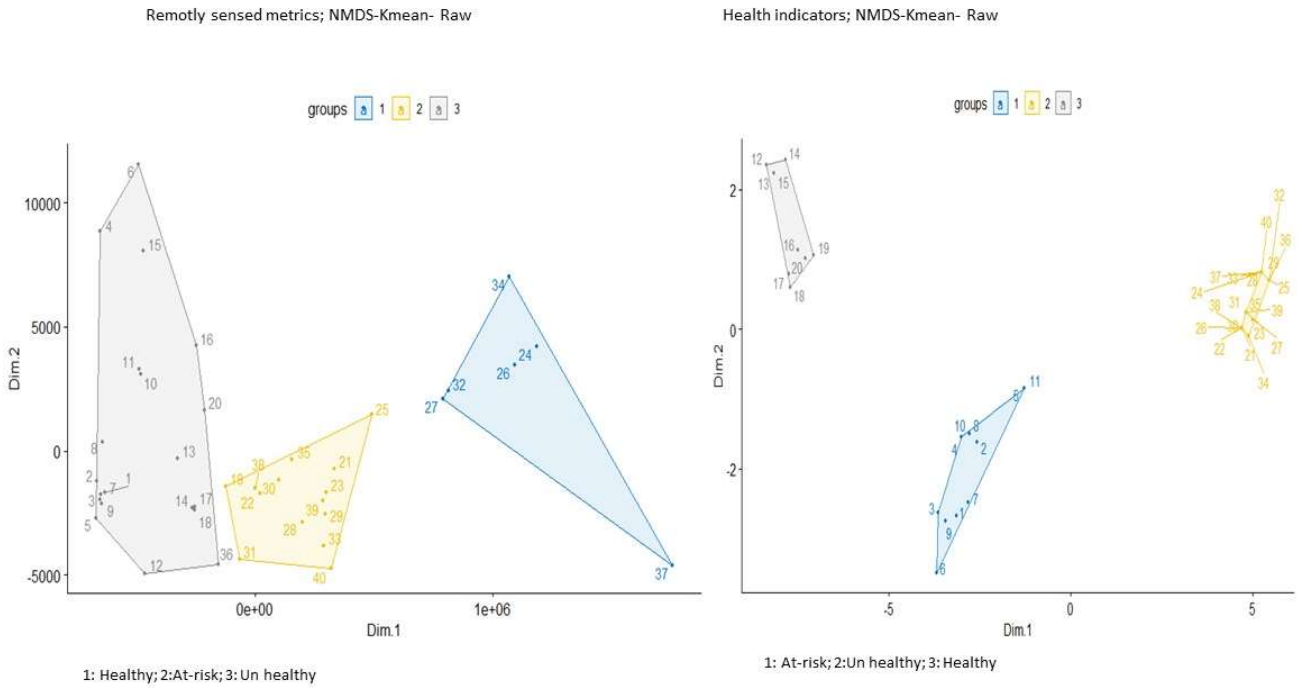

Fig S3D NMDS ordination and K-means clustering.

Supplementary file 6: Figure

The number of 25 SOM grids was determined by the Davies-Bouldin index value. SOM provides a comparison of the spatial clustering of health classes based on different health qualitative indicators and remote sensing quantitative input parameters. The spatial location of the cluster in the grid plot indicates the similarity with the other clusters and the contribution of the different variables and sites in determining the clusters. The 25 of SOM nodes were classified into three groups showing the probability of occurring each level of health. In left nodes, pink represents unhealthy class, and variables that are contained within these nodes have comparability higher unhealthy values. According to the results, the first health class for 1987 has been classified within the 19th node (Figure S. 5b). This means health classes within node number 19have higher values of edge density and leakiness of resources but low contagion values. For year the 2016, the first unhealthy class has been classified within the 24th node (Figure S. 4c) and categorized as unhealthy sites.

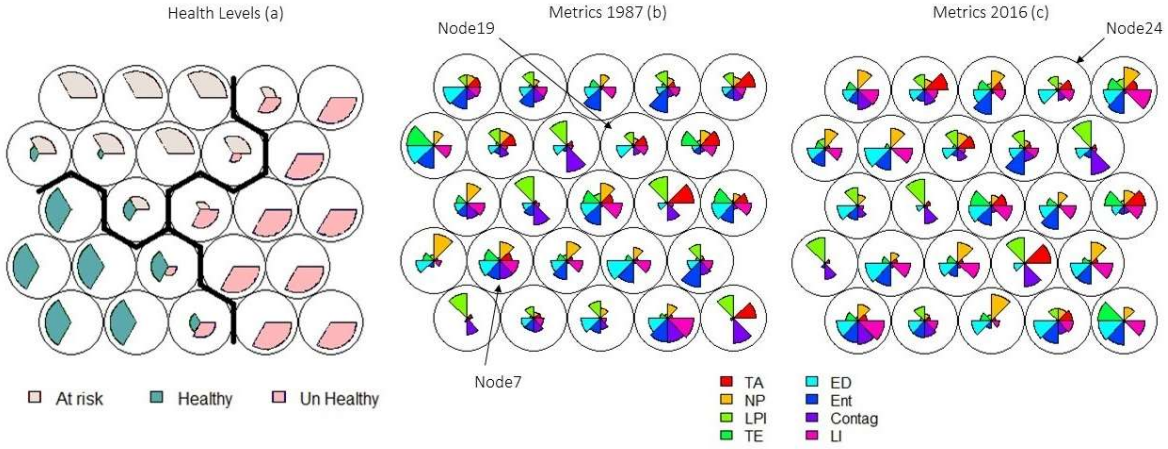

Fig. S4 These nodes contain information about different metrics in health classes. A big fan in any particular node represents higher impact of special variables. Each color in the codes plot represents one of the variables in the dataset (b and c).

Chapter 3

Tracking effects of extreme drought on coniferous forests from space using Dynamic Habitat Indices

Mojdeh Safaei[a*] Till Kleinebecker[a, b] Manuel Weis[c] André Große-Stoltenberg[a, b]

a Division of Landscape Ecology and Landscape Planning, Institute of Landscape Ecology and Resource Management, IFZ Research Centre for Biosystems, Land Use and Nutrition, Justus Liebig University Giessen, Heinrich-Buff Ring 26-32, 35392 Giessen, Germany

b Center for International Development and Environmental Research (ZEU), Senckenbergstrasse 3, 35390 Giessen, Germany

c Hessian Agency for Nature Conservation, Environment and Geology (HLNUG) Rheingaustraße 186, 65203 Wiesbaden, Germany

Corresponding authors: mojdeh.safaei@umwelt.uni-giessen.de, andre.grosse-stoltenberg@umwelt.uni-giessen.de
MS ORCiD: https://orcid.org/0000-0002-6509-8307
TK ORCiD: https://orcid.org/0000-0003-1121-2861
AGS ORCiD: https://orcid.org/0000-0001-6075-5497

Heliyon: Volume 10, Issue 7, 15 April 2024, e27864, https://doi.org/10.1016/j.heliyon.2024.e27864

Tracking effects of extreme drought on coniferous forests from space using Dynamic Habitat Indices

Abstracts

Terrestrial ecosystems such as coniferous forests in Central Europe are experiencing changes in health status following extreme droughts compounding with severe heat waves. The increasing temporal resolution and spatial coverage of earth observation data offer new opportunities to assess these dynamics. Dense time-series of optical satellite data allow for computing Dynamic Habitat Indices (DHIs), which have been predominantly used in biodiversity studies. However, DHIs cover three aspects of vegetation changes that could be affected by drought: annual productivity, minimum cover, and seasonality. Here, we evaluate the health status of coniferous forests in the federal state of Hesse in Germany over the period 2017-2020 including the severe drought year of 2018 using DHIs based on the Normalized Difference Vegetation Index (NDVI) for drought assessment. To identify the most important variables affecting coniferous forest die-off, a series of environmental variables together with the three DHIs components were used in a logistic regression (LR) model. Each DHI component changed significantly across non-damaged and damaged sites in all years (p-value 0.05). When comparing 2017 to 2019, DHI-based annual productivity decreased and seasonality increased. Most importantly, none of the DHI components had reached pre-drought conditions, which likely indicates a change in ecosystem functioning. We also identified spatially explicit areas highly affected by drought. The LR model revealed that in addition to common environmental parameters related to temperature, precipitation, and elevation, DHI components were the most important factors explaining the health status. Our analysis demonstrates the potential of DHIs to capture the effect of drought events on Central European coniferous forest ecosystems. Since the spaceborne data are available at the global level, this approach can be applied to track the dynamics of ecosystem conditions in other regions, at larger spatial scales, and for other Land Use/Land Cover types.

Keywords

dynamic habitat indices, coniferous forest, ecosystem health, extreme drought events, Germany

Introduction

Severe drought events and heatwaves currently represent major driving forces behind forest die-off, (Haberstroh et al., 2022; Senf et al., 2020; Senf and Seidl, 2018), and the risk of megadrought events is likely to increase (Cook et al., 2022). This can push forest ecosystems beyond their historic range of disturbance (Johnstone et al., 2016) and thereby posing a threat to forest resilience (Brodrick et al., 2019; Philipp et al., 2021; Senf and Seidl, 2018; Senf and Seidl, 2021a, 2021b) and can cause vast changes in vegetation dynamics (Gonçalves et al., 2020; Jiang et al., 2020; Sheffield and Wood, 2011; Zink et al., 2016). Forests in Germany, as in other central European countries, have encountered droughts and heatwaves of various magnitudes in recent years (Senf and Seidl, 2021b). The extreme droughts between 2018 (with 3.3°C higher than the long-term average from 1961 to 1990 (Schuldt et al., 2020)) and 2020 severely affected Central Germany, where in certain parts in central Germany up to two-thirds of coniferous forests died (Thonfeld et al., 2022) and certain tree species such as Spruce Scots pine (*Pinus sylvestris* L.) potentially having reached tipping point (Haberstroh et al., 2022).

Remote sensing of vegetation indices enables the monitoring of drought conditions at large spatial extents and could support monitoring and management efforts accounting for the dynamic nature of ecosystem health (Ge et al., 2021; Li et al., 2022; Philipp et al., 2021). For example, continuous space-borne measures such as phenological metrics (Eitel et al., 2023) provide more direct links to ecosystem functioning than discrete classifications (Coops and Wulder, 2019). Consequently, metrics calculated from remotely sensed time series data such as Dynamic Habitat Indices (DHIs), which rely on productivity properties, such as vegetation greenness or degree of vegetation seasonality, provide a baseline of the (natural) variability in ecosystem health and degradation (Coops et al., 2008; Razenkova et al., 2020).

DHIs are useful tools to summarize measures of vegetative productivity including the cumulative and minimum annual productivity as well as variation in annual productivity (Coops et al., 2008). DHIs have been derived at 1 km spatial resolution for Australia (Mackey et al., 2004), Canada (Coops et al. 2008), and recently at global scale (Coops et al., 2018). The availability of remote sensing products such as the Normalized Difference Vegetation Index (NDVI), Leaf Area Index (LAI), the fraction of light absorbed by the vegetation (fPAR), or estimates of Gross Primary Productivity (GPP) derived from globally available MODIS satellite data clearly facilitates the calculation of DHIs (Coops et al., 2008; Hobi et al., 2017). However, with the increasing availability of remote sensing products with high temporal resolution, for example from the European

Copernicus Land Monitoring service that provides global NDVI data at 300m resolution with an interval of 10 days (Copernicus, 2022), these high temporal scale data products have a great potential for exploring ecosystem dynamics using composite vegetation indices such as the DHI.

The increasing temporal extent of baseline data to compute DHIs also allows for analyzing changes in DHIs over successive years across Land Use Land Cover types (Safaei et al., 2023). For example, identifying significant deviations from the long-term mean or a baseline state can facilitate to demarcate regions undergoing changes in ecosystem conditions (Coops et al., 2008; Hobi et al., 2017; Razenkova et al., 2020; Savtchenko et al., 2004). To the best of our knowledge, DHIs have not been used to explore the health characteristics of coniferous forests affected by drought, yet. This is even more remarkable as DHIs may hold a substantial potential to refine the understanding between vegetation dynamics (Coops et al., 2018; Razenkova et al., 2020) and severe drought events (Thonfeld et al., 2022).

Here, we present a detailed spatiotemporal analysis of a NDVI-based DHI across coniferous forests of Hesse, Germany. The specific objectives include (1) establishing a Hessian dynamic habitat index (DHI_{Total}) using spaceborne NDVI data at 300m resolution, (2) identifying the DHI based health status of the coniferous forest before the severe drought event in 2018 and its potential recovery afterwards, (3) identifying where the drought event had strongest effects using spatiotemporal analysis, and (4) exploring the relationship between the environmental drivers, DHI components and coniferous health status.

Material and Methods

Study area

This study was conducted in the federal state of Hesse, Germany (Fig. 3-1). The mean annual temperature (1981-2010) is 8.8 °C. It increased from 8.2 °C between 1951 and 1980, and it is still rising. There is a considerable spatial variation of annual increase ranging from almost 0 in some northern parts to +1.4°C in the south. The annual precipitation increased slightly from 735mm (1901-1930) to 807mm (1981-2010). As for precipitation, there is a clear spatial variability of precipitation ranging from around 500mm in the Upper Rhine Valley to 1400mm at the higher elevations of e.g. the Vogelsberg or the Rhön (HLNUG, 2022).

According to the Climate Protection Scenario in Hesse, an increase in the number of particularly hot days with temperatures above 30 °C is very likely (HLNUG, 2022). Precipitation is predicted to shift from summer to winter and will be more likely fall as rain instead of snow in winter. The

probability and the severity of heavy precipitation and drought events will increase in the future (HLNUG, 2018).

In Hesse, forests cover more than 40 % of the land surface (about 894000 ha). More than half of these are dominated by broad-leaved tree species such as *Fagus sylvatica* L. (Beech) and *Quercus robur* L (Oak). Beech and oak together account for 43.8% of the forest area. Conifers make up almost 40%. The main coniferous tree species are *Picea abies* (L.) Karst. (Spruce), *Pinus sylvestris* L. (Scots pine), *Pseudotsuga menziesii* Franco (Douglas fir), and *Abies alba* Mill. (silver fir) (Panek, 2018). As a result of storm events (and subsequent bark beetle infestation), the area of spruce forests decreased by more than 20000 ha between 2002 and 2012. This was associated with an increase in deciduous forests and Douglas fir, which is more and more used as a "replacement" for spruce (Panek, 2018).

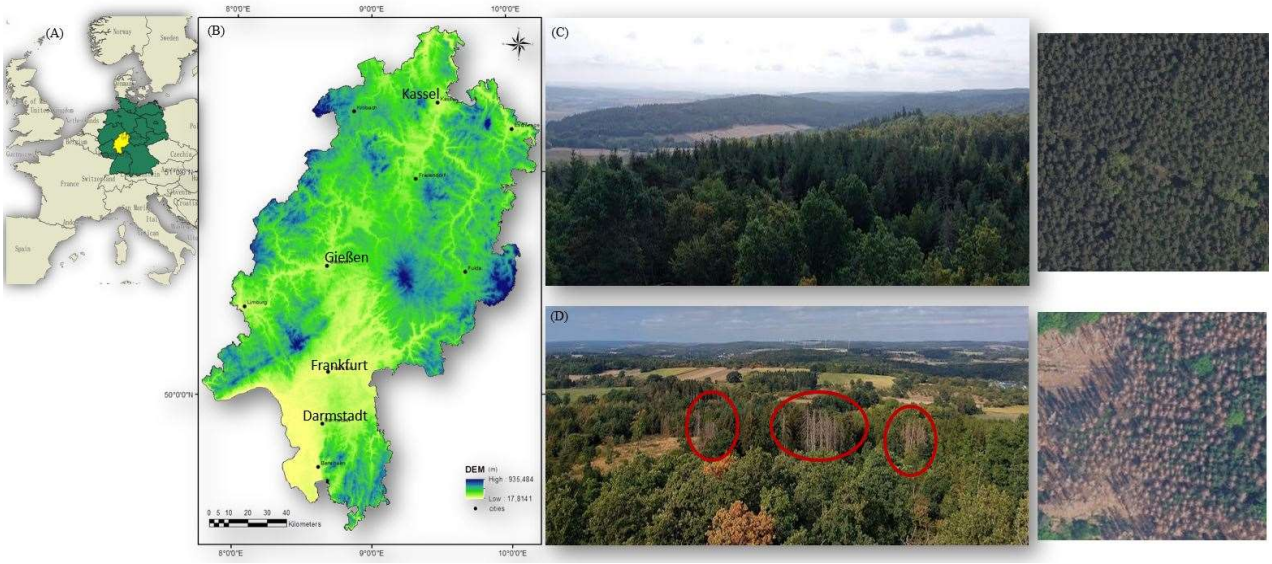

Figure 3-1 (A) Location of the federal state of Hesse in central Germany and in Europe (B) the digital elevation model (DEM) (NASA, 2020) ranging between 75 and 950 meters above sea level. Photos show some indication of the health status of coniferous forests: (C) example of a non-damaged site and (D) of a damaged site. Photos were taken by the first-author in August 2022 in the Vogelsberg region and aerial overview pictures are derived from digital orthophotos of the Hessian geoportal (Geoportal Hessen, 2022).

Data

Satellite data

To compute the DHI_{Total}, we used the NDVI product of the Copernicus Global Land Service with a spatial resolution of 300m (Copernicus, 2022). It is a 10-daily synthesis product derived from PROBA-V observations (Copernicus, 2022). We used data from Jan 01 2017 until

Dec 31 2020, that showed consistent data value ranges, to calculate the Hessian DHIs to examine the sudden effects of the extreme drought of 2018. Recent studies demonstrated the applicability of the DHI for similar temporal ranges (Silveira et al., 2023; Sun et al., 2021; Zhi et al., 2022). Further, recent analysis of annual, satellite-derived NDVI data showed the effect of the 2018 drought on ecosystem conditions in Europe (Brun et al., 2020) including central European forests (Buras et al., 2020; Schuldt et al., 2020). Notably, such data can potentially be applied to track coniferous forest health (Haberstroh et al., 2022). In addition to NDVI data, a satellite-based digital elevation model (DEM) (NASA, 2020) was used to derive elevation above sea level as an topographical predictor of the health status of coniferous forests (Table 3-1).

Climate data

Various climate datasets related to vegetation and ecophysiology of plants were obtained from the Climate Data Center (CDC) (https://cdc.dwd.de/portal/) including grids of monthly total precipitation (CDC, 2022a), monthly mean of minimum daily air temperature in 2 m height above ground (CDC, 2022b), monthly total sunshine duration (CDC, 2022c), as well as grids of monthly drought index (de Martonne index= dMI (CDC, 2022d; de Martonne, 1941)). The dMI is calculated based on Equation 1.

$$\text{(de Martonne, 1941): } dMI = \frac{P}{T+10} \qquad (1)$$

T refers to the temperature in degrees Celsius from temperature grids and P refers to the precipitation in mm from precipitation grids. This index shows the aridity of regional climate zones and provides information on the drought level at a given site (Bhuyan et al., 2017). Lower dMI values indicate drought while increased values indicate more water is available for trees. The dMI has been used to describe the extreme drought conditions for summer 2018 in Central Germany (Beloiu et al., 2022).

In order to investigate the relationship between DHI and climatic drivers, we calculated the cumulative, minimum, and variation of the climate variables (Table 3-1).

Coniferous forest data

Geodata on the damage of coniferous forests were obtained from the Hessian state forestry service (Weis, 2022). Since bark beetle outbreaks following the deep depression Friederike in January 2018, the forestry service regularly monitors coniferous forest health in early summer

(Weis, 2022). Damaged forests are detected based on multispectral Sentinel 2 data and pixel-based change detection using the NDVI (Weis, 2022). Random Forest (Breiman, 2001) was used to generate a spatial analysis mask, describing the exact distribution of coniferous forests in summer 2017, before the winter storm Friederike and the associated bark beetle outbreak. This mask allows to define sharp thresholds for damage detection resulting in complete spatiotemporal patterns of forestry damage(Weis, 2022). To identify non-damaged areas, the CORINE Land-use and Land cover (LULC) map was used to extract coniferous forests in Hesse (CORINE Land Cover Product User Manual, 2018). Coniferous forest patches displaying a homogenous green texture based on digital orthophotos (DOP) from the geoportal of Hesse (Geoportal Hessen, 2022) were classified as non-damaged. (Fig. 3-1C). After that, we applied spatial thinning using "spThin", and spatial autocorrelation was checked using "acf" R package (R Core Team, 2021). We found no spatial autocorrelation in our dataset.

Table 3-1 Datasets and extracted variables used in this study.

Dataset	Abbreviation	Temporal res. and coverage	Spatial res.	Variables
Normalized difference vegetation index Copernicus (Copernicus, 2022)	NDVI	10 days, 01.01.2017- 31.12.2020	300m	Annual Productivity Minimum cover Seasonality
Digital elevation model (NASA, 2020)	DEM	11.02.2000 to 21.02.2000	30 m	DEM
CORINE Landuse/ land cover (CORINE Land Cover Product User Manual, 2018)	LULC	2018	100 m	LULC
Monthly total precipitation (mm) (CDC, 2022a)	MTP	30 days, 01.01.2017-31.12.2020	1000m	Cumulative
Mean of the monthly averaged minimum daily air temperature (1/10°C) (CDC, 2022b)	MMT	30 days, 01.01.2017-31.12.2020	1000m	Minimum Variation of each climate dataset
Monthly total sunshine duration (h) (CDC, 2022c)	MTS	30 days, 01.01.2017-31.12.2020	1000m	
Monthly drought index (de Martonne index) (CDC, 2022d)	dMI	30 days, 01.01.2017-31.12.2020	1000 m	
Coniferous forest damage map (Weis, 2022)		2018 and 2019	10 m	Damaged area
Orthophotos ((Geoportal Hessen, 2022)		2018 and 2019	20 cm	Identify and verify Damaged and non-damaged sites

The Hessian Dynamic Habitat Index (DHI_{Total})

NDVI data from 2017 to 2020 were recorded with an interval of 10 days (Copernicus, 2022), thus three tiles were collected per month resulting in 36 tiles for each year and a total of 144 tiles for the full 4-year dataset. For each year, yearly NDVI composites were used to obtain the three DHI components, i.e., cumulative DHI (DHI_{Cum}), minimum DHI (DHI_{Min}), and variation DHI (DHI_{Var}). Here, the three components of DHI_{Total} were computed over the time period 2017-2020 from the NDVI layers based on Equation 2(Hobi et al., 2017):

$$DHI_{Cum} = \sum p_t \qquad DHI_{min} = \min(p_t) \qquad DHI_{Var} = \frac{\sigma(p_t)}{\mu(p_t)} \qquad t = 1..n \qquad (2)$$

where p represents vegetation productivity at different periods (t) during a year (Coops et al., 2008; Hobi et al., 2017). DHI_{Cum} refers to the cumulative productivity values for all time periods over a year, DHI_{Min} refers to the minimum productivity value within a year, and DHI_{Var} refers to the seasonality of the productivity calculated based on the coefficient of variation using the standard deviation and the mean ($\sigma(p_t)/\ \mu(p_t)$) (Coops et al., 2008; Hobi et al., 2017). In addition, the long-term mean of each indicator was calculated as the median over the full four-year period. Further details on DHI calculation are described by (Coops et al., 2008; Hobi et al., 2017; Michaud et al., 2012; Razenkova et al., 2020).

To reveal the extent to which the three DHI components complement each other (Radeloff et al., 2019), we performed Spearman correlation analyses between DHI_{Cum}, DHI_{Min}, and DHI_{Var}. In addition, we tested the correlation of the DHI components with the climatic variables under study.

Yearly comparison

One-way analysis of variance (ANOVA) was performed to test differences in DHI components across damaged and non-damaged coniferous forests within each of the four years using the "car" package (R Core Team, 2021). We met the assumptions of one-way ANOVA using the Shapiro-Wilk test, Q-Q plot of residuals, and Bartlett's Test (A. Zuur et al., 2009). To test for immediate or time-delayed effects of the severe drought in 2018 and for possible recovery, we calculated the change of the DHI components between each combination of years.

We performed Theil–Sen's test and Ordinary Least Squares (OLS) with a moving window

(Lu et al., 2016; Verbesselt et al., 2010) to investigate the overall trends of the three DHI components. Theil–Sen's test is a non-parametric and robust method concerning missing values and non-normal distributions (Theil, 1992).. To assess the effect of drought on the observed trends, we first classified cumulative drought into four zones including arid, semi-arid, semi-humid, and humid and identified areas with high aridity over time. These classes which indicated the aridity of regional climate zones came from equal intervals of cumulative drought maps. To figure out which cells had a considerable trend across the time we applied a 20% threshold on the DHIs components on the entire distribution of trend values (Michaud et al., 2012); (Wulder et al., 2007). Finally, we used the positive-to-negative trend ratio to understand how health status was affected by which arid zone.

Environmental variables across health status

To distinguish which variables were related to the health status, and to gain a better understanding of the trend analysis, we added further environmental variables such as cumulative, minimum, and variation precipitation, temperature, sunshine duration, and monthly drought index (Table 1) to our analysis. Strongly intercorrelated variables ($|R| > 0.8$) were removed (Hinkle et al., 2003). We used logistic regression (LR) as a subtype of generalized linear models (GLM) and chose binomial distribution (Dobson and Barnett, 1990) as the response data are binary (damaged, non-damaged) using the "glm" function in R statistical software (R Core Team, 2021). The model was built based on Equation 3.

$$p(X)\frac{e^{\beta 0 + \beta 1 X1 + \beta 2 X2 + \ldots + \beta p Xp}}{(1 + e^{\beta 0 + \beta 1 X1 + \beta 2 X2 + \ldots + \beta p Xp})} \qquad (3)$$

p: the probability of occurrence of an event, β_0: model constant, β_i: regression coefficients, and X_i: environmental variables (McCullagh, 1989). To assess how well the LR model fits the data, McFadden's R^2 using "pR2" function from the "pscl" package was employed. Values close to 0 indicate low goodness of-fit, and values over 0.40 indicate a very good model fit (McFadden, 1977). The importance of each environmental variable using the "varImp" function from the "caret" package was computed. To minimize effects of multicollinearity, variables with variance inflation factor (VIF)> 5 were removed (James et al., 2013).

All statistical and geospatial analyses were performed in R statistical software ver. 4 (R Core Team, 2021) and QGIS ver. 3.22 LTR Białowieża and gdal wrap (QGIS Development Team, 2021). The general framework of our study is summarized in Figure 3-2.

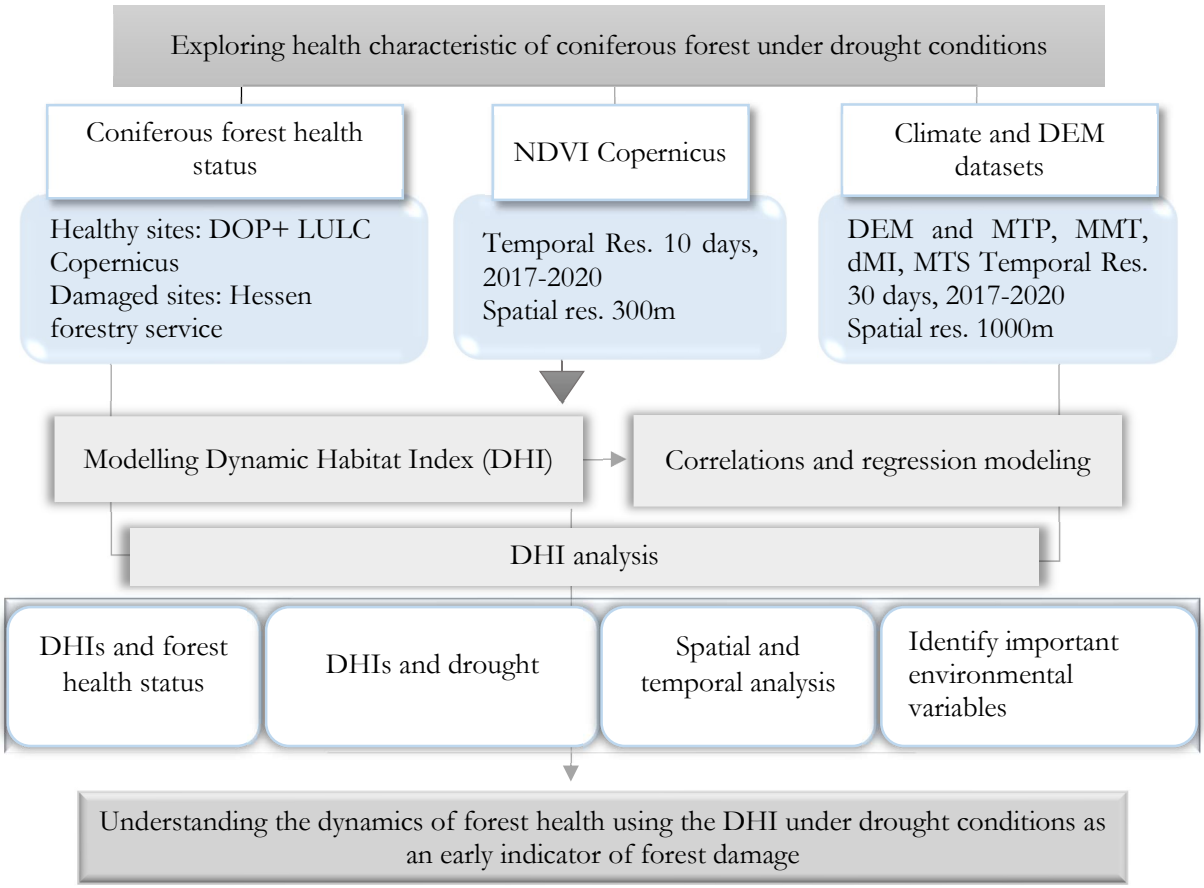

Figure 3-2 Methodological steps of the inputs, analysis, and outputs. DOP: Digital orthophotos, DEM: digital elevation model, MTP: monthly total precipitation, MMT: mean of the monthly averaged minimum daily air temperature, dMI: Monthly drought index (de Martonne index), and MTS: monthly total sunshine duration, DHI: Dynamic habitat index, and LULC: Land Use Land Cover

Results

The Hessian Dynamic Habitat Index (DHI_{Total})

The three components of the DHI_{Total} varied across time and space (Fig. 3-3A, B, C) as did the DHI_{Total} (Fig. 3-3D). DHI_{Cum} (annual productivity) dropped in 2018 (Fig. 3-3A), while DHI_{Min} (minimum coverage) clearly decreased in 2020 (Fig. 3-3B). DHI_{Var} (seasonality) in 2018 is different from all other years (Fig. 3-3C). DHI_{Total} captured the variability in the vegetative productivity patterns during 2017-2020, and the contribution of each DHI component to DHI_{Total} varied between the years (Fig. 3-3D). For example, while some regions were characterized constantly by high seasonality, low annual productivity and low minimum cover (blueish colours), the location

of areas with moderate seasonality, high annual productivity and low minimum cover (reddish purple) varied (Fig. 3-3D).

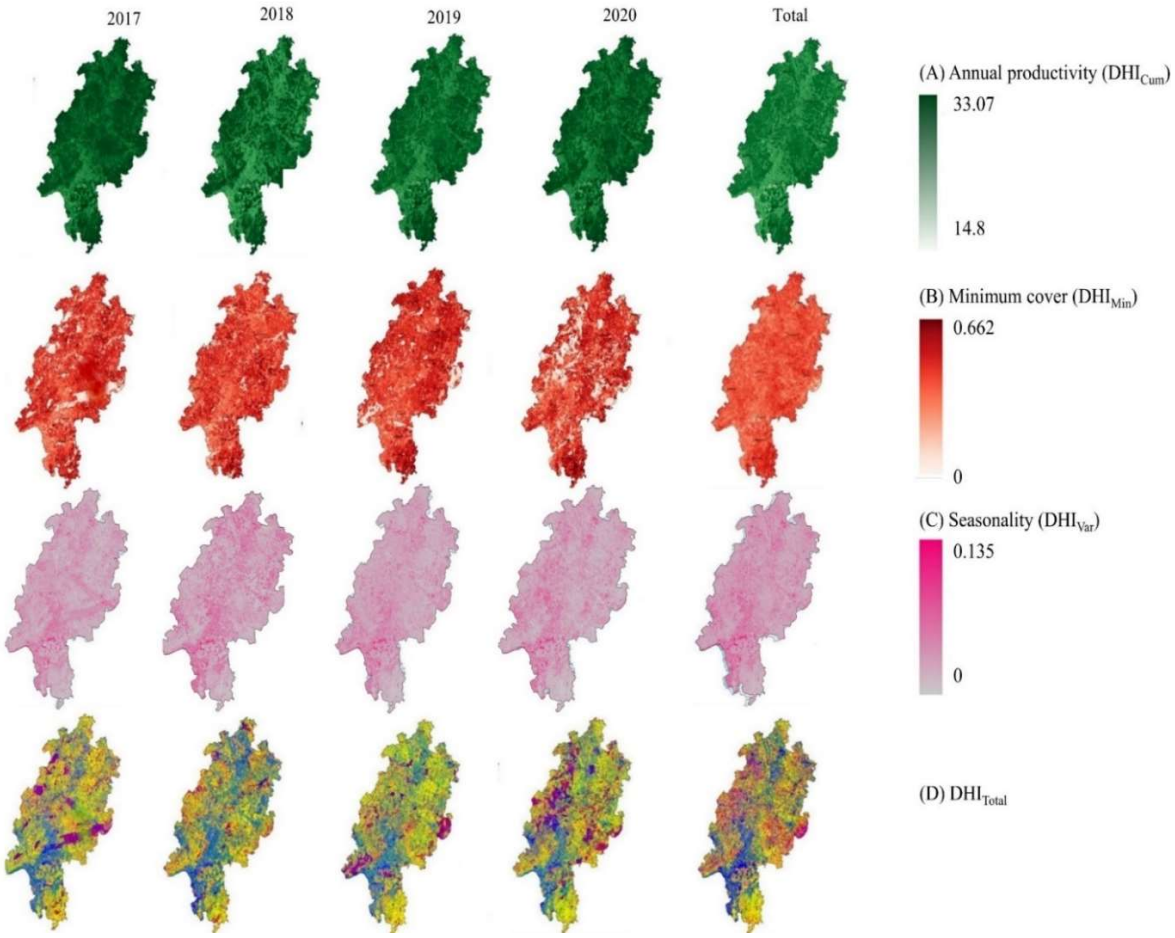

DHI's Legend						
Seasonality	Low	Moderate	Moderate	Low	High	High
Annual productivity	High	High	High	Moderate	Moderate	Low
Minimum Cover	High	High	Low	Moderate	Moderate	Low

Figure 3-3. Maps of each year and for all years combinedof the DHI components (A) annual productivity (DHI_{Cum}), (B) minimum cover (DHI_{Min}), and (C) seasonality (DHI_{Var}), which are calculated based on 10-day NDVI data per year, and (D) of the merged components (DHI_{Total}) over the 4 years of observations from 01.01.2017 to 31.12.2020.

Three DHI_{Total} components were moderately to strongly correlated with each other (Fig. 3-4). There was a positive correlation between annual productivity and minimum cover values (R^2

= 0.42). Seasonality was negatively correlated to minimum cover and annual productivity (R^2 = −0.71 and −0.66, respectively) (Fig. 3-4B, C). This indicated that the highest values of DHI_{Var} occurred at the lowest DHI_{Min} and DHI_{Cum}. The DHI components correlated moderately positively with precipitation, drought, and temperature variables (See Table S1 and Fig. S3).

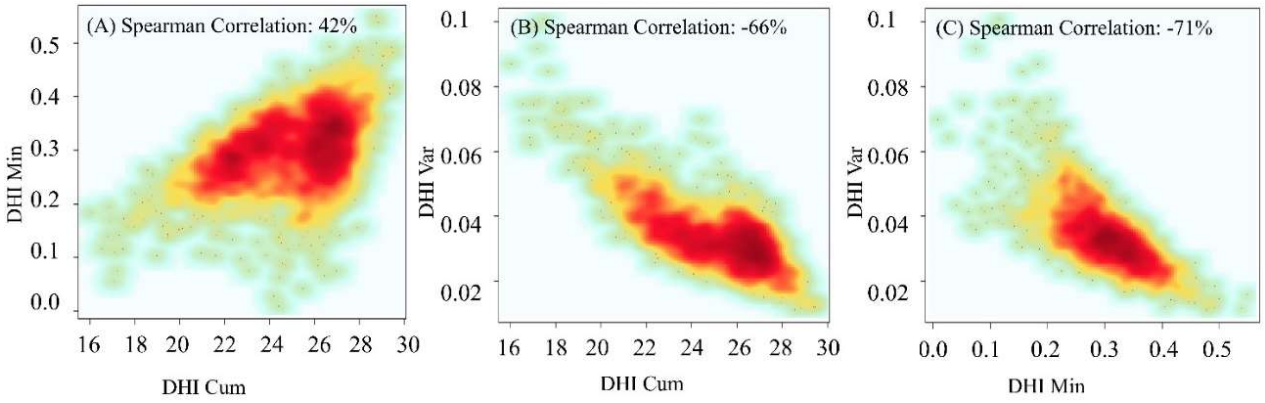

Figure 3-4 Correlations among the three DHITotal components derived from NDVI. The three DHITotal components were moderate to strongly correlated with each other. DHICum: Annual Productivity, DHIMin: Minimum cover, and DHIVar: Seasonality. The color range is based on the density of points. Dense points of each scatter plot were shown with red color and by decreasing points density it changed to orange, yellow, and then green.

Yearly comparison between non-damaged and damaged coniferous forests

Annual productivity and minimum cover were significantly higher for non-damaged sites compared to damaged sites throughout the years (Fig.3-5A and B). The seasonality component was constantly significantly lower (Fig. 3-5C) meaning that in non-damaged sites less variation (seasonality) occurred.

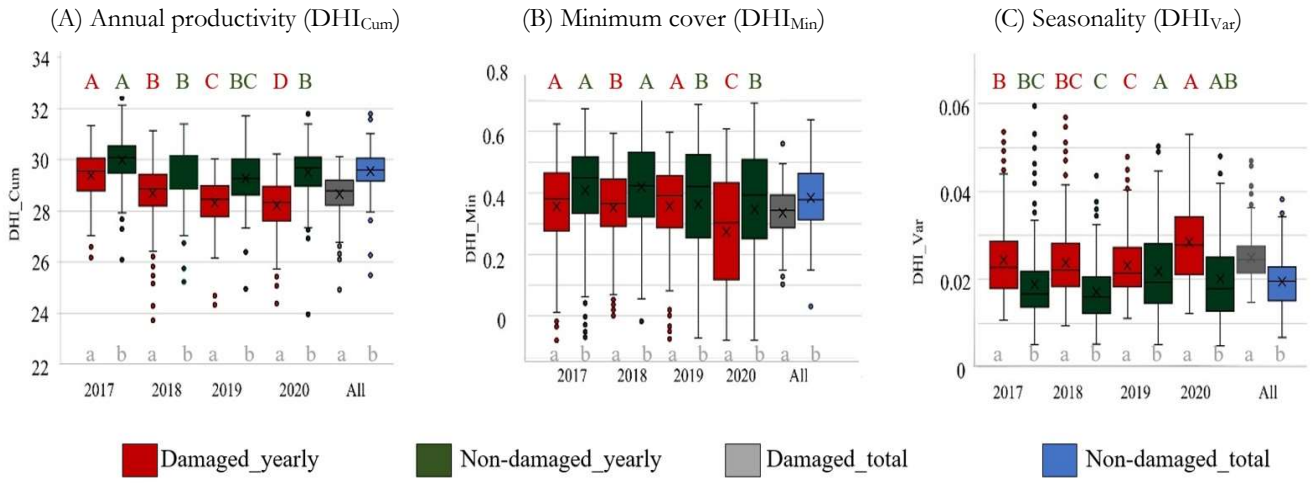

Figure 3-5 Comparison of damaged and non-damaged coniferous forests for each DHI component for each year (A, B, and C). The capital letters indicate significant differences related to the non-damaged (green letters) and damaged sites (red letters) between years. The lowercase letters in grey indicate significant differences regarding the health status within each year using the Tukey post hoc test (p-value<0.05). For example, grey lowercase letters in 2017 mean that there is a significant difference related to the non-damaged and damaged sites.

When analysing the changes of the DHI components in damaged sites between the years (Fig. 3-6A), annual productivity first decreased with the most negative changes being observed between 2017 (pre-drought) and 2019 but showed partial recovery in 2020 where it reached its maximum. In contrast, minimum coverage significant decreased in 2020 (Fig. 3-6B). So, while annual productivity and minimum cover were moderately positively correlated for the whole time span (Fig. 3-4), yearly comparison showed different and partly opposing trends. The third DHI component seasonality first decreased, but then continuously increased since 2019 (Fig. 3-6C). Thus, annual productivity in damaged sites was mostly negative, but showed a positive trend and became positive in 2020, while the seasonality increased across all the years apart from a decrease due the 2018 drought event. Minimum cover increased towards 2019 but was negative otherwise. So, all DHI components differed significantly between non-damaged and damaged sites, and they did so even before the drought event 2018 (Fig. 3-5, 6). Compared to 2017, damaged sites showed different characteristics after the drought for all DHI components. While annual productivity showed a partial recovery, minimum cover rather decreased and seasonality rather increased (Fig. 3-6 and Fig. S.1).

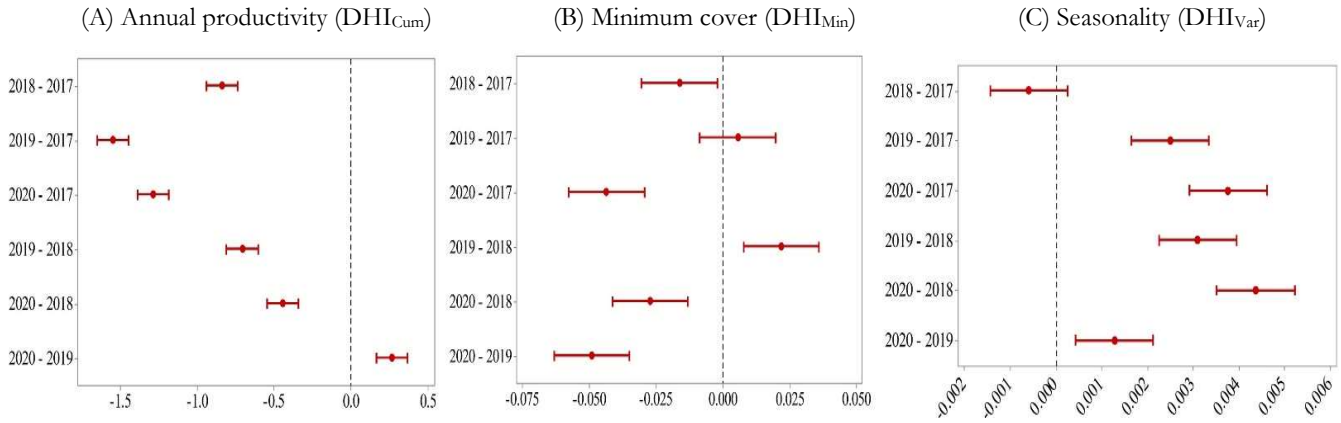

Figure 3-6. Visualizations of the drought effects across damaged sites. The plots show Tukey's simultaneous tests for differences in DHIs means within years. The confidence intervals display the likely ranges for all of

the differences in the means. If an interval does not intersect the zero line, the corresponding means are significantly different (p-value<0.05).

Spatial and temporal dimension of coniferous forest health status

We explored the spatial dimension of DHI changes of coniferous forest from 2017 to 2020 (Fig. 3-7A) and identified a set these changes into relation with the aridity zones after de Martonne index (Fig. 3-7B). We then explored the negative or positive trends of the DHI components for different aridity zones based on the dMI (Fig. 3-7C and Table 3-2).

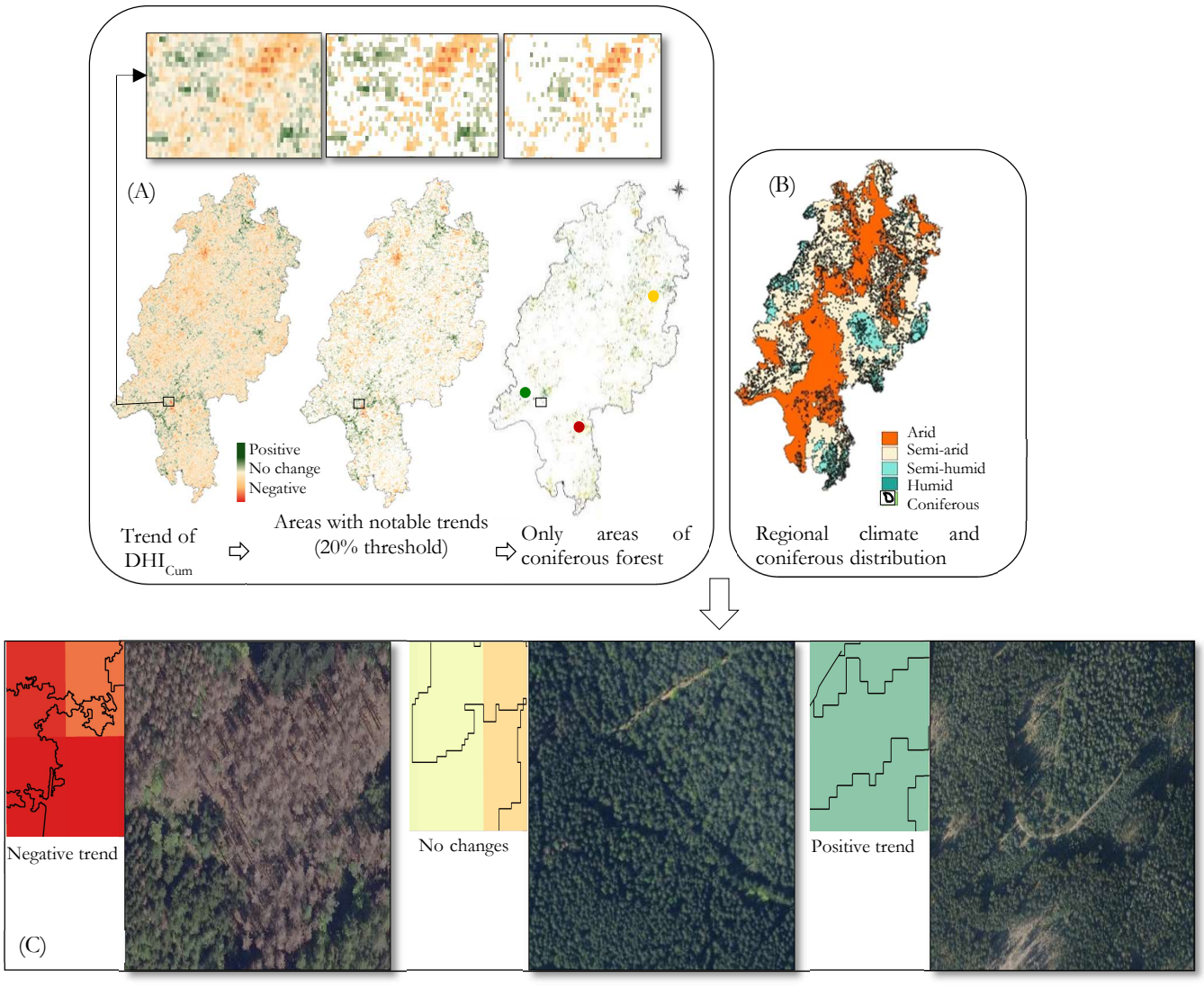

Figure 3-7. Results of spatial analysis to capture the effects of drought on the DHI's trend (A) Example of DHICum trend analysis spanning from 2017 until 2020 (See Fig. S2 for more maps) for coniferous forests. Small boxes above are zoomed in the area to see more details. (B) The accumulated drought map based on the de Martonne index (dMI) ranging from "low accumulated drought" (dark green) to "high accumulated

drought" (orange) overlaid with (in black) a coniferous forest map. (C) Examples of coniferous forests showing negative (red), indifferent (yellow) or positive (blue) trends over four years.

The area of coniferous forest for each aridity zone equalled 42284 ha for arid zone (16% of the total coniferous forest area), 165542 ha for semi-arid zone (62%), 55108 ha for semi-humid zone1 (21%), and 3243 ha for humid zone (1%). Most positive trends of the DHI components were found at the rather humid end of the dMI aridity gradient (Table 3-2). For example, the most positive trend of DHI_{Cum} considering all years (2.65, Table 3-2) was observed when the drought effect decreased (semi-humid zone), while the least positive trend (1.39) was observed when drought increased (semi-arid zone, Table 3-2). Coniferous forests rarely occurred in areas which were characterized by strong drought effect (arid zone), and this could explain the positive trend in this zone (Fig. 3-7C). The highest coniferous coverage occurred in the semi-arid zone. The overall trends were similar for non-damaged and damaged forest (Table 3-2). However, in damaged sites the positive-to-negative ratios of DHI_{Cum} were lower, but DHI_{Var} was higher compared to non-damaged sites (Table 3-2). DHI_{Min} was generally lower in damaged forest apart from rather humid zone (Table 3-2).

Table 3-2. The ratio of the positive trend to the negative trend of the area in each arid zone for each DHI component across health status. Sparklines refer to the ratios across arid zone for each DHI component.

The ratio of positive to negative trend of the area under aridity zones after de Martonne index (dMI)						
DHI Components \ arid zones		Arid	Semi-arid	Semi-humid	humid	Sparkline
Total	DHI_{Cum}	2.08	1.39	1.65	2.65	
	DHI_{Var}	0.30	0.17	0.04	0.02	
	DHI_{Min}	0.89	1.21	2.59	2.72	
Damaged	DHI_{Cum}	0,16	0.26	0,33	0,51	
	DHI_{Var}	0.55	0.43	0.09	0.04	
	DHI_{Min}	0.70	0.86	2.01	3.00	
Non-	DHI_{Cum}	1.95	1.20	1.43	2.33	
	DHI_{Var}	0.29	0.14	0.04	0.02	
	DHI_{Min}	0.90	1.29	2.69	2.70	

Analysis revealed that most damages of the coniferous forests did not occur in the areas where maximum accumulated drought was located, but rather in the semi-arid zone, where most of the coniferous forest occurred (Table 3-2). Consequently, most damaged coniferous forests were observed at altitudes lower than 350 meters with pronounced, but not maximum cumulative drought. Most of the non-damaged forests occurred at higher altitudes of 350 and lower cumulative drought (semi-humid zone, and y = 12.867x – 147.27 with R^2= 0.73) (Fig. 3-8).

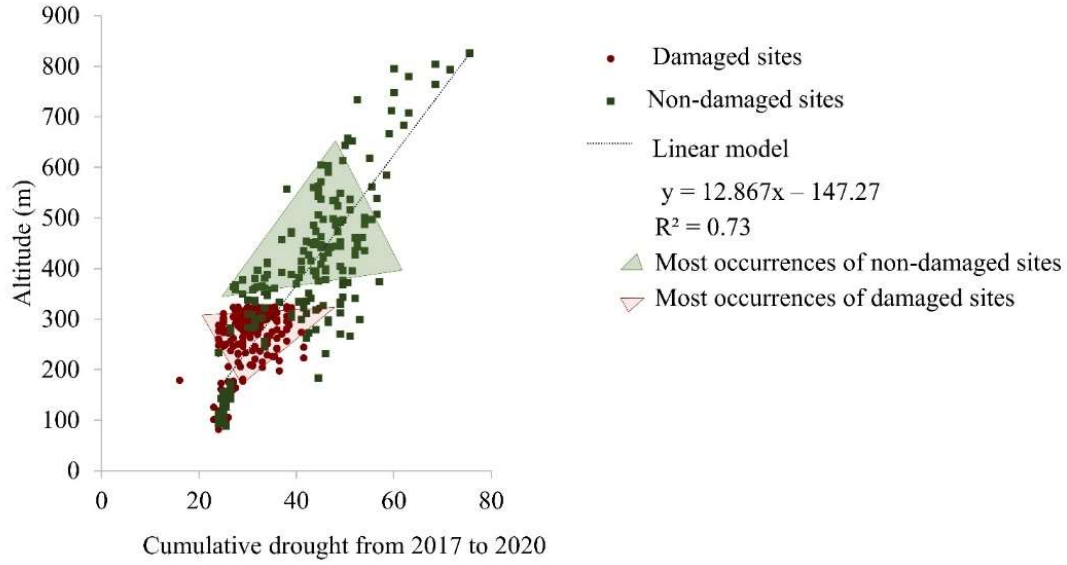

Figure 3-8. Linear regression between altitude and cumulative drought index (dMI) from 2017 to 2020. Non-damaged sites are displayed in green, and damaged sites are in red. Lower values of cumulative drought indicate stronger drought effects.

Environmental factors affecting health status

Finally, we investigated which environmental factors and which DHI components explained the coniferous health status (Table 3-3). Out of initially 16 predictors 9 (mainly climatic variables) were removed due to high correlation > 0.8 and high collinearity > 5, and 7 remained in the final model. Among them were all DHI components (Table 3-3). Logistic regression analysis revealed that the most important factors explaining the health status were the variation in temperature, annual productivity (DHI_{Cum}), altitude, minimum coverage (DHI_{Min}), cumulative drought, and minimum sunshine duration (Table 3-3, Fig. 3-9). Seasonality (DHI_{Var}) was among the most important predictors (Fig. 3-9), but it was not significant (Tab. 3-3). McFadden's R^2 value

of 0. 44 indicated that the GLM model with a binomial family fit the environmental data very well (McFadden, 1974), and the results of variable importance matched up with the *p*-values from the model (Table 3-3 and Fig. 3-9). Thus, in addition to environmental parameters, DHI components were among the most important predictors of the distinction between degraded and non-degraded coniferous.

Table 3-3. shows the Logistic regression model coefficients and p-values. DHI_{Cum}: DHI Annual Productivity. DHI_{Var}: DHI Seasonality. DHI_{Min}: DHI minimum vegetation cover. TempVar: Variation in the monthly averaged minimum daily air temperature Sun_{Min}: Minimum monthly sunshine duration. Dry_{Cum}: Cumulative monthly drought index. DEM: Digital elevation model.

Coefficients:	Estimate	Std. Error	z value	Pr(>|z|)	Significant*
(Intercept)	-54.20	5.33	-10.16	< 0.0000002	***
DHI_{Cum}	1.27	0.16	7.68	1.55E-14	***
DHI_{Min}	-5.59	2.11	-2.64	0.00821	**
DHI_{Var}	-49.42	26.13	-1.89	0.05856	.
Sun_{Min}	-0.047	0.021	-2.17	0.02931	*
$Temp_{Var}$	0.007	0.0006	11.18	< 0.000002	***
Dry_{Cum}	0.044	0.017	2.54	0.01105	*
DEM	-0.007	0.001	-6.28	3.32E-10	***

*Significant codes: 0 '***' 0.001 '**' 0.01 '*' 0.05 '.' 0.1 ' ' 1

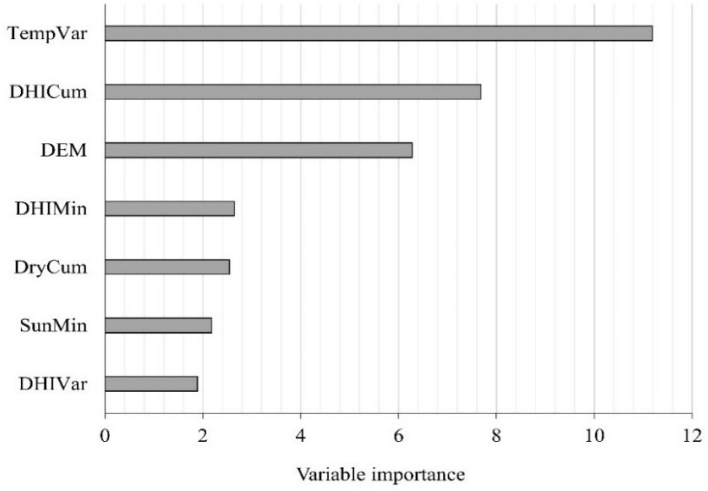

Figure 3-9. The importance of each predictor variable in the model. Higher values indicate more importance. DHI_{Cum}: DHI Annual Productivity. DHI_{Var}: DHI Seasonality. DHI_{Min}: DHI minimum vegetation cover.

$Temp_{Var}$: Variation in the monthly averaged minimum daily air temperature Sun_{Min}: Minimum monthly sunshine duration. Dry_{Cum}: Cumulative monthly drought index. DEM: Digital elevation model.

Discussion

In this study we show how vegetation information derived from satellite time series in the form of Dynamic Habitat Indices (DHI) can be used as indicators and diagnostic tools to assess forest damages caused by drought. All three components of the DHI (annual productivity, minimum cover, and seasonality) were able to capture the response of the coniferous forest to drought, but overall temporal trends differed. We highlight that the drought effect is clearly altitude dependent, but that DHI components are important in addition to climatic variables to distinguish non-damaged from damaged sites.

The potential of the Dynamic Habitat Index to capture the effect of drought on coniferous forest health

DHI was developed as an integrated remote sensing metric to track dynamics of vegetative productivity (Coops et al., 2008), and to relate these dynamics to biodiversity patterns(Razenkova et al., 2023). As it is based on spaceborne NDVI time series data, it informs on the dynamics of vegetation greenness (Coops et al., 2008). The 2018 drought event had a strong negative impact on forest health (Beloiu et al., 2022), including coniferous species such as Spruce (*Picea abies*) and Scots pine (*Pinus sylvestris*) (Haberstroh et al., 2022; Schuldt et al., 2020).We found that the DHI based on dense NDVI time series data proved to be a promising diagnostic tool to capture the dynamic changes and drought assessment (Pettorelli et al., 2005) including forest dieback in the health status of central European coniferous forests as a consequence of the severe drought events.

While surrogates of single components of the DHI such as seasonality (Xu et al., 2013) or vegetation productivity (Ivits et al., 2014), or minimum NDVI (Rahimzadeh Bajgiran et al., 2008) have been used to assess effects of droughts on vegetation, their combination as DHI as rarely used although they combination allows new insights. In this study, each of three DHI components provided useful information to assess forest health status. Coniferous forests generally have high vegetation productivity (Ji et al., 2020), making both the DHI_{Cum} and DHI_{Min} suitable health indicators for these ecosystems. For example, coniferous forests with high minimum vegetation cover (DHI_{Min}) remained healthier in 2018. The lowest values and the largest value ranges of DHI_{Min} occurred in 2020 after two years of drought stress, which could indicate a partial or

complete canopy dieback (Schuldt et al., 2020) together with a legacy effect (Margalef-Marrase et al., 2020). Importantly, not only damaged but also non-damaged sites suffered after two years of drought events. At the same time, partial recovery after the drought year 2018, e.g., related to minimum cover, also occurred, so both positive and negative could be mapped using DHI. However, such increases in NDVI might at least partly be the result of herbaceous vegetation resprouting after partial or complete forest die-off (Smith et al., 2022), so the forest type might have changed. An indicator for strong drought effects might be the altered vegetation (see (Ivits et al., 2014)). Here, non-damaged sites showed the least amount of variation (DHI_{Var}) compared to the damaged sites. The marked differences for all DHI components value between non-damaged and damaged sites underpin their potential as warning indicators of forest degradation.

Advantages of remote sensing metrics based on times series data

Multiple-year and extended droughts have additive effects on the response of trees in terms of e.g. leaf area (Miller et al., 2022) and vegetation productivity (Zhang et al., 2022). So, analysis of temporal changes using time series provides more detailed information about the effects of global change events such as severe droughts on vegetation health compared to a single NDVI tile (Prăvălie et al., 2022). We demonstrated that each of the three DHIs components can be useful in terms of drought assessment and showed that Hessian coniferous forests did not fully recover to pre-drought conditions yet. Recovery time as one important component of ecosystem stability is particularly relevant if the frequency and intensities of droughts increase (Češljar et al., 2022). Ecosystems with longer drought recovery times are more likely to experience a new drought event before fully recovering which leads to increased plant mortality and a potential transition to a new state (Luo et al., 2015). These legacy effects are often characterized by ecological responses to water availability and temperature (Ogle et al., 2015). Therefore, extended droughts affect the recovery time associated with canopy mortality and may push forests beyond a tipping point (Beloiu et al., 2022) and ultimately lead to changes in LULC (Miller et al., 2022). Our results showed that the time series of NDVIs expressed as DHI indices are helpful for recognizing where damages are considerable and can thus be used as a potential early indicator of forest damage. For example, March 2018 was the start of the drought period that never showed complete recovery by the end of 2020. Similar to our results, (Beloiu et al., 2022) reported that mean precipitation in April-August 2018 for the growing season was less than half of the normal amount (450-500 mm) in Bavaria in central European forests, and in our study the de Martonne aridity index showed a summer with arid to semi-arid climate (Fig. S. 3 and Fig. S. 4). Decreasing NDVI has been linked to tipping

points of *P. sylvestris* forests in Southwest Germany, where the coniferous forest is changing towards a broadleaf forest (Haberstroh et al., 2022). Thus, DHI analysis including spatial trends could be used to characterize forest die-off and subsequent recovery. So, changes in DHI might serve as early indicators of forest damage and could be used together with remotely sensed data on tree species identity to explore if there shift towards alternative states such as broadleaf forests or open ecosystems with distinct DHI signatures.

Environmental factors together with the DHIs explain coniferous health status

Severe droughts and heatwaves cause forest die-off in the Antropocene (Allen et al., 2015; Margalef-Marrase et al., 2020) and mortality of coniferous tree species is increasing (Gazol and Camarero, 2022; Obladen et al., 2021; Philipp et al., 2021; Schuldt et al., 2020; Senf et al., 2020; Senf and Seidl, 2021b). Here, in addition to environmental parameters, DHI components were among most important predictors to distinguish non-damaged from damaged coniferous forests, which emphasizes their usefulness in assessing forest drought. An advantage of DHIs derived from satellite data collections (e.g. (Copernicus, 2022)) over other climatic datasets (such as precipitation, drought and, temperature) could be that the latter are derived from interpolation techniques and can suffer from potential biases (Hobi et al., 2017). Nevertheless, variation in temperature was the most important factor to predict health status in our study. Indeed, tree mortality in Europe is triggered by global-change-type drought (Schuldt and Ruehr, 2022). Temperature stress and drought could limit the capability of plants to refill cavitated xylem to support metabolism and therefore disable recoverability from drought (Luo et al., 2015). It also has a negative impact on wood formation of coniferous forest species (Larysch et al., 2022). Such drought-affected growth processes are species-specific, show seasonal dynamics and might be altitude dependant (Larysch et al., 2022). Altitude is also an important factor concerning the magnitude of potential post-drought legacy effects (Li et al., 2020). We found that the drought was particularly severe (cumulative dMI<28) at lower altitude where the area of coniferous forests is relatively small. For coniferous forests, less drought effects occurred at higher altitudes with higher precipitation and lower temperature, which indicated more suitable habitat conditions. In the lower altitudes, the magnitude of the damages to the coniferous on the DHI components increased as precipitation decreased, and coniferous forests were not able to recover in these very dry regions. Thus, the patterns of coniferous forest damage generally followed the altitudinal patterns of drought (Fig. 3-9). This highlights the importance of considering both the meteorological and other environmental condition particularly to identify cumulative drought effects of a series of dry

and vulnerability of coniferous to drought due to the legacy effect possibly persists for a few years after a drought event (Margalef-Marrase et al., 2020), and DHIs based on dense time series data could play an important role in analysing such legacy effects.

Future directions

Our findings clearly show that the use of DHIs is a promising and straightforward approach to monitor the health status of coniferous forests at larger spatial scales that could contribute additional spatio-temporal information about global change effects such as drought. Previous studies on DHIs were performed at a 1km spatial resolution on a global scale (Radeloff et al., 2019). Latest DHI developments emphasized the combination of the DHIs, climate, and human-related variables in modelling approaches related to the abundance patterns due to high explanatory power (Razenkova et al., 2023). While we were interested in exploiting the globally available NDVI from the Copernicus program (Copernicus, 2022; Toté, 2016) whose spatial resolution corresponds to earlier DHI studies (Coops et al., 2008; Hobi et al., 2017) as well as to the climate data set used here, future studies should explore the potential of high to very high spatial resolution NDVI products based on for example PlanetScope, Sentinel-2 or Landsat data (Silveira et al., 2023). Further, combination of DHIs with ecophysiological measurements (Schuldt et al., 2020) and sensory networks (Lausch et al., 2017) together with high-resolution bioclimatic data sets (Haesen et al., 2023) and synthetic aperture radar (SAR)-based maps on soil moisture (Zhang et al., 2019) and forest drought (Kaiser et al., 2022) that potentially identify tree damage even before visible evidence (Filizzola et al., 2022)could create new insights into forest-die off due to drought events. While the binary forest damage mask based on freely available Sentinel-2 and a random forest model (Weis, 2022) could be further improved using public aerial imagery and methods of deep learning (Hamdi et al., 2019), composite remote sensing indices such as the DHI can be computed at high spatial resolution (Silveira et al., 2023), and could provide a continuous metric to assess forest damage, e.g. to map decreasing annual productivity or stagnation at low level after disturbance. Adding structural data and canopy height information from LiDAR data (Coops et al., 2018) supported by automated field measurements for calibration (Calders et al., 2023) would be the next step to improve the identification of tipping points and regime shifts to other types of (forest) ecosystems. A long-term networked monitoring system with relatively high-frequency data is needed to understand the underlying forest dynamics (see (Zweifel et al., 2023)). Depending on the availability of the satellite data and acquisitions date, there are numerous existing images with coarser spatial resolutions at the global scale or finer resolutions at the regional or

local scale. Dense NDVI times series can be derived from publicly available Landsat and Sentinel-2 imagery at 30m (Yang et al., 2023) or even 10m resolution (Thonfeld et al., 2022), and vegetation information can be further scaled down to 3m resolution using PlanetScope imagery (Moon et al., 2022). In addition to NDVI-based information, indices that also include the shortwave infrared spectral bands and that are sensitive to vegetation moisture content can be derived from Landsat imagery and bear high potential to assess climate change effects (Requena Suarez et al., 2023). So, if the annual DHI profiles of healthy and damaged forests are known and calibrated against ecophysiological field data and if the effects of abiotic factors on DHI profiles are explored (e.g., (Safaei et al., 2023)) and computational challenges are met, then such time-series based information could contribute to an automated warning system, e.g., by indicating deviations from healthy forest DHI profiles in a spatially explicit way.

Conclusion

Progress in earth technology facilitates its application in ecosystem studies, e.g., to quantify landscape dynamics and capture changes due to extreme droughts, particularly when using time series of remotely sensed and freely accessible data. The DHI based on the multiyear NDVI time series clearly illustrated the strong effect of the drought year 2018 on coniferous forests, so it could support monitoring health status in central European coniferous forest ecosystems or further LULC types. Comparing the values of three DHI components across non-damaged and damaged sites could help to develop early warning indicators of ecosystem degradation and changes in ecosystem functioning. This study also highlighted the importance of considering meteorological and environmental conditions to interpret the remote sensing-based assessment of ecosystem condition. Therefore, we suggest testing this approach across different LULCs types or to assess potential additive effects of multiple extreme events. Future avenues include the use of very high-resolution optical time series data as well as the integration of other data types such as LiDAR to map changes in vegetation structure, or SAR time series data to explore, e.g., changes in vegetation structure and soil moisture especially in areas where the use of optical data is limited.

Availability of data: Data available on request from the authors

Authorship: Mojdeh Safaei: Conceptualization; Data curation; Formal analysis; Investigation; Methodology; Software; Validation; Visualization; Writing- original draft– review. Till

Kleinebecker: Conceptualization; Writing- review & editing; Resources. Manuel Weis: Data curation; Writing- review & editing. André Große-Stoltenberg: Conceptualization; Methodology; Writing- review & editing; Supervision.

References

Allen, C.D., Breshears, D.D., McDowell, N.G., 2015. On underestimation of global vulnerability to tree mortality and forest die-off from hotter drought in the Anthropocene. Ecosphere 6, art129. https://doi.org/10.1890/ES15-00203.1

Beloiu, M., Stahlmann, R., Beierkuhnlein, C., 2022. Drought impacts in forest canopy and deciduous tree saplings in Central European forests. Forest Ecology and Management 509, 120075. https://doi.org/10.1016/j.foreco.2022.120075

Bhuyan, U., Zang, C., Menzel, A., 2017. Different responses of multispecies tree ring growth to various drought indices across Europe. Dendrochronologia 44, 1–8. https://doi.org/10.1016/j.dendro.2017.02.002

Breiman, L., 2001. Random Forests. Machine Learning 45, 5–32. https://doi.org/10.1023/A:1010933404324

Brodrick, P.G., Anderegg, L.D.L., Asner, G.P., 2019. Forest Drought Resistance at Large Geographic Scales. Geophysical Research Letters 46, 2752–2760. https://doi.org/10.1029/2018GL081108

Brun, P., Psomas, A., Ginzler, C., Thuiller, W., Zappa, M., Zimmermann, N.E., 2020. Large-scale early-wilting response of Central European forests to the 2018 extreme drought. Global Change Biology 26, 7021–7035. https://doi.org/10.1111/gcb.15360

Buras, A., Rammig, A., Zang, C.S., 2020. Quantifying impacts of the 2018 drought on European ecosystems in comparison to 2003. Biogeosciences 17, 1655–1672. https://doi.org/10.5194/bg-17-1655-2020

Calders, K., Brede, B., Newnham, G., Culvenor, D., Armston, J., Bartholomeus, H., Griebel, A., Hayward, J., Junttila, S., Lau, A., Levick, S., Morrone, R., Origo, N., Pfeifer, M., Verbesselt, J., Herold, M., 2023. StrucNet: a global network for automated vegetation structure monitoring. Remote Sensing in Ecology and Conservation 9, 587–598. https://doi.org/10.1002/rse2.333

CDC, 2022a. Climate Data Center, Grids of monthly total precipitation (mm) over Germany.

CDC, 2022b. Climate Data Center, Grids of mean of the monthly averaged minimum daily air temperature (1/10°C) over Germany.

CDC, 2022c. Climate Data Center, Grids of monthly total sunshine duration (h) over Germany.

CDC, 2022d. Climate Data Center, Grids of monthly drought index (de Martonne) over Germany, version v1.0.

Češljar, G., Jovanović, F., Brašanac-Bosanac, L., Đorđević, I., Mitrović, S., Eremija, S., Ćirković-Mitrović, T., Lučić, A., 2022. Impact of an Extremely Dry Period on Tree Defoliation and Tree Mortality in Serbia. Plants 11. https://doi.org/10.3390/plants11101286

Cook, B.I., Smerdon, J.E., Cook, E.R., Williams, A.P., Anchukaitis, K.J., Mankin, J.S., Allen, K., Andreu-Hayles, L., Ault, T.R., Belmecheri, S., Coats, S., Coulthard, B., Fosu, B., Grierson, P., Griffin, D., Herrera, D.A., Ionita, M., Lehner, F., Leland, C., Marvel, K., Morales, M.S., Mishra, V., Ngoma, J., Nguyen, H.T.T., O'Donnell, A., Palmer, J., Rao, M.P., Rodriguez-Caton, M., Seager, R., Stahle, D.W., Stevenson, S., Thapa, U.K., Varuolo-Clarke, A.M., Wise, E.K., 2022. Megadroughts in the Common Era and the Anthropocene. Nature Reviews Earth & Environment 3, 741–757. https://doi.org/10.1038/s43017-022-00329-1

Coops, N.C., Kearney, S.P., Bolton, D.K., Radeloff, V.C., 2018. Remotely-sensed productivity clusters capture global biodiversity patterns. Scientific Reports 8, 16261. https://doi.org/10.1038/s41598-018-34162-8

Coops, N.C., Wulder, M.A., 2019. Breaking the Habit(at). Trends in Ecology & Evolution 34, 585–587. https://doi.org/10.1016/j.tree.2019.04.013

Coops, N.C., Wulder, M.A., Duro, D.C., Han, T., Berry, S., 2008. The development of a Canadian dynamic habitat index using multi-temporal satellite estimates of canopy light absorbance. Ecological Indicators 8, 754–766. https://doi.org/10.1016/j.ecolind.2008.01.007

Copernicus, 2022. Normalized Difference Vegetation Index, Copernicus global land service, Providing bio-geophysical products of global land surface.

CORINE Land Cover Product User Manual, 2018. Copernicus Land Monitoring Service (CLMS) European Environment Agency (EEA). Copenhagen K. – Denmark.

de Martonne, E., 1941. Nouvelle carte mondiale de l' indice d' aridite. La Meteorologie.

Dobson, A.J., Barnett, A.G., 1990. An Introduction to Generalized Linear Models (4th ed.). Chapman and Hall/CRC. https://doi.org/10.1201/9781315182780

Eitel, J.U.H., Basler, D., Braun, S., Buchmann, N., D'Odorico, P., Etzold, S., Gessler, A., Griffin, K.L., Krejza, J., Luo, Y., Maguire, A.J., Rao, M.P., Vitasse, Y., Walthert, L., Zweifel, R., 2023. Towards monitoring stem growth phenology from space with high resolution satellite data. Agricultural and Forest Meteorology 339, 109549. https://doi.org/10.1016/j.agrformet.2023.109549

Filizzola, C., Carlucci, M.A., Genzano, N., Ciancia, E., Lisi, M., Pergola, N., Ripullone, F., Tramutoli, V., 2022. Robust Satellite-Based Identification and Monitoring of Forests Having Undergone Climate-Change-Related Stress. Land 11. https://doi.org/10.3390/land11060825

Gazol, A., Camarero, J.J., 2022. Compound climate events increase tree drought mortality across European forests. Science of The Total Environment 816, 151604. https://doi.org/10.1016/j.scitotenv.2021.151604

Ge, W., Han, J., Zhang, D., Wang, F., 2021. Divergent impacts of droughts on vegetation phenology and productivity in the Yungui Plateau, southwest China. Ecological Indicators 127, 107743. https://doi.org/10.1016/j.ecolind.2021.107743

Geoportal Hessen, 2022. Hessische Verwaltung für Bodenmanagement und Geoinformation.

Gonçalves, N.B., Lopes, A.P., Dalagnol, R., Wu, J., Pinho, D.M., Nelson, B.W., 2020. Both near-surface and satellite remote sensing confirm drought legacy effect on tropical forest leaf phenology after 2015/2016 ENSO drought. Remote Sensing of Environment 237, 111489. https://doi.org/10.1016/j.rse.2019.111489

Haberstroh, S., Werner, C., Grün, M., Kreuzwieser, J., Seifert, T., Schindler, D., Christen, A., 2022. Central European 2018 hot drought shifts scots pine forest to its tipping point. Plant Biology n/a. https://doi.org/10.1111/plb.13455

Haesen, S., Lembrechts, J.J., De Frenne, P., Lenoir, J., Aalto, J., Ashcroft, M.B.,… Van Meerbeek, K., 2023. ForestClim—Bioclimatic variables for microclimate temperatures of European forests. Global Change Biology 29, 2886–2892. https://doi.org/10.1111/gcb.16678

Hamdi, Z.M., Brandmeier, M., Straub, C., 2019. Forest Damage Assessment Using Deep Learning on High Resolution Remote Sensing Data. Remote Sensing 11. https://doi.org/10.3390/rs11171976

Hinkle, D.E., Wiersma, W., Jurs, S.G., 2003. Applied statistics for the behavioral sciences. Houghton Mifflin College Division.

HLNUG, 2022. Beobachteter Klimawandel. Klimawandel in Hessen. Hessisches Landesamt für Naturschutz, Umwelt und Geologie (HLNUG).

HLNUG, 2018. Klimawandel in Hessen. Herausgeber, © und Vertrieb: Hessisches Landesamt für Naturschutz, Umwelt und Geologie Fachzentrum Klimawandel und Anpassung Rheingaustraße 186 65203 Wiesbaden.

Hobi, M.L., Dubinin, M., Graham, C.H., Coops, N.C., Clayton, M.K., Pidgeon, A.M., Radeloff, V.C., 2017. A comparison of Dynamic Habitat Indices derived from different MODIS products as predictors

of avian species richness. Remote Sensing of Environment 195, 142–152. https://doi.org/10.1016/j.rse.2017.04.018

Ivits, E., Horion, S., Fensholt, R., Cherlet, M., 2014. Drought footprint on European ecosystems between 1999 and 2010 assessed by remotely sensed vegetation phenology and productivity. Global Change Biology 20, 581–593. https://doi.org/10.1111/gcb.12393

James, G., Witten, D., Hastie, T., Robert, T., 2013. An Introduction to Statistical Learning. Springer New York, NY. https://doi.org/10.1007/978-1-4614-7138-7

Ji, Y., Zhou, G., Luo, T., Dan, Y., Zhou, L., Lv, X., 2020. Variation of net primary productivity and its drivers in China's forests during 2000–2018. Forest Ecosystems 7, 15. https://doi.org/10.1186/s40663-020-00229-0

Jiang, H., Xu, X., Guan, M., Wang, L., Huang, Y., Jiang, Y., 2020. Determining the contributions of climate change and human activities to vegetation dynamics in agro-pastural transitional zone of northern China from 2000 to 2015. Science of The Total Environment 718, 134871. https://doi.org/10.1016/j.scitotenv.2019.134871

Johnstone, J.F., Allen, C.D., Franklin, J.F., Frelich, L.E., Harvey, B.J., Higuera, P.E., Mack, M.C., Meentemeyer, R.K., Metz, M.R., Perry, G.L., Schoennagel, T., Turner, M.G., 2016. Changing disturbance regimes, ecological memory, and forest resilience. Frontiers in Ecology and the Environment 14, 369–378. https://doi.org/10.1002/fee.1311

Kaiser, P., Buddenbaum, H., Nink, S., Hill, J., 2022. Potential of Sentinel-1 Data for Spatially and Temporally High-Resolution Detection of Drought Affected Forest Stands. Forests 13. https://doi.org/10.3390/f13122148

Larysch, E., Stangler, D.F., Puhlmann, H., Rathgeber, C.B.K., Seifert, T., Kahle, H.-P., 2022. The 2018 hot drought pushed conifer wood formation to the limit of its plasticity: Consequences for woody biomass production and tree ring structure. Plant Biology 24, 1171–1185. https://doi.org/10.1111/plb.13399

Lausch, A., Erasmi, S., King, D.J., Magdon, P., Heurich, M., 2017. Understanding Forest Health with Remote Sensing-Part II—A Review of Approaches and Data Models. Remote Sensing 9. https://doi.org/10.3390/rs9020129

Li, M., Ge, C., Zong, S., Wang, G., 2022. Drought Assessment on Vegetation in the Loess Plateau Using a Phenology-Based Vegetation Condition Index. Remote Sensing 14. https://doi.org/10.3390/rs14133043

Li, P., Zhu, D., Wang, Y., Liu, D., 2020. Elevation dependence of drought legacy effects on vegetation greenness over the Tibetan Plateau. Agricultural and Forest Meteorology 295, 108190. https://doi.org/10.1016/j.agrformet.2020.108190

Lu, M., Pebesma, E., Sanchez, A., Verbesselt, J., 2016. Spatio-temporal change detection from multidimensional arrays: Detecting deforestation from MODIS time series. ISPRS Journal of Photogrammetry and Remote Sensing 117, 227–236. https://doi.org/10.1016/j.isprsjprs.2016.03.007

Luo, Y., Keenan, T.F., Smith, M., 2015. Predictability of the terrestrial carbon cycle. Global Change Biology 21, 1737–1751. https://doi.org/10.1111/gcb.12766

Mackey, B., Bryan, J., Randall, L., 2004. Australia's Dynamic Habitat Template 2003, in: MODIS Vegetation Workshop II.

Margalef-Marrase, J., Pérez-Navarro, M.Á., Lloret, F., 2020. Relationship between heatwave-induced forest die-off and climatic suitability in multiple tree species. Global Change Biology 26, 3134–3146. https://doi.org/10.1111/gcb.15042

McCullagh, P., 1989. Generalized Linear Models (2nd ed.). Routledge. https://doi.org/10.1201/9780203753736.

McFadden, D., 1977. Quantitative Methods for Analyzing Travel Behaviour of Individuals: Some Recent Developments. Cowles Foundation for Research in Economics, Yale University.

McFadden, D., 1974. Quantitativ Quantitative Methods for Analyzing T e Methods for Analyzing Travel Beha el Behaviour of viour of Individuals: Some Recent Developments.

Michaud, J.-S., Coops, N.C., Andrew, M.E., Wulder, M.A., 2012. Characterising spatiotemporal environmental and natural variation using a dynamic habitat index throughout the province of Ontario. Ecological Indicators 18, 303–311. https://doi.org/10.1016/j.ecolind.2011.11.027

Miller, D.L., Wetherley, E.B., Roberts, D.A., Tague, C.L., McFadden, J.P., 2022. Vegetation cover change during a multi-year drought in Los Angeles. Urban Climate 43, 101157. https://doi.org/10.1016/j.uclim.2022.101157

Moon, M., Richardson, A.D., Milliman, T., Friedl, M.A., 2022. A high spatial resolution land surface phenology dataset for AmeriFlux and NEON sites. Scientific Data 9, 448. https://doi.org/10.1038/s41597-022-01570-5

NASA, 2020. NASA DEM Merged DEM Global 1 arc second. NASA EOSDIS Land Processes DAAC.

Obladen, N., Dechering, P., Skiadaresis, G., Tegel, W., Keßler, J., Höllerl, S., Kaps, S., Hertel, M., Dulamsuren, C., Seifert, T., Hirsch, M., Seim, A., 2021. Tree mortality of European beech and Norway spruce induced by 2018-2019 hot droughts in central Germany. Agricultural and Forest Meteorology 307, 108482. https://doi.org/10.1016/j.agrformet.2021.108482

Ogle, K., Barber, J.J., Barron-Gafford, G.A., Bentley, L.P., Young, J.M., Huxman, T.E., Loik, M.E., Tissue, D.T., 2015. Quantifying ecological memory in plant and ecosystem processes. Ecology Letters 18, 221–235. https://doi.org/10.1111/ele.12399

Panek, N., 2018. Hessens Wälder im Fokus der dritten Bundeswaldinventur Herausgegeben vom Bund für Umwelt und Naturschutz in Deutschland (BUND) Landesverband Hessen e.V. aus naturschutzfachlicher Sicht.

Pettorelli, N., Vik, J.O., Mysterud, A., Gaillard, J.-M., Tucker, C.J., Stenseth, N.Chr., 2005. Using the satellite-derived NDVI to assess ecological responses to environmental change. Trends in Ecology & Evolution 20, 503–510. https://doi.org/10.1016/j.tree.2005.05.011

Philipp, M., Wegmann, M., Kübert-Flock, C., 2021. Quantifying the Response of German Forests to Drought Events via Satellite Imagery. Remote Sensing 13. https://doi.org/10.3390/rs13091845

Prăvălie, R., Sîrodoev, I., Nita, I.-A., Patriche, C., Dumitraşcu, M., Roşca, B., Tişcovschi, A., Bandoc, G., Săvulescu, I., Mănoiu, V., Birsan, M.-V., 2022. NDVI-based ecological dynamics of forest vegetation and its relationship to climate change in Romania during 1987–2018. Ecological Indicators 136, 108629. https://doi.org/10.1016/j.ecolind.2022.108629

QGIS Development Team, 2021. QGIS Geographic Information System. Open Source Geospatial Foundation Project. http://qgis.osgeo.org.

R Core Team, 2021. R: A language and environment for statistical computing. R Foundation for Statistical Computing, Vienna, Austria.

Radeloff, V.C., Dubinin, M., Coops, N.C., Allen, A.M., Brooks, T.M., Clayton, M.K., Costa, G.C., Graham, C.H., Helmers, D.P., Ives, A.R., Kolesov, D., Pidgeon, A.M., Rapacciuolo, G., Razenkova, E., Suttidate, N., Young, B.E., Zhu, L., Hobi, M.L., 2019. The Dynamic Habitat Indices (DHIs) from MODIS and global biodiversity. Remote Sensing of Environment 222, 204–214. https://doi.org/10.1016/j.rse.2018.12.009

Rahimzadeh Bajgiran, P., Darvishsefat, A.A., Khalili, A., Makhdoum, M.F., 2008. Using AVHRR-based vegetation indices for drought monitoring in the Northwest of Iran. Journal of Arid Environments 72, 1086–1096. https://doi.org/10.1016/j.jaridenv.2007.12.004

Razenkova, E., Dubinin, M., Pidgeon, A.M., Hobi, M.L., Zhu, L., Bragina, E.V., Allen, A.M., Clayton, M.K., Baskin, L.M., Coops, N.C., Radeloff, V.C., 2023. Abundance patterns of mammals across Russia explained by remotely sensed vegetation productivity and snow indices. Journal of Biogeography 50, 932–946. https://doi.org/10.1111/jbi.14588

Razenkova, E., Radeloff, V.C., Dubinin, M., Bragina, E.V., Allen, A.M., Clayton, M.K., Pidgeon, A.M., Baskin, L.M., Coops, N.C., Hobi, M.L., 2020a. Vegetation productivity summarized by the Dynamic Habitat Indices explains broad-scale patterns of moose abundance across Russia. Scientific Reports 10, 836. https://doi.org/10.1038/s41598-019-57308-8

Requena Suarez, D., Rozendaal, D.M.A., De Sy, V., Decuyper, M., Málaga, N., Durán Montesinos, P., Arana Olivos, A., De la Cruz Paiva, R., Martius, C., Herold, M., 2023. Forest disturbance and recovery in Peruvian Amazonia. Global Change Biology 29, 3601–3621. https://doi.org/10.1111/gcb.16695

Safaei, M., Kleinebecker, T., Große-Stoltenberg, A., 2023. Potential of the satellite-based Dynamic Habitat Index (DHI) to capture changes in soil properties and drought conditions across Land Use/Land Cover types in a Central European landscape. Geocarto International 38, 2292162. https://doi.org/10.1080/10106049.2023.2292162

Savtchenko, A., Ouzounov, D., Ahmad, S., Acker, J., Leptoukh, G., Koziana, J., Nickless, D., 2004. Terra and Aqua MODIS products available from NASA GES DAAC. Advances in Space Research 34, 710–714. https://doi.org/10.1016/j.asr.2004.03.012

Schuldt, B., Buras, A., Arend, M., Vitasse, Y., Beierkuhnlein, C., Damm, A., Gharun, M., Grams, T.E.E., Hauck, M., Hajek, P., Hartmann, H., Hiltbrunner, E., Hoch, G., Holloway-Phillips, M., Körner, C., Larysch, E., Lübbe, T., Nelson, D.B., Rammig, A., Rigling, A., Rose, L., Ruehr, N.K., Schumann, K., Weiser, F., Werner, C., Wohlgemuth, T., Zang, C.S., Kahmen, A., 2020a. A first assessment of the impact of the extreme 2018 summer drought on Central European forests. Basic and Applied Ecology 45, 86–103. https://doi.org/10.1016/j.baae.2020.04.003

Schuldt, B., Ruehr, N.K., 2022. Responses of European forests to global change-type droughts. Plant Biology 24, 1093–1097. https://doi.org/10.1111/plb.13484

Senf, C., Buras, A., Zang, C.S., Rammig, A., Seidl, R., 2020. Excess forest mortality is consistently linked to drought across Europe. Nature Communications 11, 6200. https://doi.org/10.1038/s41467-020-19924-1

Senf, C., Seidl, R., 2021a. Storm and fire disturbances in Europe: Distribution and trends. Global Change Biology 27, 3605–3619. https://doi.org/10.1111/gcb.15679

Senf, C., Seidl, R., 2021b. Persistent impacts of the 2018 drought on forest disturbance regimes in Europe. Biogeosciences 18, 5223–5230. https://doi.org/10.5194/bg-18-5223-2021

Senf, C., Seidl, R., 2018. Natural disturbances are spatially diverse but temporally synchronized across temperate forest landscapes in Europe. Global Change Biology 24, 1201–1211. https://doi.org/10.1111/gcb.13897

Sheffield, J., Wood, E., 2011. Drought: Past Problems and Future Scenarios.

Silveira, E.M.O., Pidgeon, A.M., Farwell, L.S., Hobi, M.L., Razenkova, E., Zuckerberg, B., Coops, N.C., Radeloff, V.C., 2023. Multi-grain habitat models that combine satellite sensors with different resolutions explain bird species richness patterns best. Remote Sensing of Environment 295, 113661. https://doi.org/10.1016/j.rse.2023.113661

Smith, T., Traxl, D., Boers, N., 2022. Empirical evidence for recent global shifts in vegetation resilience. Nature Climate Change 12, 477–484. https://doi.org/10.1038/s41558-022-01352-2

Sun, C., Beirne, C., Burgar, J.M., Howey, T., Fisher, J.T., Burton, A.C., 2021. Simultaneous monitoring of vegetation dynamics and wildlife activity with camera traps to assess habitat change. Remote Sensing in Ecology and Conservation 7, 666–684. https://doi.org/10.1002/rse2.222

Theil, H., 1992. A Rank-Invariant Method of Linear and Polynomial Regression Analysis, in: Raj, B., Koerts, J. (Eds.), Henri Theil's Contributions to Economics and Econometrics: Econometric Theory and Methodology. Springer Netherlands, Dordrecht, pp. 345–381. https://doi.org/10.1007/978-94-011-2546-8_20

Thonfeld, F., Gessner, U., Holzwarth, S., Kriese, J., da Ponte, E., Huth, J., Kuenzer, C., 2022. A First Assessment of Canopy Cover Loss in Germany's Forests after the 2018–2020 Drought Years. Remote Sensing 14. https://doi.org/10.3390/rs14030562

Toté, C., 2016. Gio Global Land Component - Lot I "Operation of the Global Land Component" Framework Service Contract N° 388533 (JRC) Algorithm theoretical basis document Normalized Difference Vegetation Index (NDVI) collection 300M version 1 Issue I1.02 Organization name of lead contractor for this deliverable: VITO Book Captain: Else Swinnen (VITO) Contributing.

Verbesselt, J., Hyndman, R., Zeileis, A., Culvenor, D., 2010. Phenological change detection while accounting for abrupt and gradual trends in satellite image time series. Remote Sensing of Environment 114, 2970–2980. https://doi.org/10.1016/j.rse.2010.08.003

Weis, M., 2022. Kalamitätsmonitoring der Nadelwälder in Hessen mit Sentinel-2-Satellitendaten. gis. business, 1/2022, 24-27.

Wulder, M.A., White, J.C., Coops, N.C., Nelson, T., Boots, B., 2007. Using local spatial autocorrelation to compare outputs from a forest growth model. Ecological Modelling 209, 264–276. https://doi.org/10.1016/j.ecolmodel.2007.06.033

Xu, L., Myneni, R.B., Chapin III, F.S., Callaghan, T.V., Pinzon, J.E., Tucker, C.J., Zhu, Z., Bi, J., Ciais, P., Tømmervik, H., Euskirchen, E.S., Forbes, B.C., Piao, S.L., Anderson, B.T., Ganguly, S., Nemani, R.R., Goetz, S.J., Beck, P.S.A., Bunn, A.G., Cao, C., Stroeve, J.C., 2013. Temperature and vegetation seasonality diminishment over northern lands. Nature Climate Change 3, 581–586. https://doi.org/10.1038/nclimate1836

Yang, J., Dong, J., Liu, L., Zhao, M., Zhang, X., Li, X., Dai, J., Wang, H., Wu, C., You, N., Fang, S., Pang, Y., He, Y., Zhao, G., Xiao, X., Ge, Q., 2023. A robust and unified land surface phenology algorithm for diverse biomes and growth cycles in China by using harmonized Landsat and Sentinel-2 imagery. ISPRS Journal of Photogrammetry and Remote Sensing 202, 610–636. https://doi.org/10.1016/j.isprsjprs.2023.07.017

Zhang, K., Ali, A., Antonarakis, A., Moghaddam, M., Saatchi, S., Tabatabaeenejad, A., Chen, R., Jaruwatanadilok, S., Cuenca, R., Crow, W.T., Moorcroft, P., 2019. The Sensitivity of North American Terrestrial Carbon Fluxes to Spatial and Temporal Variation in Soil Moisture: An Analysis Using Radar-Derived Estimates of Root-Zone Soil Moisture. Journal of Geophysical Research: Biogeosciences 124, 3208–3231. https://doi.org/10.1029/2018JG004589

Zhang, W., Wei, F., Horion, S., Fensholt, R., Forkel, M., Brandt, M., 2022. Global quantification of the bidirectional dependency between soil moisture and vegetation productivity. Agricultural and Forest Meteorology 313, 108735. https://doi.org/10.1016/j.agrformet.2021.108735

Zhi, X., Du, H., Zhang, M., Long, Z., Zhong, L., Sun, X., 2022. Mapping the habitat for the moose population in Northeast China by combining remote sensing products and random forests. Global Ecology and Conservation 40, e02347. https://doi.org/10.1016/j.gecco.2022.e02347

Zink, M., Samaniego, L., Kumar, R., Thober, S., Mai, J., Schäfer, D., Marx, A., 2016. The German drought monitor. Environmental Research Letters 11, 074002. https://doi.org/10.1088/1748-9326/11/7/074002

Zuur, A., Ieno, E.N., Walker, N., Saveliev, A.A., Smith, G.M., 2009. Mixed Effects Models and Extensions in Ecology with R. Springer New York.

Zweifel, R., Pappas, C., Peters, R.L., Babst, F., Balanzategui, D., Basler, D., Bastos, A., … Sterck, F., 2023. Networking the forest infrastructure towards near real-time monitoring – A white paper. Science of The Total Environment 872, 162167. https://doi.org/10.1016/j.scitotenv.2023.162167

Appendix

Table S1

Correlation between the DHI component and environmental components is presented in Table S1 (*p*-value<0.001). Annual productivity, precipitation and drought variables correlated moderately and positively. In the case of the drought variable derived from dMI, higher values indicate humid environmental conditions. A moderate and positive correlation between the annual productivity and minimum as well as temperature. Relatively weak relationships were obtained for sunshine components and no correlation with DEM data was found. In the case of DHI_{Var}, the highest correlation with the precipitation cumulative and variation were only −0.35 and -0.34, and correlation with cumulative and variation of the drought were -0.33 and -0.31. DHI_{Min} was (at maximum) weakly correlated with climate variables and DEM data.

Table S1 Correlations between the three DHITotal components derived from NDVI and the environmental variables (p-value < 0.001)

Variables \ DHI Components		Annual productivity	Minimum cover	Seasonality
Precipitation	Cumulative	0.54	0.10	-0.35
	Minimum	0.38	0.01	-0.21
	Variation	0.52	0.10	-0.34
Temperature	Cumulative	-0.31	0.05	0.15
	Minimum	-0.38	-0.01	0.26
	Variation	0.10	0.11	-0.07
Sunshine duration	Cumulative	0.01	0.07	-0.08
	Minimum	0.19	0.11	-0.17
	Variation	-0.21	-0.07	0.12
Drought	Cumulative	0.55	0.06	-0.33
	Minimum	0.33	0.01	-0.22
	Variation	0.52	0.05	-0.30
DEM		0.0	-0.23	0.05

Figure S1

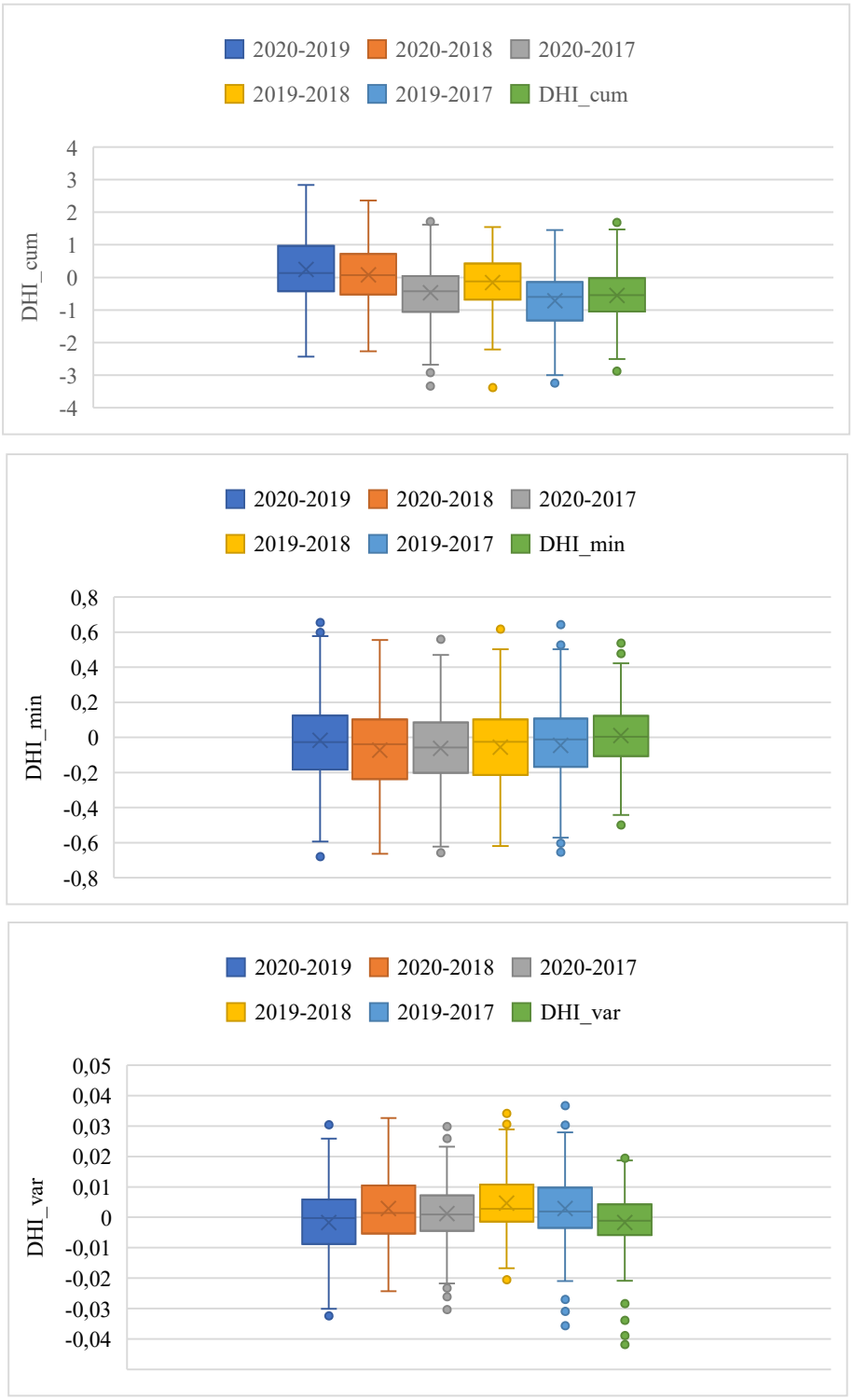

Fig. S. 1. Differences between DHI components across different years in healthy sites.

Figure S2

(A) Annual production (B) Minimum cover (C) seasonality

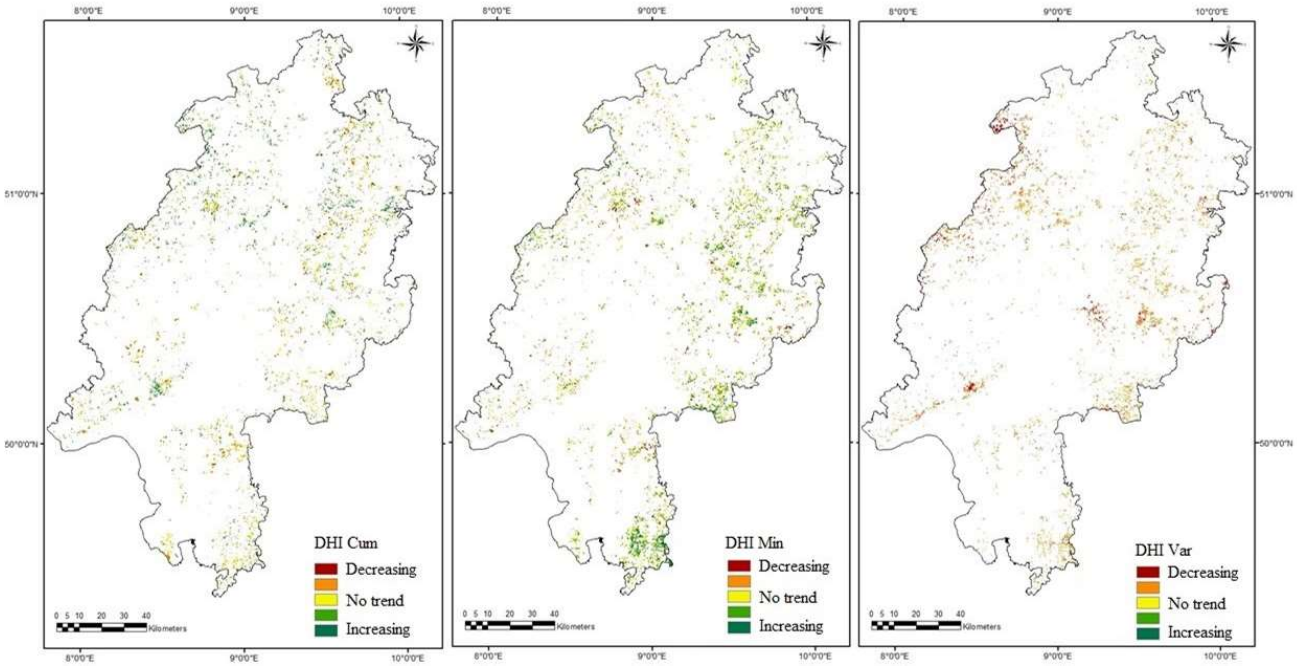

Fig. S2. Results of trend analysis to capture the effects of drought on the DHI components (A) DHICum (B) DHIMin and (C) DHIVar. Trend analysis was performed using Theil–Sen's test. A 20% threshold was applied to the DHIs components on the entire distribution of trend values to figure out which cells had a considerable trend spanning over the 2017–2020 period.

Figure S3

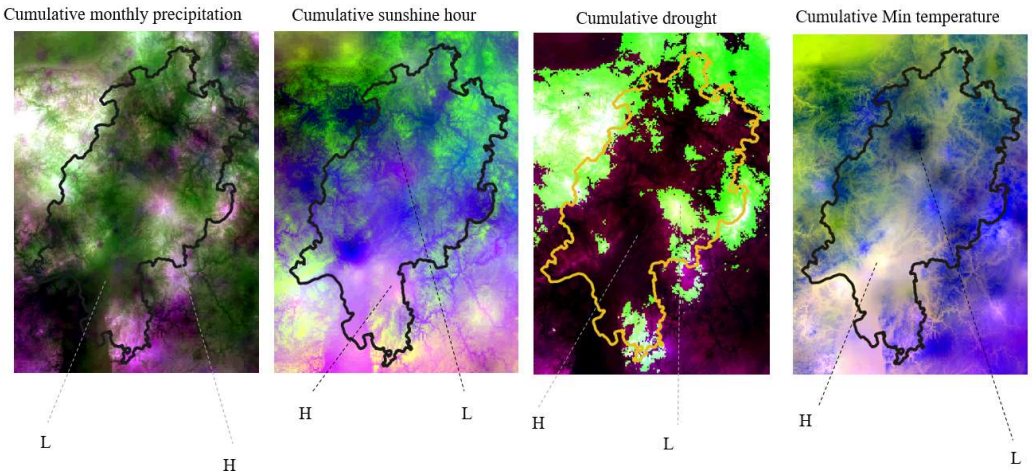

Fig S3. Environmental variable maps. H:Higher values and L: Lower values.

Figure S4

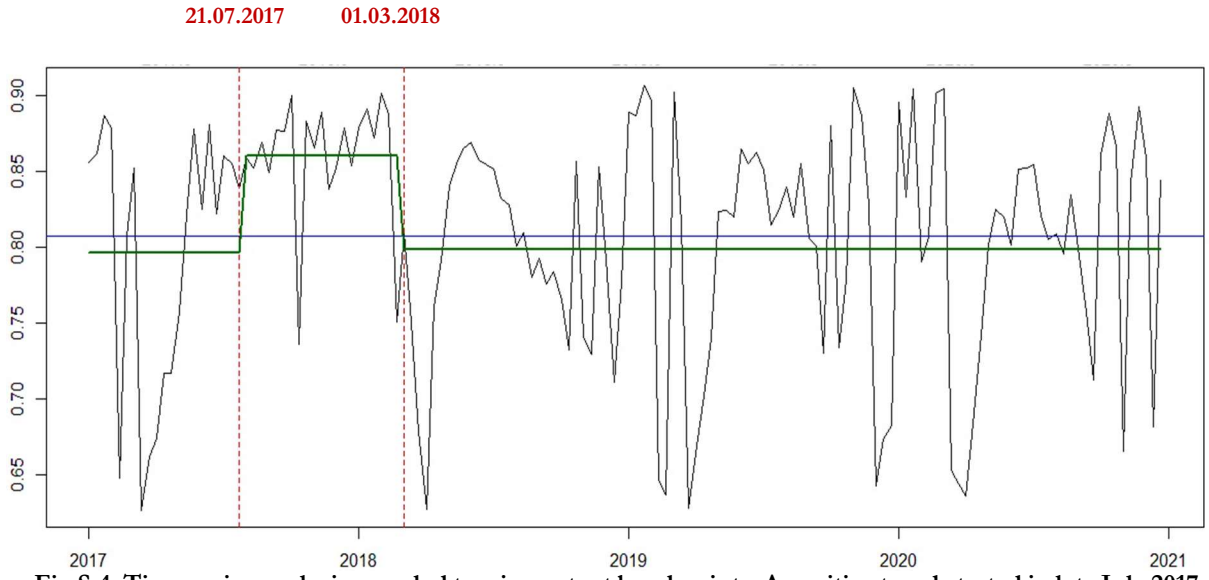

Fig S.4. Time series analysis revealed two important breakpoints. A positive trend started in late July 2017 until the end of February 2018 and then a decreasing trend in NDVI was identified in March 2018. This pattern was partly in line with precipitation trends, where in 2017 the amount of precipitation was markedly higher than in 2018 and a negative breakpoint was identified in February 2018. By the end of August 2018, the amount of precipitation increased (second positive breakpoint) but did not fully recover to the level of 2017.

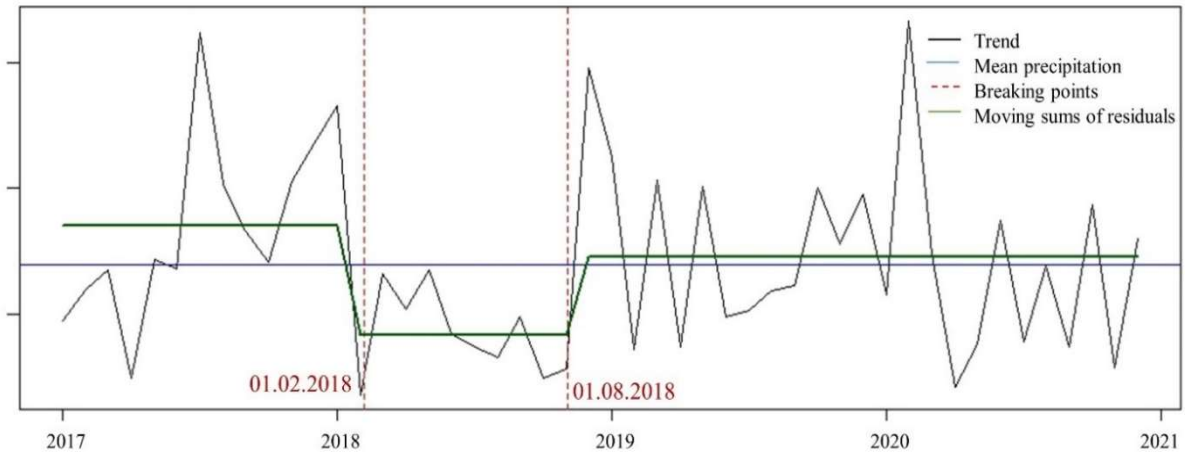

Monthly precipitation trends: in 2017 the amount of precipitation was higher than in 2018 and a negative breakpoint started from February 2018 to August 2018 and covered the complete growing season in 2018, and by the end of August 2018, the amount of precipitation increased as the second positive breakpoint but failed to match the 2017 trend.

Chapter 4

Potential of the satellite-based Dynamic Habitat Index (DHI) to capture changes in soil properties and drought conditions across Land Use/ Land Cover types in a central European landscape

Mojdeh Safaei[a*] Till Kleinebecker[a, b] André Große-Stoltenberg[a, b]

a Division of Landscape Ecology and Landscape Planning, Institute of Landscape Ecology and Resource Management, IFZ Research Centre for Biosystems, Land Use and Nutrition, Justus Liebig University Giessen, Heinrich-Buff Ring 26-32, 35392 Giessen, Germany

b Center for International Development and Environmental Research (ZEU), Senckenbergstrasse 3, 35390 Giessen, Germany

Corresponding authors: mojdeh.safaei@umwelt.uni-giessen.de, andre.grosse-stoltenberg@umwelt.uni-giessen.de
MS ORCiD: https://orcid.org/0000-0002-6509-8307
TK ORCiD: https://orcid.org/0000-0003-1121-2861
AGS ORCiD: https://orcid.org/0000-0001-6075-5497

Geocarto International Volume 38, 2023 -Issue1 https://doi.org/10.1080/10106049.2023.2292162

Potential of the satellite-based Dynamic Habitat Index (DHI) to capture changes in soil properties and drought conditions across Land Use/ Land Cover types in a central European landscape

Abstract

Land Use/ Land Cover (LULC) maps deliver essential information on landscape structure and functions, but such maps are usually considered static, and more progress is needed towards dynamic LULC products. The Dynamic Habitat Index (DHI), for example, has revealed high potential in biodiversity studies, but its capability to capture the variability of different LULC types under differing environmental conditions, which in turn affect biodiversity, is underexplored. In this study, we used NDVI products of the Copernicus Global Land Service to test if DHIs are sensitive to changing environmental conditions across LULC types over a 4-year period (2017–2020) in a central European landscape in Germany. We found that (1) all LULC types had distinct DHI characteristics, (2) DHI components responded to an extreme drought year in 2018 with no return to pre-drought conditions except for deciduous forests, and DHIs captured the spatio-temporal variability of pedo-climatic conditions. Thus, the DHI is sensitive towards environmental conditions. Integrated with ancillary geodata it could add a continuous and quantitative component to common categorical LULC maps with broad application in biodiversity and ecosystem research. Such integrated products could serve as valuable tools for decision makers to formulate sustainable land management strategies and contribute to Sustainable Develop Goal (SDG) indicators related to land degradation, e.g. by identifying deviations from typical DHI profiles of a given environmental context as a response to disturbance and environmental stress.

Keywords

Land Use/Land Cover; vegetation productivity; Dynamic Habitat Index; usable Field Capacity.

Introduction

Land Use/ Land Cover (LULC) maps provide essential information on landscape structure, functions, and dynamics (Belay et al., 2022). Changes in LULC have a crucial impact on ecosystem services (Belay et al., 2022; Sharma et al., 2019, 2023) and biodiversity assessments (Akodéwou et al., 2020; Musetsho et al., 2021; Sharma et al., 2018) by affecting ecosystem patterns (Gashaw et al., 2018) as well as hydrological processes (Wagner et al. 2016; Aghsaei et al. 2020; Yonaba et al. 2021a). Methods of remote sensing are widely applied to produce and update LULC maps (Chaves et al., 2020; Talukdar et al., 2020) with the aim to identify ecosystem degradation and to guide sustainable land management (Aghsaei et al. 2020; Yonaba et al. 2021b; Safaei et al. 2023). Consequently, LULC maps are continuously produced by public agencies, e.g. in Europe within the frame of the Copernicus Land Monitoring Service (CORINE Land Cover, 2018), and global products are being developed using novel methods such as deep-learning (Karra et al., 2021). However, these maps are mostly static and categorical representations of LULC. There have been various discussions about moving towards dynamic LULC models that are quantitative and continuous to account for the dynamics of habitat or ecosystem conditions (Coops and Wulder, 2019; Le et al., 2022). Quantitative approaches to assess the LULC dynamics are important to understand and manage the landscape variability (Mas et al., 2017; Talukdar et al., 2020). These variabilities have impacts on both environment and human livelihood such as increased flood probability (Avand et al., 2021), drought vulnerability (Fathi-Taperasht et al., 2023), loss of ecosystem services (Belay et al., 2022), soil quality (Safaei et al., 2019) as well as habitat suitability and future species distribution (Marshall et al. 2018).

The increasing availability of earth observation data with high temporal resolution allows for exploring ecosystem properties based on time series data in a spatially and temporally continuous way (Ramirez-Reyes et al., 2019; Runge et al., 2019). This includes mapping of LULC based on patterns of vegetation productivity (Gemitzi et al., 2019; Le et al., 2022) for ecosystem service assessments (Kooistra et al., 2023). Consequently, there has been an increasing interest in composite remote sensing indices such as Dynamic Habitat Indices (DHI), which offer new opportunities to assess the dynamics of habitats related to vegetation productivity (Coops et al., 2008; Hobi et al., 2017; Razenkova et al., 2020). DHIs summarize three measures of vegetative productivity and include the annual productivity and minimum cover as well as seasonality (Coops et al., 2008). The DHI approach showed great potential in biodiversity assessments using a range of satellite data products such as Normalized Difference Vegetation Index (NDVI), Leaf Area

Index (LAI), Gross Primary Production (GPP), and fraction of Photosynthetically Active Radiation (fPAR) at 1 km spatial resolution in Australia (Mackey et al., 2004), Canada (Coops et al., 2008), the United States (US) (Hobi et al., 2017), Russia (Razenkova et al., 2023, 2020), Thailand (Suttidate et al., 2019), global scale (Coops et al., 2018) and recently at 3 and 5m spatial resolutions in the US (Silveira et al., 2023). However, the application of the DHI is mainly restricted to biodiversity aspects. Integration of the DHI with drivers of vegetation productivity such as precipitation regimes (Zeng et al., 2022) as well as soil conditions (Zhang et al., 2022) in the context of LULC analysis needs to be explored further. Combining the DHI with additional spatial information on ecosystem properties could enhance the understanding of ecosystem dynamics at the landscape scale (Michaud et al., 2012), which in turn would be relevant for applications of the DHI in biodiversity studies.

To our knowledge, a comprehensive assessment of how the DHI changes for different LULC types across different environmental conditions related to precipitation and soil conditions has not yet been studied. Information on the usable field capacity of the soil is essential to understand plant growth particularly in dry years as the response of different LULC types will depend on soil physical and chemical properties (Safaei et al., 2019; Zhang et al., 2021). The integration of DHI with explanatory spatial data sets (Michaud et al., 2012) such as soil texture and field capacity under different LULCs and drought conditions would provide more details into drivers of productivity dynamics and underpin the relevance of DHIs to evaluate ecosystem dynamics.

Therefore, the main goal of this study is to investigate if DHIs are sensitive to changing environmental conditions across LULC types. In this case, it will highlight potential to use DHIs in ecosystem studies and could provide further added information to static LULC maps. Our study area is a central European landscape, which experienced a strong drought in 2018 (Haberstroh et al., 2022; C. Senf and Seidl, 2021; Thonfeld et al., 2022). We investigated the effect of soil-related factors such as usable Field Capacity (uFC) and climatic factors on the DHIs of different LULC types such as coniferous forest, deciduous forest, mixed forest, pasture, croplands, and built-up areas in the light of the aforementioned drought. Our specific research questions were: (1) Do LULC types have distinct DHI profiles? (2) Do LULC types and their respective DHIs differ specifically regarding their response to the extreme drought in 2018? (3) Do LULC types and their respective DHIs differ in general regarding climatic and soil conditions? Such insights are expected to be particularly valuable for monitoring activities, management decisions, and landscape protection.

Materials and methods

Study area

The state of Hesse is located in the centre of the Federal Republic of Germany. It has about 6.3 Million inhabitants, 2.4 Million people living in the Frankfurt-Rhine/Main region in the southern part of the federal state (Kallert et al. 2021). Outside the urbanized areas, the landscape is characterized by a high proportion of forests (ca. 42%), particularly in the northeast and east with forest cover up to 50% (HLNUG, 2018), but also intensively used agricultural regions, e.g. in the Wetterau north of Frankfurt (Jauker et al. 2009) where forest cover drops down to 15% (HMUKLV 2023), or non-intensively used grasslands in the Lahn-Dill (Reger et al. 2009) or Rhön region (Klinger et al. 2019). In eastern Hesse, the highest mountain with almost 950 m a.s.l is in the Rhön, and the largest continuous basalt area in Europe is the Vogelsberg area (Leßmann et al., 2000). Hesse's geological features include the crystalline Odenwald in the South, the expanse of the Rhenish Slate Mountains in the West, the extensive deposits from the Triassic period (Buntsandstein, Muschelkalk, Keuper) in the North, areas with volcanic rocks, like the above-mentioned Vogelsberg, and the regions where Tertiary and Quaternary sedimentary rocks are distributed, e.g. the upper Rhine valley in the South (Becker and Reischmann 2021). Small-scale farming is still widespread and cultivated land lies on the limestone uplands and on the loess soils of the river lowlands. Wheat is the most widely grown crop, followed by potatoes and sugar beets. Poultry, pigs, and cattle are the main livestock (HLNUG, 2018). Figure 4-1 shows the location of the federal state of Hessen in Germany and a CORINE Land Cover map from 2018 with a spatial resolution of 100m (CORINE Land Cover, 2018) taken from the Copernicus land portal to show different LULC types across Hesse. CORINE land cover maps can be considered a standard for land monitoring in Europe (Feranec et al., 2016)

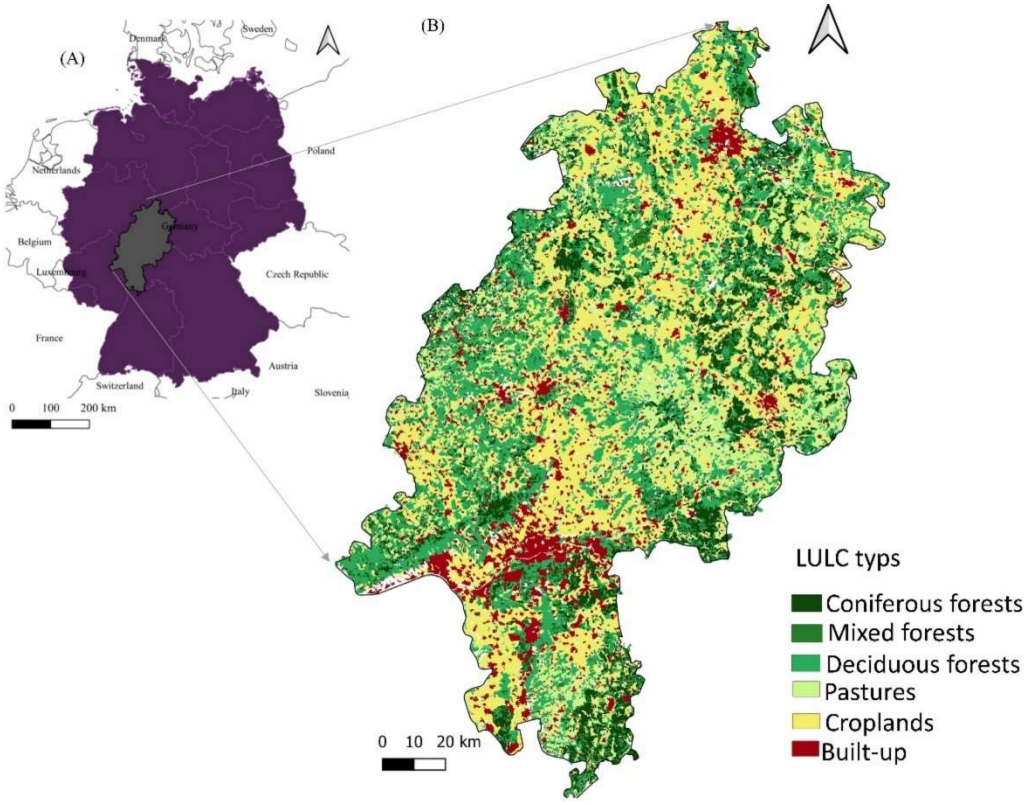

Figure 4-1 (A) Location of the federal state of Hesse in central Germany and (B) the CORINE Land Cover map from 2018 (CORINE Land Cover, 2018).

The climate of Hesse has rather continental features. The average rainfall is between 600 and 800 mm per year ranging from approximately 500mm in the Upper Rhine Valley to as high as 1400mm in elevated regions such as the Vogelsberg or the Rhön (HLNUG 2022a). The average annual temperature for the period 1981-2010 stands at 8.8°C. This marks an increase from the previous period, 1951-1980, during which it was at 8.2°C (HLNUG 2022a), and the trend shows that it continues to rise, i.e., up to 10.4°C in 2020 (HLNUG 2020). Considerable variations in annual temperature can be observed, primarily oriented along a North-South axis (HLNUG 2022a, b, Huebener et al. 2022). These variations range from minimal temperature changes in the northern regions to a notable 1.4°C increase in the South (HLNUG 2022a). In addition, clear differences between urban (hot spots) and rural regions (cold spots) exist (HLNUG 2022b). The annual precipitation levels have also experienced a modest uptick, progressing from 735mm (1901-1930) to 807mm (1981-2010). According to the Climate Protection Scenario in Hesse, it is anticipated that average temperatures will continue to rise, leading to an increase in the number of particularly warm days with temperatures exceeding 30°C (HLNUG 2022a). Nonetheless, there remains a

possibility of occasional cold spells in winter and spring, including late frosts. Furthermore, precipitation maxima are expected to shift from summer to winter, with a greater likelihood of rain as opposed to snow during the winter season. Alongside changes in mean temperatures and precipitation, there is a projected increase in the probability and intensity of heavy precipitation events and droughts in the future (HLNUG 2018). In 2018, large parts of Europe including Hesse were affected by an extreme drought (Beloiu et al., 2022; C. Senf and Seidl, 2021; Thonfeld et al., 2022). Such unprecedented hot droughts in Central Europe are expected to have strong effects, for example, on forest disturbance regimes (Senf and Seidl 2021). Further, nine priority habitat types as defined by the European Habitats Directive (92/43/EEC) occur in Hesse, and seven of them are a likely to be negatively affected by climate change (Schwenkmezger 2019). According to the monthly drought index after de Martonne (CDC, 2022), the year 2018 had the highest amount of variation of monthly drought from 2014 to 2021 in Hesse (Fig. 4-2).

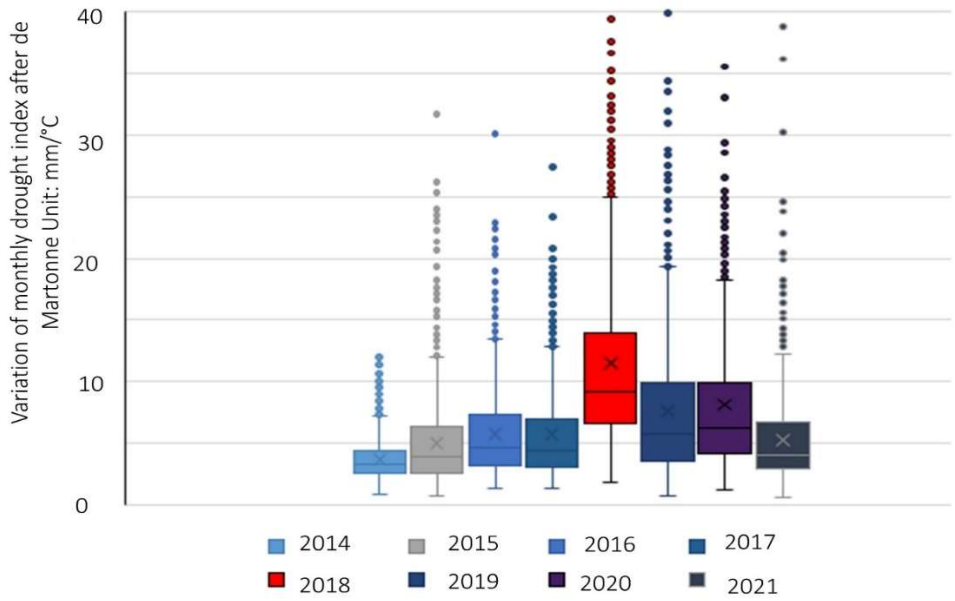

Figure 4-2 Variation of monthly drought index after de Martonne from 2014 to 2021 in Hesse/Germany (CDC, 2022). Maximum variation and drought happened in 2018.

Data and analysis

Dynamic Habitat Index (DHI)

The flowchart in Fig. 4-3 shows the conceptual framework of this study. The NDVI products of the Copernicus Global Land Service (Copernicus 2022) that are derived from top-of-

canopy PROBA-V satellite data with 300m spatial resolution (Copernicus 2022) were the basis to compute the three components of the DHI related to vegetation productivity. For this study, we used NDVI data from 01.01.2017 until 31.12.2020 with an interval of 10 days, which totaled up to 144 tiles for the full 4-year dataset. For each year, the three DHI components were computed: cumulative DHI ($\boldsymbol{DHI_{Cum} = \sum p_t}$) indicating annual cumulative productivity, minimum DHI ($\boldsymbol{DHI_{min} = \min(p_t)}$) indicating minimum cover, and seasonality ($\boldsymbol{DHI_{Var} = \frac{\sigma(p_t)}{\mu(p_t)}}$) based on the coefficient of variation using the standard deviation and the mean (p represents vegetation productivity at different periods (t)). The DHI_{Total} was generated from the composite of these three components. All details on DHI calculation are described by Coops et al. (2008), Hobi et al. (2017), Michaud et al. (2012), and Razenkova et al. (2020).

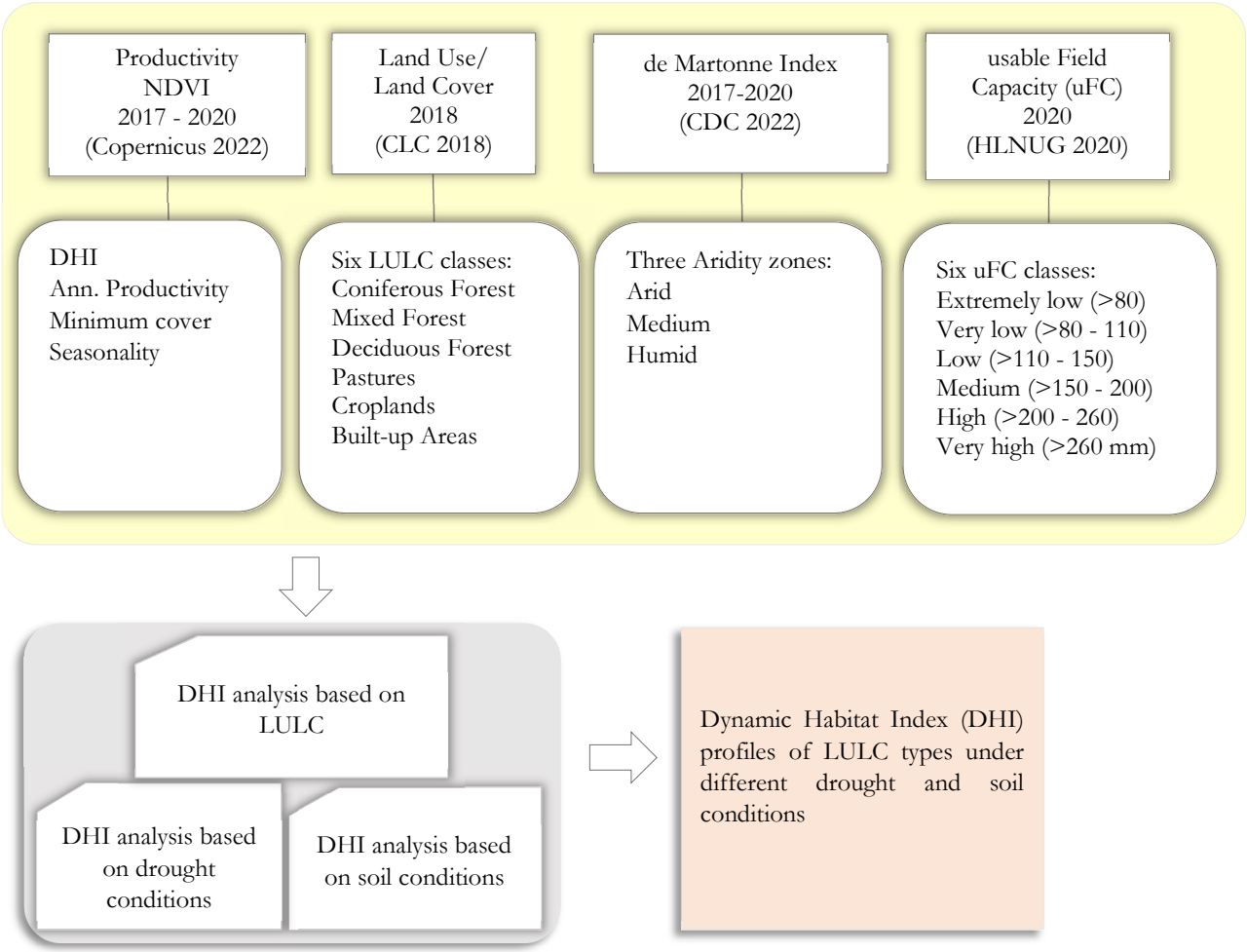

Figure 4-3: Conceptual framework of the study. The green box contains all input data and their categories. The grey boxes below show the methodological steps and analysis to reach the target in the yellow box.

Land Use/Land Cover (LULC)

The 2018 CORINE Land Cover data set was used to extract six major LULC types in Hesse: coniferous, mixed, and deciduous forests, pastures, croplands, and built-up areas and a spatial resolution of 100 m (CORINE Land Cover, 2018) using 'Raster' and 'SF' packages in R statistical software version 4 (R Core Team, 2021)for raster and vector analysis. To visually control each LULC, the LULC maps and digital orthophotos (DOP) with 20 cm spatial resolution were overlaid (Geoportal Hessen, 2022) in QGIS ver. 3.22 LTR Białowieża (QGIS Development Team, 2021) (Fig. 4B).

Precipitation Conditions: De Martonne index (dMI)

The de Martonne Index (dMI) is based on the relationship of precipitation and temperature for a given area ($dMI = \frac{P}{T+10}$ where T refers to the temperature in degrees Celsius and P refers to the precipitation in mm (de Martonne, 1941)). Low dMI values indicate aridity while increased values indicate humidity. Thus, the dMI provides information on the drought level at a given site and reflect the aridity of regional climate zones (Bhuyan et al., 2017) and has been used before in Central Germany to describe the extreme drought conditions in summer 2018 (Beloiu et al., 2022). We used monthly grids of the dMI from 01.01.2017 until 31.12.2020 provided by the German Climate Data centre (CDC, 2022) to generate regional aridity zones map at 1km spatial resolution based on a total of 48 tiles for the full 4-year dataset (CDC, 2022). To do so, we defined three aridity zones (arid, medium, humid) based on cumulative drought in the study area (dMI_{Cum}) for four years using the equation $dMI_{Cum} = \sum dMI_t$, where It refers to the cumulative drought for period t. We used the 'Raster' package to calculate the dMI_{Cum} in R statistical software version 4 (R Core Team, 2021). We then used natural break (Jenks), which accounts for non-uniform distributions and gives an unequal class width with varying frequency of observations per class, to identify the aridity zones.

Soil conditions: usable Field Capacity (uFC)

Spatial data on usable Field Capacity (uFC) data was used to study the variation of the DHI across different soil conditions (Table 4-1). The term field capacity is interchangeably used with the term water holding capacity and refers to the amount of water content held in soil after drainage of excess water (Rai et al., 2017). The uFC of a soil or a horizon describes the available part of the field capacity for vegetation. It thus includes the amount of water that a soil can retain against gravity. The data at a scale of 1:50 000 and a reference depth of 1m were provided as vector data

by Hessian State Agency for Nature Conservation, Environment and Geology (HLNUG_BFD50, 2020). There are six main groups of uFC in Hessen ranging from very low to (0 - 80 mm) to very high (>260 mm) (Table 4-1). The highest coverage mainly belonged to low uFC (>110 - 150 mm) with almost 38% of the area, followed by medium uFC (>150 - 200 mm) with 26% and high uFC (>200 - 260 mm) with 16.5% of the area.

Table 4-2: Overview of the different usable Field Capacity (uFC) categories and the proportional areas in Hesse based on data by (HLNUG_BFD50, 2020)

usable Field Capacity categories	Level	Area (m2)	Proportional Area in Hesse
Extremely low	0 - 80 mm	567495992	2.99
Very low	>80 - 110 mm	2831954494	14.95
Low	>110 - 150 mm	7199682409	38.00
Medium	>150 - 200 mm	4885629371	25.79
High	>200 - 260 mm	3125752490	16.50
Very high	>260 mm	333763646,7	1.76

To answer the question whether the DHIs are susceptible to changes in soil conditions, we extracted the DHI component values across the six uFC categories for each LULC type in QGIS. When extracting the raster data including the DHIs based on vector categories such as uFC and LULC, pixels smaller than the native DHI pixel size (300 m) at the border of each vector were excluded. For each zone and LULC type the values for the three DHI components were extracted to explore whether the DHI is sensitive towards changing precipitation regimes across LULC types.

We also examined whether yearly DHI components from 2017 to 2020 differed across LULCs and whether they returned to their previous state after the severe drought in 2018. To test it, one-way analysis of variance (ANOVA) and post hoc Tukey test (p-value <0.05) was employed using the "car" package (R Core Team, 2021). Normality of data was checked using the Shapiro-Wilk test and the Q-Q plot of residuals, and Bartlett's Test was used to check the equality of variances (A Zuur et al., 2009).

Results

All LULC revealed distinct DHI profiles (Fig. 4-4) in terms of annual productivity, minimum cover, and seasonality. In the map, the colour patterns refer to different amounts of

productivity and we could differentiate LULCs visually using digital orthophotos with 20 cm spatial resolution (Geoportal Hessen, 2022). For example, blue colour indicates the built-up areas with low annual productivity, low minimum cover, and high seasonality. The yellow areas are coniferous forests that are characterized by high annual productivity and minimum cover, but low seasonality. On the other hand, pastures with purple colour have intermediate annual productivity and minimum cover, but low seasonality (Fig. 4-4A and B). The three-dimensional scatterplot indicates that the areas with high seasonality have lower annual productivity and minimum cover than the areas with low seasonality (Fig. 4-4C).

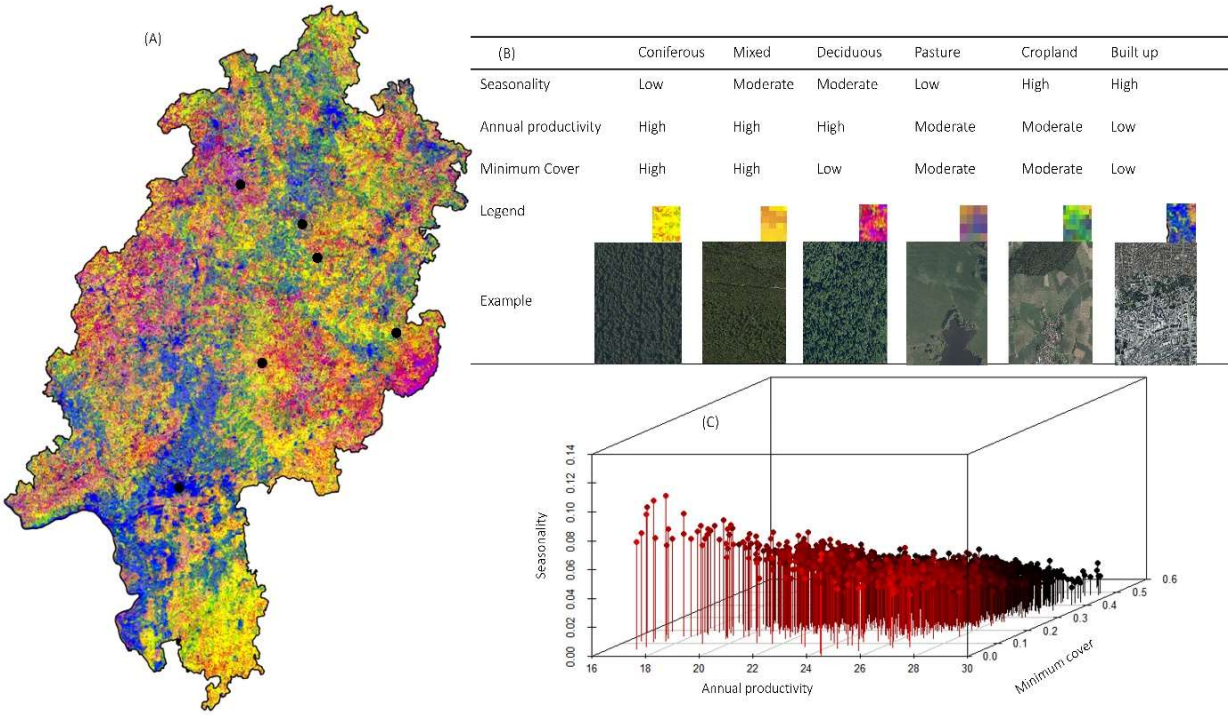

Figure 4-4 The combined components of the dynamic habitat index derived from 2017 to 2020 (A). This composite image was developed by assigning the annual productivity to the red band, the minimum cover to the green band, and the seasonality to the blue band. Blue areas have low annual productivity, low minimum cover, and high seasonal variability. Thus, blue areas indicate the locations of the built-up areas. Bright yellow areas have a high annual productivity, a high minimum cover, and low variability and represent locations with coniferous forests that were consistently green throughout the year. Purple areas or pastures indicate landscapes with medium annual productivity, medium minimum cover, and low variability. Green areas or croplands indicate moderate landscape greenness that varies throughout the year. Red areas or deciduous forest have high annual production, moderate minimum cover, and high seasonality. Black points on the map refer to the example areas (B) the three-dimensional scatterplot indicates three components of the DHI. The areas with high seasonality have lower annual productivity and minimum cover than the areas with low seasonality.

Response of the DHI to drought across LULC types

From 2017 to 2020, the annual productivity (DHI_{Cum}) for all LULCs had their maximum in 2017 (Fig. 4-5). In 2018 and 2019, the annual productivity decreased for all LULC types and then started to recover. Except for deciduous forests, none of the other LULCs had fully returned to the pre-drought conditions in 2017. The highest values of annual productivity belonged to forests and pastures (range from 28 to 30) and built-up areas revealed the lowest annual productivity (range from 23 to 25).

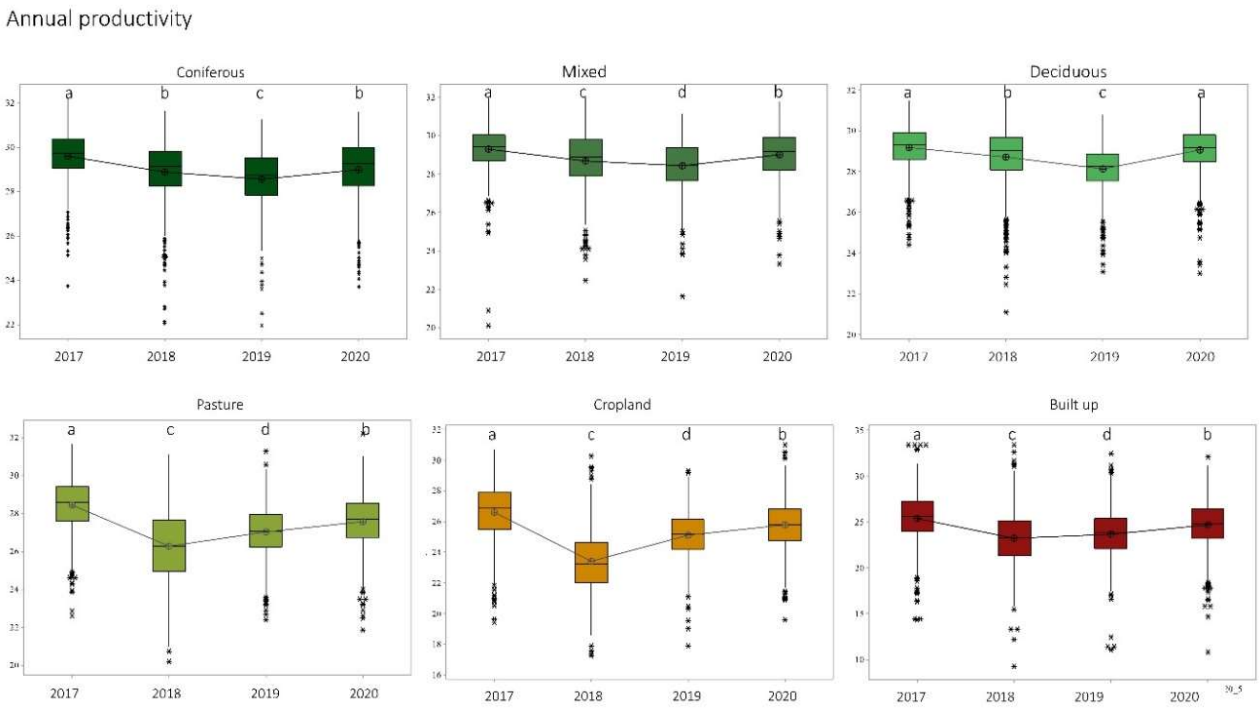

Figure 4-5: Cumulative annual productivity (DHI_{Cum}) from 2017 to 2020 including the severe drought year 2018 for the six main Land Use/Land Cover types in Hesse, Germany, namely coniferous, mixed, and deciduous forests, pastures, croplands, and built-up areas. The black line connects the median of annual productivity. Small letters on the columns indicate significant differences in values based on one-way analysis of variance (ANOVA) and the Tukey post hoc test.

Minimum cover increased from 2018 to 2019 for all LULC types, and, in general, the highest values of DHI_{Min} belonged to the forest types. (Fig. 4-6). The highest values of minimum cover occurred in the drought year, which contrasts the output of DHI_{Cum}.

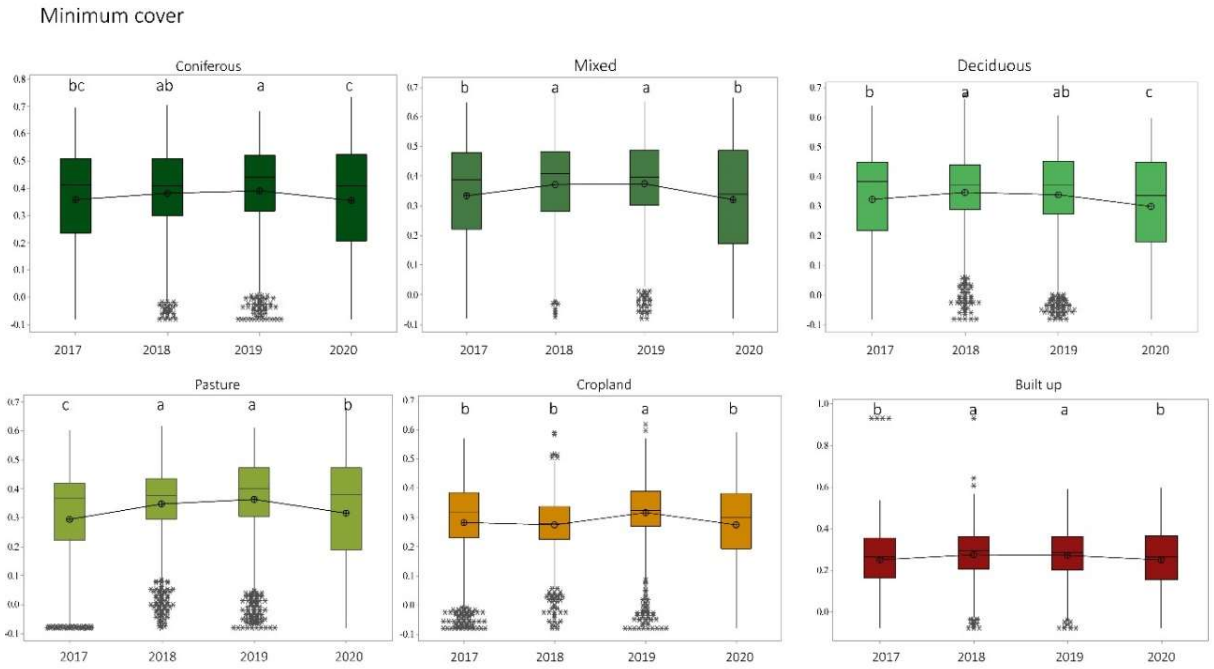

Figure 4-6: Minimum cover (DHI_{Min}) from 2017 to 2020 including the severe drought year 2018 for the six main Land Use/Land Cover types in Hesse, Germany, namely coniferous, mixed, and deciduous forests, pastures, croplands, and built-up areas. The black line connects the medians of minimum cover. Small letters on the columns indicate significant differences in values based on one-way analysis of variance (ANOVA) and the Tukey post hoc test.

Forests and pastures showed less seasonality than croplands and built-up areas (Fig. 4-7). After the drought 2018, the seasonality of the forest LULC types increased. In pastures and croplands, most variation occurred in 2018. In the built-up areas, seasonality was almost constant over the years.

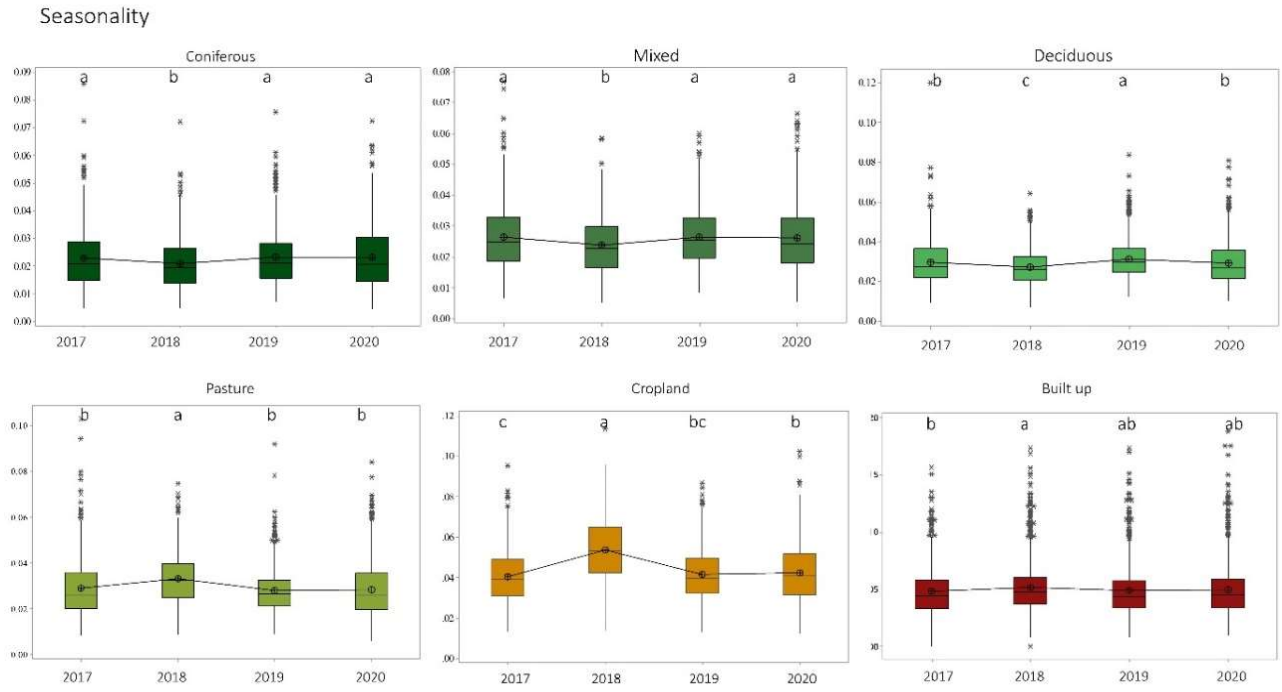

Figure 4-7: Seasonality (DHI_{Var}) from 2017 to 2020 including the severe drought year 2018 for the six main Land Use/Land Cover types in Hesse, Germany, namely coniferous, mixed, and deciduous forests, pastures, croplands, and built-up areas. The black line connects the medians of seasonality. Small letters on the columns indicate significant differences in values based on one-way analysis of variance (ANOVA) and the Tukey post hoc test.

Effect of aridity zones on DHI components across LULC types

In general, for all LULC types, annual productivity and minimum cover were significantly higher in the humid zone than in the medium and arid zone (Fig. 4-8A and B, p <0.05). On the other hand, seasonality in arid zones was significantly higher compared to the other two zones (Fig. 4-8C, p <0.05). More precisely, the annual productivity in the three forest types, pasture and built-up areas was significantly higher in the humid zone, but there is no significant difference between the medium and arid zones of coniferous and mixed forests and built-up areas (Fig. 4-8A). In terms of minimum cover, again the highest values for all LULC types were observed in the humid zone (Fig. 4-8B). The maximum seasonality mainly occurred in the arid zone in all LULCs (Fig. 4-8C) and the seasonality in forest LULC types was less pronounced than that of pastures, croplands, and built-up areas.

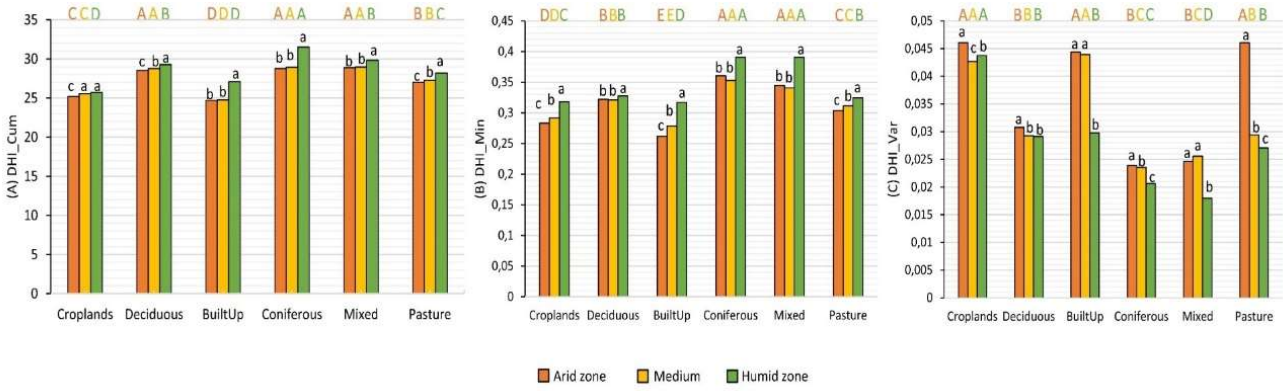

Figure 4-8: The three components of the Dynamic Habitat Index (DHI), namely (A) DHI_{Cum} (annual productivity), (B) DHI_{Min} (minimum cover), and (C) DHI_{Var} (seasonality) based on NDVI data from 2017 - 2020 are shown for six LULC types (coniferous, mixed, and deciduous forests, pastures, croplands, and built-up areas) and three aridity zones. The orange columns represent the arid zone, the yellow columns represent the medium zone, and the green columns represent the humid zone. The capital letter above the graph indicates the significance of the comparisons within each aridity zone separately, and the small letters inside the graph indicate the significance of the comparisons within each LULC type (p-value <0.05).

Effect of uFC on DHI components across LULC types

With decreasing uFC, annual productivity decreased in all LULC types except built-up areas (Fig. 4-9A). In forest types, pasture, and croplands lowest annual productivity was obtained for extremely low (0 - 80 mm) and very low (>80 - 110 mm) uFC, whereas maximum annual productivity values were obtained for high (>200 - 260 mm) and very high (>260 mm) uFc. In built-up areas, annual productivity was not affected by uFc (Fig. 4-9A).

In terms of minimum cover, except of built-up areas, a decreasing trend was observed with decreasing uFC (Fig. 4-9B). In forest types, pasture and croplands, the maximum values of minimum cover occurred in the areas with highest uFC. Seasonality showed a trend opposite to the previous two DHI components. Thus, in forests and pastures lowest seasonality occurred where the uFC was the highest (>260 mm), and seasonality increased when uFC decreased (Fig. 4-9C). Cropland and built-up areas showed different trends. For croplands, seasonality was higher in areas with very high uFC (>260 mm), while for built-up areas the changes were not in a particular order.

Figure 4-9: (A) Annual productivity (DHI_{Cum}), (B) Minimum cover (DHI_{Min}), and (C) Seasonality (DHI_{Var}) of each LULC type (namely coniferous, mixed, and deciduous forests, pastures, croplands, and built-up

areas) depending on the usable Field Capacity (uFC). Small letters on the columns indicate significant differences between uFC classes (p-value < 0.05).

Discussion

We found that all LULC types had distinct and plausible DHI profiles (e.g., high productivity and minimum cover, but low intra-seasonal variability for all forest LULC types) that differed due to regional environmental changes related to soil and drought conditions. Annual productivity and seasonality clearly captured the response of the LULC types to different uFC classes and aridity zones, but minimum cover had different temporal trends. Indeed, heat stress and disturbances associated with droughts affect water availability in soil and reduce vegetation productivity (Xu et al., 2019), which is in line with the response of the DHI components to changing climatic and soil conditions. Therefore, the DHI provided a continuous measure to characterize LULC types which could provide more direct connections to ecosystem functions and health than purely static classifications (Coops and Wulder, 2019). So, we see potential for composite vegetation indices or other land surface phenological products derived from satellite time-series data to complement common LULC maps to allow for a more detailed analysis of links between LULC and ecosystem functioning and services.

The DHI components responded to the severe drought year 2018. The DHI_{Cum} showed that apart from the deciduous forest none of the LULC types had returned to their original level after the drought event, which could be a sign of weakened resilience and vegetation degradation (Lloret et al., 2022; Manrique-Alba et al., 2022). Indeed, forests are facing several drought events with different intensities and magnitudes during their lifetime and therefore resilience to dry conditions may be critical to long-term survival (DeSoto et al., 2020). Understanding forest productivity and its variation under different environmental conditions is important especially when climate change is likely to strongly affect the productivity of temperate European forests (Morin et al., 2018). Capturing the effect of current droughts based on DHI in the forests can be a promising proxy to assess future tree mortality risk (e.g., by identifying DHI profiles of forests typical for die-off), especially when producing the DHI using high-resolution optical data like Planet Scopes or Rapid eye images (Silveira et al., 2023). However, the computation of the DHI with a relatively large pixel size comparable to the initial study by (Coops et al., 2008) allows retrospective studies, for example using MODIS satellite data. In cases where the use of the NDVI might be limited, for example in semi-arid regions where vegetation cover is low or in the Tropics where the NDVI tends to saturate, other vegetation indices that can partially overcome these

limitations such as the Enhanced Vegetation Index (EVI) or the Soil-Adjusted Vegetation Index (SAVI) (Pettorelli et al. 2005) could be tested. Another alternative could be a biophysical parameter such as the LAI, which has been used in combination with precipitation indices for vegetation drought monitoring (Kim et al. 2017) and which has been computed in DHI studies (Hobi et al. 2017). A further limitation of using vegetation indices derived from passive optical remote sensing data might be the presence of clouds (Pettorelli et al. 2005). Latest development in forest drought monitoring includes the use of freely available SAR data (Kaiser et al., 2022; Schellenberg et al., 2023), so further potential exists to improve the power of DHI to detect and interpret changes or ecosystem degradation using high-temporal resolution active remote sensing data.

The integration of the DHI with spatial environmental information provides a more comprehensive understanding of ecosystem dynamics at the landscape scale (Michaud et al., 2012), which is extremely valuable for biodiversity assessments (Razenkova et al., 2023; Silveira et al., 2023). In addition, NDVI-based measurements from space have the potential to identify site-specific and climate-induced degradation of vegetation health (Margalef-Marrase et al. 2020), but productivity related effects might show time lags of one to two years (Ogle et al. 2015), so combining the DHI with abiotic factors has the potential to provide insight into ecosystem degradation. Such integrated products could help decision makers to develop sustainable land management strategies and contribute to Sustainable Develop Goal (SDG) indicators such as SDG 15.3.1 that is related to land degradation (Sims et al. 2021), e.g. by identifying deviations of a LULC type from its typical DHI profile within its environmental context as a response to disturbance and environmental stress. Here, examining uFC for different LULCs revealed decreasing annual productivity with decreasing water holding capacity of the soil for all LULCs except built-up areas. The DHI was also able to clearly capture forest and pasture productivity depending on the uFC. Availability of more water is essential for forest growth and thus production, particularly in the context of global change and increased probabilities of severe droughts (Piedallu et al., 2011). In croplands, uFC can have a significant impact on the efficiency of crop productivity under given climate conditions (Fang and Su, 2019; He and Wang, 2019), and in this study the DHIs were able to capture such variation. Due to management in croplands (ploughing) and intensive human activities in built-up areas (sealing) the seasonality was higher, and annual productivity was lower compared to forests and pastures. A reason for almost no differences in the built-up area could be the relatively large pixel size as fine urban landscape structures might require spectral unmixing approaches to map urban vegetation greenness even from Landsat time series data (Czekajlo et al., 2020), or the use of very high-resolution Planet Scope imagery (Silveira et al., 2023). On the other

hand, the seasonality of urban heat islands has been mapped using a MODIS-based data product (Sismanidis et al., 2022). Quantifying sealed surfaces and their effect on productivity has been emphasized since it is important in a wide range of strategies to reduce impervious surfaces and their impacts on water resources and vegetation cover for site-level planning, and land use regulation (Arnold and Gibbons, 1996). Thus, future avenues of research particularly for urban areas could include the combination of the DHI based on the NDVI (or similar parameters) with high temporal thermal remote sensing data.

Conclusion

We show that composite remote sensing indices such as the DHI based on NDVI time series data are useful to characterize LULC types including their variation due to changing soil and drought conditions including effects of severe drought years in Central European landscapes. We argue that DHIs are an appropriate metric to complement or even replace discrete and static LULC maps especially for biodiversity and ecosystem research and application, for example within the frame of Sustainable Development Goals related to sustainable use of terrestrial ecosystems and ongoing land degradation such as SDG 15. Limitations due to coarse spatial resolution could be solved in the future due the availability of free high resolution optical satellite data, and the integration with high temporal resolution thermal and SAR satellite data is to our knowledge still underexplored. The methodological approach was based on publicly available data as well as free and open-source software, so we see potential for further studies in the field of monitoring impacts of climate change, landscape planning and management of ecosystems.

Date availability statement: Data available on request from the authors.

Disclosure statement: All authors declare that they have no conflicts of interest.

References

Aghsaei, H., Dinan, NM., Moridi, A., Asadolahi, Z., Delavar, M., Fohrer, N., Wagner, PD., 2020. Effects of dynamic land use/land cover change on water resources and sediment yield in the Anzali wetland catchment, Gilan, Iran. Science of the Total Environment. 712: 136449. https://doi.org/10.1016/j.scitotenv.2019.136449

Akodéwou, A., Oszwald, J., Saïdi, S., Gazull, L., Akpavi, S., Akpagana, K., Gond, V., 2020. Land Use and Land Cover Dynamics Analysis of the Togodo Protected Area and Its Surroundings in Southeastern Togo, West Africa. Sustainability. 12(13). https://doi.org/10.3390/su12135439

Arnold, CL., Gibbons, CJ., 1996. Impervious Surface Coverage: The Emergence of a Key Environmental Indicator. Journal of the American Planning Association. 62(2):243–258. https://doi.org/10.1080/01944369608975688

Avand, M., Moradi, H., lasboyee, MR., 2021. Using machine learning models, remote sensing, and GIS to investigate the effects of changing climates and land uses on flood probability. Journal of Hydrology. 595:125663. https://doi.org/10.1016/j.jhydrol.2020.125663

Becker, R., Reischmann, T., 2021. Geologie von Hessen. Hessisches Landesamt für Naturschutz, Umwelt und Geologie (HLNUG). Wiesbaden, Germany.

Belay, T., Melese, T., Senamaw, A., 2022. Impacts of land use and land cover change on ecosystem service values in the Afroalpine area of Guna Mountain, Northwest Ethiopia. Heliyon. 8(12):e12246. https://doi.org/10.1016/j.heliyon.2022.e12246

Beloiu, M., Stahlmann, R., Beierkuhnlein, C., 2022. Drought impacts in forest canopy and deciduous tree saplings in Central European forests. Forest Ecology and Management. 509:120075. https://doi.org/10.1016/j.foreco.2022.120075

Bhuyan, U., Zang, C., Menzel, A., 2017. Different responses of multispecies tree ring growth to various drought indices across Europe. Dendrochronologia. 44:1–8. https://doi.org/10.1016/j.dendro.2017.02.002

CDC., 2022. Climate Data Center, Grids of monthly drought index (de Martonne) over Germany, version v1.0. Index of /climate_environment/CDC/grids_germany/monthly/drought_index/ (dwd.de).

Chaves, M., Picoli, M., Sanches, I., 2020. Recent Applications of Landsat 8/OLI and Sentinel-2/MSI for Land Use and Land Cover Mapping: A Systematic Review. Remote Sensing. 12(18). https://doi.org/10.3390/rs12183062

CLC, 2018. Copernicus Land Monitoring Service (CLMS) European Environment Agency (EEA). Copenhagen K. – Denmark.

Coops, NC., Kearney, SP., Bolton, DK., Radeloff, VC., 2018. Remotely-sensed productivity clusters capture global biodiversity patterns. Scientific Reports. 8(1):16261. https://doi.org/10.1038/s41598-018-34162-8

Coops, NC., Wulder, MA., 2019. Breaking the Habit(at). Trends in Ecology & Evolution. 34(7):585–587. https://doi.org/10.1016/j.tree.2019.04.013

Coops, NC., Wulder, MA., Duro, DC., Han, T., Berry, S., 2008. The development of a Canadian dynamic habitat index using multi-temporal satellite estimates of canopy light absorbance. Ecological Indicators. 8(5):754–766. https://doi.org/10.1016/j.ecolind.2008.01.007

Copernicus, 2022. Normalized Difference Vegetation Index, Copernicus global land service, Providing bio-geophysical products of global land surface.

Czekajlo, A., Coops, NC., Wulder, MA., Hermosilla, T., Lu, Y., White, JC., van den Bosch, M., 2020. The urban greenness score: A satellite-based metric for multi-decadal characterization of urban land dynamics. International Journal of Applied Earth Observation and Geoinformation. 93:102210. https://doi.org/10.1016/j.jag.2020.102210

DeSoto, L., Cailleret, M., Sterck, F., Jansen, S., Kramer, K., Robert, EMR., Aakala, T., Amoroso, MM., Bigler, C., Camarero, JJ., et al. 2020. Low growth resilience to drought is related to future mortality risk in trees. Nature Communications. 11(1):545. https://doi.org/10.1038/s41467-020-14300-5

Fang, J., Su, Y., 2019. Effects of Soils and Irrigation Volume on Maize Yield, Irrigation Water Productivity, and Nitrogen Uptake. Scientific Reports. 9(1):7740. https://doi.org/10.1038/s41598-019-41447-z

Fathi-Taperasht, A., Shafizadeh-Moghadam, H., Sadian, A., Xu, T., Nikoo, MR., 2023. Drought-induced vulnerability and resilience of different land use types using time series of MODIS-based indices. International Journal of Disaster Risk Reduction. 91:103703. https://doi.org/10.1016/j.ijdrr.2023.103703

Feranec, T., Soukup, G., Hazeu, G., 2016. European landscape dynamics. Corine land cover data, CRC-Press, Boca Raton.

Gashaw, T., Tulu, T., Argaw, M., Worqlul, AW., Tolessa, T., Kindu, M., 2018. Estimating the impacts of land use/land cover changes on Ecosystem Service Values: The case of the Andassa watershed in the Upper Blue Nile basin of Ethiopia. Ecosystem Services. 31:219–228. https://doi.org/10.1016/j.ecoser.2018.05.001

Gemitzi, A., Banti, MA., Lakshmi, V., 2019. Vegetation greening trends in different land use types: natural variability versus human-induced impacts in Greece. Environmental Earth Sciences. 78(5):172. https://doi.org/10.1007/s12665-019-8180-9

Geoportal Hessen., 2022. Hessische Verwaltung für Bodenmanagement und Geoinformation. Metadaten (hessen.de).

Haberstroh, S., Werner, C., Grün, M., Kreuzwieser, J., Seifert, T., Schindler, D., Christen, A., 2022. Central European 2018 hot drought shifts scots pine forest to its tipping point. Plant Biology. 24(7):1186–1197. https://doi.org/10.1111/plb.13455

He, D., Wang, E., 2019. On the relation between soil water holding capacity and dryland crop productivity. Geoderma. 353:11–24. https://doi.org/10.1016/j.geoderma.2019.06.022

HLNUG. 2018. Klimawandel in Hessen. Hessisches Landesamt für Naturschutz, Umwelt und Geologie (HLNUG), Fachzentrum Klimawandel und Anpassung, Wiesbaden, Germany.

HLNUG. 2020. Gewässerkundlicher Jahresbericht 2020. Hydrologie in Hessen 23.

HLNUG. 2022a. Beobachteter Klimawandel. Klimawandel in Hessen. Hessisches Landesamt für Naturschutz, Umwelt und Geologie (HLNUG), Wiesbaden, Germany.

HLNUG. 2022b. Satellitenfernerkundung in Hessen. Mit Hitzekarten Hessens Hot Spots erkennen. Hessisches Landesamt für Naturschutz, Umwelt und Geologie (HLNUG), Wiesbaden, Germany.

HLNUG. 2023. Hessisches Ministerium für Umwelt, Landwirtschaft und Forsten Geologische Entwicklung in Hessen. https://www.hlnug.de/themen/geologie/geo-info-hessen/geologische-entwicklung-in-hessen/naturraum.

HLNUG_BFD50. 2020. Nutzbare Feldkapazität des Bodens. Hessisches Landesamt für Naturschutz, Umwelt und Geologie (HLNUG), Wiesbaden, Germany.

HMUKLV. 2023. Naturnah & vielfältig. Wir machen den Wald klimastabil. Hessisches Ministerium für Umwelt, Klimaschutz, Landwirtschaft und Verbraucherschutz (HMUKLV). https://umwelt.hessen.de/wald. Accessed 09.10.2023.

Hobi, ML., Dubinin, M., Graham, CH., Coops, NC., Clayton, MK., Pidgeon, AM., Radeloff, VC., 2017. A comparison of Dynamic Habitat Indices derived from different MODIS products as predictors of avian species richness. Remote Sensing of Environment. 195:142–152. https://doi.org/10.1016/j.rse.2017.04.018

Huebener, H., Gelhardt, U., Lang, J., 2022. Improved representativeness of simulated climate using natural units and monthly resolution. Frontiers in Climate, 4, 991082. https://doi.org/10.3389/fclim.2022.991082

Jauker, F., Diekoetter, T., Schwarzbach, F., Wolters, V., 2009. Pollinator dispersal in an agricultural matrix: opposing responses of wild bees and hoverflies to landscape structure and distance from main habitat. Landscape Ecology, 24, 547-555. https://doi.org/10.1007/s10980-009-9331-2

Kaiser, P., Buddenbaum, H., Nink, S., Hill, J., 2022. Potential of Sentinel-1 Data for Spatially and Temporally High-Resolution Detection of Drought Affected Forest Stands. Forests. 13(12). https://doi.org/10.3390/f13122148

Karra, K., Kontgis, C., Statman-Weil, Z., Mazzariello, CJ., Mathis, M., Brumby, SP., 2021. Global land use / land cover with Sentinel 2 and deep learning. In: 2021 IEEE International Geoscience and Remote Sensing Symposium IGARSS. [place unknown]; p. 4704–4707. https://doi.org/10.1109/IGARSS47720.2021.9553499

Kim, K., Wang, MC., Ranjitkar, S., Liu, SH., Xu, JC., Zomer, RJ., 2017. Using leaf area index (LAI) to assess vegetation response to drought in Yunnan province of China. Journal of Mountain Science. 14(9): 1863-1872. https://doi.org/10.1007/s11629-016-3971-x

Klinger, YP., Harvolk-Schöning, S., Eckstein, RL., Hansen, W., Otte, A., Ludewig, K., 2019. Applying landscape structure analysis to assess the spatio-temporal distribution of an invasive legume in the Rhön UNESCO Biosphere Reserve. Biological Invasions, 21(8), 2735-2749. https://doi.org/10.1007/s10530-019-02012-x

Kooistra, L., Berger, K., Brede, B., Graf, LV., Aasen, H., Roujean, J-L., Machwitz, M., Schlerf, M., Atzberger, C., Prikaziuk, E., et al. 2023. Reviews and syntheses: Remotely sensed optical time series for monitoring vegetation productivity. Biogeosciences Discussions. 2023:1–67. https://doi.org/10.5194/bg-2023-88

Le, TDH., Pham, LH., Dinh, QT., Hang, NTT., Tran, TAT., 2022. Rapid method for yearly LULC classification using Random Forest and incorporating time-series NDVI and topography: a case study of Thanh Hoa province, Vietnam. Geocarto International. 37(27):17200–17215. https://doi.org/10.1080/10106049.2022.2123959

Leßmann, B., Scharpff, H-J., Wedel, A., Wiegand, K., 2000. Grundwasser im Vogelsberg, Hessisches Ministerium für Umwelt, Landwirtschaft und Forsten, ISBN 3-89274-206-5. https://www.hlnug.de/fileadmin/dokumente/wasser/hydrogeologie/grundwasser_im_vogelsberg.pdf.

Lloret, F., Jaime, LA., Margalef-Marrase, J., Pérez-Navarro, MA., Batllori, E., 2022. Short-term forest resilience after drought-induced die-off in Southwestern European forests. Science of The Total Environment. 806:150940. https://doi.org/10.1016/j.scitotenv.2021.150940

Mackey, B., Bryan, J., Randall, L., 2004. Australia's Dynamic Habitat Template 2003.

Manrique-Alba, À., Beguería, S., Camarero, JJ., 2022. Long-term effects of forest management on post-drought growth resilience: An analytical framework. Science of The Total Environment. 810:152374. https://doi.org/10.1016/j.scitotenv.2021.152374

Margalef-Marrase, J., Pérez-Navarro, MÁ., Lloret, F., 2020. Relationship between heatwave-induced forest die-off and climatic suitability in multiple tree species. Global Change Biology. 26(5): 3134-3146. https://doi.org/ 10.1111/gcb.15042

Marshall, L., Biesmeijer, JC., Rasmont, P., Vereecken, NJ., Dvorak, L., Fitzpatrick, U., Francis, F., Neumayer, J., Ødegaard, F., Paukkunen, JPT., Pawlikowski, T., Reemer M, Roberts SPM, Straka J, Vray S, Dendoncker, N., 2018. The interplay of climate and land use change affects the distribution of EU bumblebees. Global Change Biology. 24(1): 101-116. https://doi.org/10.1111/gcb.13867

de Martonne, E., 1941. Nouvelle carte mondiale de l' indice d' aridite. La Meteorologie. Annales de géographie.

Mas, J-F., Lemoine-Rodríguez, R., González-López, R., López-Sánchez, J., Piña-Garduño, A., Herrera-Flores, E., 2017. Land use/land cover change detection combining automatic processing and visual interpretation. European Journal of Remote Sensing. 50(1):626–635. https://doi.org/10.1080/22797254.2017.1387505

Michaud, J-S., Coops, NC., Andrew, ME., Wulder, MA., 2012. Characterising spatiotemporal environmental and natural variation using a dynamic habitat index throughout the province of Ontario. Ecological Indicators. 18:303–311. https://doi.org/10.1016/j.ecolind.2011.11.027

Morin, X., Fahse, L., Jactel, H., Scherer-Lorenzen, M., García-Valdés, R., Bugmann, H., 2018. Long-term response of forest productivity to climate change is mostly driven by change in tree species composition. Scientific Reports. 8(1):5627. https://doi.org/10.1038/s41598-018-23763-y

Musetsho, KD., Chitakira, M., Nel, W., 2021. Mapping Land-Use/Land-Cover Change in a Critical Biodiversity Area of South Africa. International Journal of Environmental Research and Public Health. 18(19). https://doi.org/10.3390/ijerph181910164

Ogle, K., Barber, JJ., Barron-Gafford, GA., Bentley, LP., Young, JM., Huxman, TE., Loik, ME., Tissue, DT., 2015. Quantifying ecological memory in plant and ecosystem processes. Ecology Letters. 18(3):221-35. https://doi.org/10.1111/ele.12399

Pettorelli, N., Vik, JO., Mysterud, A., Gaillard, JM., Tucker, CJ., Stenseth, NC., 2005. Using the satellite-derived NDVI to assess ecological responses to environmental change. Trends in Ecology & Evolution. 20(9): 503-510. https://doi.org/10.1016/j.tree.2005.05.011

Piedallu, C., Gégout, J-C., Bruand, A., Seynave, I., 2011. Mapping soil water holding capacity over large areas to predict potential production of forest stands. Geoderma. 160(3):355–366. https://doi.org/10.1016/j.geoderma.2010.10.004

QGIS Development Team. 2021. QGIS Geographic Information System. Open Source Geospatial Foundation Project. http://qgis.osgeo.org.

R Core Team. 2021. R: A language and environment for statistical computing. R Foundation for Statistical Computing, Vienna, Austria.

Rai, RK., Singh, VP., Upadhyay, A., 2017. Chapter 17 - Soil Analysis. In: Rai RK, Singh VP, Upadhyay A, editors. Planning and Evaluation of Irrigation Projects [Internet]. [place unknown]: Academic Press; p. 505–523. https://doi.org/10.1016/B978-0-12-811748-4.00017-0

Ramirez-Reyes, C., Brauman, KA., Chaplin-Kramer, R., Galford GL, Adamo SB,, Anderson, CB., Anderson, C., Allington GRH, Bagstad KJ, Coe MT, et al., 2019. Reimagining the potential of Earth observations for ecosystem service assessments. Science of The Total Environment. 665:1053–1063. https://doi.org/10.1016/j.scitotenv.2019.02.150

Razenkova, E., Dubinin, M., Pidgeon, AM., Hobi, ML., Zhu, L., Bragina, EV., Allen, AM., Clayton MK, Baskin LM., Coops, NC., Radeloff, VC., 2023. Abundance patterns of mammals across Russia

explained by remotely sensed vegetation productivity and snow indices. Journal of Biogeography. 50(5):932–946. https://doi.org/10.1111/jbi.14588

Razenkova, E., Radeloff, VC., Dubinin, M., Bragina EV, Allen AM, Clayton MK, Pidgeon AM, Baskin LM, Coops, NC., Hobi, ML., 2020. Vegetation productivity summarized by the Dynamic Habitat Indices explains broad-scale patterns of moose abundance across Russia. Scientific Reports. 10(1):836. https://doi.org/10.1038/s41598-019-57308-8

Reger, B., Mattern, T., Otte, A., Waldhardt, R., 2009. Assessing the spatial distribution of grassland age in a marginal European landscape. Journal of Environmental Management, 90(9), 2900-2909. https://doi.org/10.1016/j.jenvman.2007.10.015

Runge, J., Bathiany, S., Bollt, E., Camps-Valls, G., Coumou, D., Deyle, E., Glymour C, Kretschmer M, Mahecha MD, Muñoz-Marí J, et al., 2019. Inferring causation from time series in Earth system sciences. Nature Communications. 10(1):2553. https://doi.org/10.1038/s41467-019-10105-3

Safaei, M., Bashari, H., Mosaddeghi, MR., Jafari, R., 2019. Assessing the impacts of land use and land cover changes on soil functions using landscape function analysis and soil quality indicators in semi-arid natural ecosystems. CATENA. 177:260–271. https://doi.org/10.1016/j.catena.2019.02.021

Safaei, M., Bashari, H., Kleinebecker, T., Fakheran, S., Jafari, R., Große-Stoltenberg, A., 2023. Mapping terrestrial ecosystem health in drylands: comparison of field-based information with remotely sensed data at watershed level. Landscape Ecology, 38(3), 705-724. https:// doi.org/ 10. 1007/ s10980- 022- 01454-4

Schellenberg, K., Jagdhuber, T., Zehner, M., Hese, S., Urban, M., Urbazaev, M., Hartmann H, Schmullius C., Dubois, C., 2023. Potential of Sentinel-1 SAR to Assess Damage in Drought-Affected Temperate Deciduous Broadleaf Forests. Remote Sensing. 15(4). https://doi.org/10.3390/rs15041004

Schwenkmezger, L., 2019. Auswirkungen des Klimawandels auf hessische Arten und Lebensräume: Liste potentieller Klimaverlierer. Hessisches Landesamt für Naturschutz, Umwelt und Geologie (HLNUG), Wiesbaden, Germany.

Senf, C., Seidl, R., 2021. Persistent impacts of the 2018 drought on forest disturbance regimes in Europe. Biogeosciences. 18(18):5223–5230. https://doi.org/10.5194/bg-18-5223-2021

Sharma, R., Nehren, U., Rahman, SA., Meyer, M., Rimal, B., Aria, Seta G., Baral, H., 2018. Modeling Land Use and Land Cover Changes and Their Effects on Biodiversity in Central Kalimantan, Indonesia. Land. 7(2). https://doi.org/10.3390/land7020057

Sharma, R., Rimal, B., Baral, H., Nehren, U., Paudyal, K., Sharma, S., Rijal, S., Ranpal S, Acharya RP, Alenazy AA., Kandel, P., 2019. Impact of Land Cover Change on Ecosystem Services in a Tropical Forested Landscape. Resources. 8(1). https://doi.org/10.3390/resources8010018

Sharma, S., Hussain, S., Singh, AN., 2023. Impact of land use and land cover on urban ecosystem service value in Chandigarh, India: a GIS-based analysis. Journal of Urban Ecology. 9(1):juac030. https://doi.org/10.1093/jue/juac030

Silveira, EMO., Pidgeon, AM., Farwell, LS., Hobi, ML., Razenkova, E., Zuckerberg, B., Coops, NC., Radeloff, VC., 2023. Multi-grain habitat models that combine satellite sensors with different resolutions explain bird species richness patterns best. Remote Sensing of Environment. 295:113661. https://doi.org/10.1016/j.rse.2023.113661

Sims, NC., Newnham, GJ., England, JR., Guerschman, J., Cox, SJD., Roxburgh, SH., Viscarra Rossel, RA., Fritz, S., Wheeler, I., 2021. Good Practice Guidance. SDG Indicator 15.3.1, Proportion of Land That Is Degraded Over Total Land Area. Version 2.0. United Nations Convention to Combat Desertification, Bonn, Germany. https://www.unccd.int/ publications/good-practice-guidance-sdg-indicator-1531proportion-land-degraded-over-total-land

Sismanidis, P., Bechtel, B., Perry, M., Ghent, D., 2022. The Seasonality of Surface Urban Heat Islands across Climates. Remote Sensing. 14(10). https://doi.org/10.3390/rs14102318

Suttidate, N., Hobi, ML., Pidgeon, AM., Round, PD., Coops, NC., Helmers, DP., Keuler, NS., Dubinin, M., Bateman, BL., Radeloff, VC., 2019. Tropical bird species richness is strongly associated with patterns of primary productivity captured by the Dynamic Habitat Indices. Remote Sensing of Environment. 232:111306. https://doi.org/10.1016/j.rse.2019.111306

Talukdar, S., Singha, P., Mahato, S., Shahfahad, Pal S., Liou, Y-A., Rahman, A., 2020. Land-Use Land-Cover Classification by Machine Learning Classifiers for Satellite Observations—A Review. Remote Sensing. 12(7). https://doi.org/10.3390/rs12071135

Thonfeld, F., Gessner, U., Holzwarth, S., Kriese, J., da Ponte, E., Huth, J., Kuenzer, C., 2022. A First Assessment of Canopy Cover Loss in Germany's Forests after the 2018–2020 Drought Years. Remote Sensing. 14(3). https://doi.org/10.3390/rs14030562

Wagner, PD., Bhallamudi, SM., Narasimhan, B., Kantakumar, LN., Sudheer, KP., Kumar, S., Schneider, K., Fiener, P., 2016. Dynamic integration of land use changes in a hydrologic assessment of a rapidly developing Indian catchment. Science of the Total Environment, 539, 153-164. https://doi.org/10.1016/j.scitotenv.2015.08.148

Xu, C., McDowell, NG., Fisher, RA., Wei, L., Sevanto, S., Christoffersen, BO., Weng, E., Middleton, RS., 2019. Increasing impacts of extreme droughts on vegetation productivity under climate change. Nature Climate Change. 9(12):948–953. https://doi.org/10.1038/s41558-019-0630-6

Yonaba, R., Biaou, AC., Koïta, M., Tazen, F., Mounirou, LA., Zouré, CO., Queloz, P., Karambiri, H., Yacouba, H., 2021a. A dynamic land use/land cover input helps in picturing the Sahelian paradox: Assessing variability and attribution of changes in surface runoff in a Sahelian watershed. Science of the Total Environment, 757: 143792. https://doi.org/10.1016/j.scitotenv.2020.143792

Yonaba, R., Koïta, M., Mounirou, LA., Tazen, F., Queloz, P., Biaou, AC., Niang, D., Zouré, C., Karambiri, H., Yacouba, H., 2021b. Spatial and transient modelling of land use/land cover (LULC) dynamics in a Sahelian landscape under semi-arid climate in northern Burkina Faso. Land Use Policy, 103: 105305. https://doi.org/10.1016/j.landusepol.2021.105305

Zeng, X., Hu, Z., Chen, A., Yuan, W., Hou, G., Han, D., Liang, M., Di, K., Cao, R., Luo, D., 2022. The global decline in the sensitivity of vegetation productivity to precipitation from 2001 to 2018. Global Change Biology. 28(22):6823–6833. https://doi.org/10.1111/gcb.16403

Zhang, W., Wei, F., Horion, S., Fensholt, R., Forkel, M., Brandt, M., 2022. Global quantification of the bidirectional dependency between soil moisture and vegetation productivity. Agricultural and Forest Meteorology. 313:108735. https://doi.org/10.1016/j.agrformet.2021.108735

Zhang, Y., Wang, K., Wang, J., Liu, C., Shangguan, Z., 2021. Changes in soil water holding capacity and water availability following vegetation restoration on the Chinese Loess Plateau. Scientific Reports. 11(1):9692. https://doi.org/10.1038/s41598-021-88914-0

Zuur, A., Leno, EN., Walker, N., Saveliev, AA., Smith, GM., 2009. Mixed Effects Models and Extensions in Ecology with R. Springer. New York.

Abstract

Climate change, Land Use/Land Cover Changes (LULCCs), and biological invasions are transforming ecosystems globally, posing significant challenges to human well-being. Understanding and monitoring ecosystem health—a multifaceted concept reflecting an ecosystem's structure, function, resilience, and recovery capacity—is essential for sustainable development. Combining ground-based methods with advanced remote sensing technologies makes it possible to assess and monitor ecosystem health over extensive spatial scales, providing critical insights for Sustainable Development Goals (SDGs).

This research focused on evaluating ecosystem health in two contrasting regions: the semi-arid landscapes of central Iran and the temperate suboceanic forests of central Germany. The study pursued three key objectives: (1) comparing ground-based and remote sensing methods for ecosystem health assessment, (2) employing the Dynamic Habitat Index (DHI) to monitor ecosystem dynamics over time, and (3) analyzing the sensitivity of DHIs to environmental changes across diverse LULC types.

In Iran, ground-based assessments provided factors such as biotic integrity, site stability, and hydrological functions to classify ecosystem health as healthy, at risk, or unhealthy. Complementing this, Landsat imagery and machine learning techniques produced detailed ecosystem health maps, closely aligned with field-based findings. Historical health maps derived from Landsat and evaluated using aerial orthophotos historical changes in ecosystem health. However, the specific climatic and ecological context of the region limited the generalizability of these methods.

In Germany, the study shifted to exploring the potential of DHIs—derived from Normalized Difference Vegetation Index (NDVI) data—to evaluate the health of coniferous forests under extreme drought conditions. We also evaluated the sensitivity of the DHI to changing environmental conditions across various Land Use/Land Cover (LULC) types. The analysis highlighted the effectiveness of DHIs in capturing the impacts of drought on Central European coniferous forest ecosystems. DHIs successfully distinguished between damaged and nondamaged forest areas, showing promise as an early warning system for ecosystem degradation and functional changes. Integrating DHIs with meteorological and ancillary geodata enhanced their interpretive power, highlighting the dynamic interplay of pedo-climatic factors in shaping ecosystem health.

The findings illustrate the strengths and limitations of different approaches, emphasizing the importance of indicator selection related to regional contexts, historical background, and environmental conditions. The integrated methodologies developed in this research offer valuable tools for land managers and decision-makers, contributing to sustainable land use strategies and advancing SDG indicators related to land degradation.

Keywords: Land Use/Land Cover, Ecosystem Health, Climate Change, Dynamic Habitat Index, NDVI, Germany, Iran, Rangelands, Coniferous Forests, Vegetation Seasonality, Machine Learning.

Zusammenfassung

Klimawandel, Landnutzungs- und Landbedeckungsänderungen (LULCCs) sowie biologische Invasionen verändern Ökosysteme weltweit und stellen bedeutende Herausforderungen für das menschliche Wohlergehen dar. Das Verständnis und die Überwachung der Gesundheit von Ökosystemen – ein vielschichtiges Konzept, das die Struktur, Funktion, Resilienz und Regenerationsfähigkeit von Ökosystemen widerspiegelt – sind essenziell für nachhaltige Entwicklung. Die Kombination von bodengestützten Methoden mit fortschrittlichen Fernerkundungstechnologien ermöglicht es, die Gesundheit von Ökosystemen auf großen räumlichen Skalen zu bewerten und zu überwachen, und liefert dabei wichtige Erkenntnisse für die Erreichung der Nachhaltigkeitsziele (SDGs). Diese Forschung konzentrierte sich auf die Bewertung der Gesundheit von Ökosystemen in zwei sehr unterschiedlichen Regionen: den semi-ariden Landschaften Zentralirans und den gemäßigt-subozeanischen Wäldern Zentraldeutschlands. Die Studie verfolgte drei Hauptziele: (1) Vergleich bodengestützter und fernerkundungsbasierter Methoden zur Bewertung der Ökosystemgesundheit, (2) den Einsatz des Dynamic Habitat Index (DHI), um die Dynamik von Ökosystemen im Zeitverlauf zu überwachen (3) die Analyse der Empfindlichkeit des DHI gegenüber Umweltveränderungen in verschiedenen LULC-Typen. Im Iran lieferten Felderfassungen Faktoren wie biotische Integrität, Standortstabilität und hydrologische Funktionen, um die Gesundheit von Ökosystemen als gesund, gefährdet oder ungesund zu klassifizieren. Ergänzend dazu wurden mit Landsat-Satellitenbildern und maschinellen Lernverfahren detaillierte Karten der Ökosystemgesundheit erstellt, die eng mit den feldbasierten Ergebnissen übereinstimmten. Historische Gesundheitskarten, abgeleitet aus Landsat-Daten und bewertet mit Hilfe von Orthofotos, lieferten historische Veränderungen in der Ökosystemgesundheit. Die spezifischen klimatischen und ökologischen Gegebenheiten der Region schränkten jedoch die Generalisierbarkeit dieser Methoden ein. In Deutschland lag der Fokus der Untersuchung auf dem Potenzial des DHI, abgeleitet aus dem Normalized Difference Vegetation Index (NDVI), zur Bewertung der Gesundheit von Nadelwäldern unter extremen Dürrebedingungen. Zudem wurde die Empfindlichkeit des DHI gegenüber Umweltveränderungen in verschiedenen Landnutzungs- und Landbedeckungstypen analysiert. Die Analyse zeigte die Effektivität des DHI bei der Erfassung der Auswirkungen von Dürre auf mitteleuropäische Nadelwaldökosysteme. DHIs unterschieden erfolgreich zwischen geschädigten und ungeschädigten Wäldern und zeigten Potenzial als Frühwarnsystem für Ökosystemdegradation und funktionale Veränderungen. Die Verknüpfung von DHIs mit meteorologischen und ergänzenden Geodaten verstärkte die Aussagekraft und unterstrich die Bedeutung des dynamischen Zusammenspiels von pedo-klimatischen Faktoren für die Ökosystemgesundheit. Die Ergebnisse verdeutlichen die Stärken und Grenzen verschiedener Ansätze und unterstreichen die Bedeutung der Indikatorauswahl im Hinblick auf regionale Kontexte, historische Hintergründe und Umweltbedingungen. Die in dieser Forschung entwickelten integrierten methodischen Ansätze bieten wertvolle Werkzeuge für Landmanager und Entscheidungsträger, unterstützen nachhaltige Landnutzungsstrategien und tragen zur Verbesserung von SDG-Indikatoren im Zusammenhang mit Landdegradation bei.

Acknowledgments

The journey to completing this PhD dissertation has been both challenging and rewarding, and it would not have been possible without the support, guidance, and encouragement of many wonderful individuals.

First and foremost, I am deeply thankful to my supervisor, Prof. Dr. Till Kleinebecker, for the opportunity to work at the Division of Landscape Ecology, as well as for his steadfast support, insightful guidance, kindness, and openness. His expertise and encouragement have been fundamental in shaping my academic growth. Furthermore, I would like to thank Prof. Dr. Lutz Breuer, who agreed to be the second supervisor of this dissertation.

I want to express my heartfelt gratitude to Dr. André Große-Stoltenberg. His unwavering support, insightful ideas, and expert guidance have been instrumental in shaping this dissertation and my research. I am truly grateful for his mentorship and for believing in my potential. What I learned under their guidance, particularly that of Dr. André Große-Stoltenberg and Prof. Dr. Till Kleinebecker, goes beyond science and scientific writing.

My warm thanks go to my colleagues and friends at the Division of Landscape Ecology and Landscape Planning, especially for the friendly and supportive working atmosphere.

I am extremely grateful to my family for their unwavering love and support. To my parents, and my wonderful sister, Maryam, thank you for your endless encouragement and for instilling in me the value of education. To my dear husband, Jalal, his patience, endless support, understanding, and sacrifices have been essential in helping me navigate the highs and lows of this journey.

I dedicate this work to my little Armin, who has given me a new perspective on life and creation. After all, not everything is written in books!!

I am sincerely grateful to each one of you for your contributions and support.

Thank you
Mojdeh Safaei